Modeling, Validation, and Evaluation of the NIST Net Zero Energy Residential Test Facility

by

Elizabeth C. Balke

A thesis submitted in partial fulfillment of

the requirements for the degree of:

MASTER OF SCIENCE

(MECHANICAL ENGINEERING)

at the

UNIVERSITY OF WISCONSIN – MADISON

2016

This page intentionally left blank

Approved by:

_____ _____

Professor Gregory F. Nellis Date

This page intentionally left blank

Abstract

The Net Zero Energy Residential Test Facility (NZERTF) is a highly instrumented single-family net zero energy house occupied by a virtual family of four and containing a variety of commercially-available building technologies. Two detailed TRNSYS models of the NZERTF were created including the accompanying HVAC and domestic hot water heating equipment. One model was created using only information known before the NZERTF operation, and a second model was created by tuning the first model using data collected during the first year of NZERTF operation. The models were evaluated by comparing the predictions with measured results. The first model under-predicted the measured total energy consumption by 13.8 %, while the second, tuned model under-predicted the measurements by only 1.6 %. Both models predicted the total energy generation from the photovoltaic system within 3.1 % of the measurements. This thesis shows a detailed comparison of the models' predicted results and the measured data collected from the NZERTF, and discusses the challenges of creating an accurate model for this type of facility.

The tuned model of the NZERTF and the energy equipment in the house was then used as a base for comparing alternate energy equipment and control logic. Eight different domestic hot water systems were modeled. The energy consumption of the hot water systems as well as the impact they have on space conditioning were compared. Additionally, alternate HVAC equipment and controls were evaluated, including an energy recovery ventilation system, heat pump thermostat control logic with no time-out limits, and a ground-source heat pump.

Acknowledgements

Foremost I would like to thank my advisors, Greg Nellis and Sandy Klein. Your advice, encouragement, and constructive criticism kept me on track and without your expertise and realism I would not have been able to accomplish as much as I have.

I would also like to thank the National Institute of Standards and Technology for funding this project and for enabling me to spend a summer working at the NIST campus in Gaithersburg, MD. My deepest gratitude goes to Harrison Skye, Tania Ullah, Bill Healy, Farhad Omar, Vance Payne, Lisa Ng, Hunter Fanney, Josh Kneifel, and others at NIST with whom I interacted. The passion, expertise, and comradery I observed while there was inspiring. Thank you for your patience in answering so many questions from me, for your attention to detail when reviewing my work, and for your encouragement along the way.

Thank you to Amy Van Asselt, Ana Dyreson, Chris Hummel, and others in the Solar Energy Laboratory. I have enjoyed the time we have spent together and I appreciate your help on homework assignments.

Many, many thanks go to my family. Mom, thank you for giving me my work ethic and for helping me keep things in perspective. Dad, thank you for teaching me to first adjust my attitude when a situation seems dreary or overwhelming. Mel, thank you for believing in me even when I do not believe in myself.

Finally, I would like to thank Corey Noone, who pushes me to be a better version of myself while simultaneously supporting me and whose constant love never ceases to amaze me. Thank you for being by my side throughout graduate school.

Table of Contents

List of Figures

List of Tables

This page intentionally left blank

Introduction

Recent events and trends indicate that climate change is a growing concern and reducing greenhouse gas emissions is becoming a priority. Examples include the growing number of "green" certified buildings [1][2], the increasing percentage that renewables contribute to the total energy generation in the U.S. [3], the increasing number and stringency of policies restricting greenhouse gas emissions (e.g. the Clean Power Plan [4]), and the engagement of world leaders in discussions on how to curb climate change at the 2015 United Nations Climate Change Conference [5]. One sector in which energy consumption reduction could have significant impact on the greenhouse gas emissions is the residential building sector. The residential sector emissions come from both direct fuel consumption from heating and cooking and, because the majority of electricity in the U.S. is generated by burning coal or natural gas, from electricity used for space conditioning and plug loads. Buildings accounted for 40 % of the total energy consumption in the U.S. in 2014, with residential buildings alone accounting for 22 % of the energy consumption [6], and residential buildings accounted for approximately 38 % of the retail sales of electricity in 2014 [7]. This large amount of energy consumption resulted in the residential sector accounting for approximately 21 % of the total carbon dioxide emissions in the U.S. in 2014 [8]. Therefore, advancements in the energy efficiency of residential homes could make a significant impact on greenhouse gas emission reduction. It is toward this end that this project on the modeling and evaluation of a net zero energy house and of various energy equipment configurations and controls was completed.

A net zero energy building is defined here as a building that produces at least as much energy as it uses in a year when accounted for at the site [9]. The Net Zero Energy Residential Test

Facility (NZERTF) is a net-zero energy house built by the National Institute of Standards and Technology (NIST) on the NIST campus in Gaithersburg, Maryland. It was built for two purposes: (1) to prove that it is possible to achieve net-zero energy operation with a home that is similar to a typical Maryland house and (2) to evaluate various energy system configurations and control strategies in this context [10]. The NZERTF contains an assortment of commercially-available building technologies, including three separate ground source heat exchangers, an air source heat pump, a heat recovery ventilation system, a radiant basement floor heating system, a solar hot water system with two differently sized storage tanks, a heat pump water heater, and a solar photovoltaic system. A subset of the available technology was used during the first year operation, which took place from July 2013 to June 2014. The house is not occupied, but the activities associated with a family of four are simulated by activating appliances, plug loads, lighting, water draws, and devices that generate latent and sensible heat consistent with occupants according to weekly schedules.

Two detailed models of the NZERTF and the HVAC equipment that was used during the first year of operation have been created using the TRNSYS software, a transient systems simulation program [11]. The first model was created using information known or estimated before the first year of operation (with the exception of the weather data). The parameters required for the first model are determined from sources such as equipment specifications, supplementary information from the manufacturers, and ASHRAE standards. The second model was created by tuning the first model using data collected during the first year of operation. This tuned model will be used subsequently to carry out studies of various energy system configurations and control strategies that would be difficult or time-consuming to do

experimentally. This paper discusses these two models and compares the predicted performance of the NZERTF to measurements taken during the first year of operation.

There are a number of net zero energy buildings constructed around the world and a significant number of articles and papers documenting their construction and their measured energy generation and consumption. A study by Musali et al. as a result of the International Agency Solar Heating & Cooling Programme Task 40/Annex 52 was an analysis of 280 international net zero energy buildings [12]. This analysis found many variations in building design, but each of the 50 exemplary net zero energy buildings highlighted in this study used photovoltaic energy generation to reach the net zero energy goal. Furthermore, it found that typical net zero energy residential buildings used passive house concepts with solar thermal collectors, energy efficient appliances, and heat pumps. Another noteworthy publication on net zero energy residential buildings is a report by Norton et al. that discusses the measured energy consumption and generation of a net zero energy home built by the National Renewable Energy Laboratory (NREL) and Habitat for Humanity of Metro Denver in Denver, CO [13]. A Canadian program called EQuilibrium Sustainable Housing Demonstration Initiative was launched in 2006 in order to advance sustainable housing in Canada by helping developers by modeling near zero energy or net zero energy homes. As a result of that initiative a number of articles have been published discussing the construction and energy usage of the constructed homes funded by that initiative [14 - 17]. However, these and other net zero energy homes differ from the NIST NZERTF because the NZERTF serves as a highly controlled and measured testbed for a number of various energy technologies. The occupancy, plug loads, and water draws are carefully controlled. The

energy consumed by each end use, the thermal conditions within the house, and the energy generated are all closely monitored.

In addition to the studies on the construction, the trends, and the measured energy consumption and generation of net zero energy buildings, there have also been many publications on building energy simulations of net zero energy buildings. In general, these simulations are performed for the purpose of assessing and optimizing the economics, the energy consumption and generation, or a combination of economic and energy optimization. An example of simulation done for economic assessment is a study by Leckner and Zmeureanu performing a life cycle cost analysis to determine the payback time for converting a code-compliant house in Montreal to a predicted net zero energy house [18] (and found that payback is never reached). An example of how computer simulations can inform design decisions is a book published in 2015 as another result of the previously mentioned International Agency Solar Heating & Cooling Programme Task 40/Annex 52 to discuss how to optimally use simulation tools in designing net zero energy buildings called "Modeling, Design, and Optimization of Net-Zero Energy Buildings" [19]. The modeling work discussed in this thesis differs from modeling work based on other net zero energy houses because of the large amount of measured data available to validate the model. Because of this data, a highly detailed, accurate model was created and validated.

Previous work has also been done on modeling the NIST NZERTF. Kneifel created a model of the NZERTF using EnergyPlus and compared the predicted results to the measured data [20-22]. Leyde used TRNSYS to model the NZERTF [23]. However, at the time Leyde was modeling the house, not all of the necessary information was available and only a few

months of data had been collected and post-processed. The models discussed in this thesis differ from Kneifel's EnergyPlus model because the TRNSYS software is more versatile than EnergyPlus, allowing for certain equipment and control strategies to be modeled that are not possible using EnergyPlus. This thesis builds on the work of Leyde by revising Leyde's model, validating the model, and using this validated model to evaluated alternate energy equipment and control strategies.

Chapter 1 discusses the NZERTF envelope, each subsystem in the NZERTF, and modeling the envelope and subsystems using only information known before the house was in operation and measured data was collected. Results from this un-tuned model are compared to the data collected over the first year of operation. In Chapter 2, tuning the model using the collected data from the NZERTF is discussed and the results from this tuned model are compared to the data collected over the first year of operation. Next, alternate domestic hot water systems are modeled and evaluated in Chapter 3. Finally, Chapter 4 evaluates alternate HVAC systems and control strategies. These include alternate ventilation systems, a different thermostat control strategy, and a ground-source heat pump with and without a separate dehumidifier.

Chapter 1: Modeling the NZERTF

The first model of the NZERTF was created with TRNSYS software and used only the information known before the first year of operation of the NZERTF. Much of the information needed to create the model was found in manufacturer specifications, other information gained from communication with manufacturers, the NZERTF as-built construction plans, and ASHRAE standards. In this chapter, the physical house itself and its

energy equipment subsystems are described, the methods by which the model was created are explained, and the results of a year-long simulation using this un-tuned model are compared to the measured data collected over the first year of operation.

1.1. Building Envelope

Before any models of the energy equipment were created, the building envelope geometry and properties were modeled. Estimates of the infiltration, the internal air flow, thermal capacitance, and humidity capacitance ratio were then modeled or specified.

1.1.1 *House Structure*

The NZERTF is a 251 m^2, two story house with a conditioned basement and a detached garage. The basement level of the house is an open space containing most of the house's mechanical and electrical equipment. The main floor consists of the kitchen, dining room, living room, office, a bathroom, and a foyer that extends to the second floor. The thermostat for the HVAC system is located in the living room on the main floor. The second floor consists of a hallway, three bedrooms, and two bathrooms. The unconditioned attic contains the inverters for the photovoltaic system. The detached garage contains the data acquisition equipment and is not conditioned or modeled.

The NZERTF CAD model, shown in Figure 1, was created using the TRNSYS3d plug-in for Google SketchUp and was based the Building Science Corporation's NIST Net Zero Energy Residential Test Facility As Built Architectural Plans [23] [24]. The layers of material used in the external walls, roof, floors, and ceilings were specified in the TRNSYS utility program, TRNBuild, in accordance with the NZERTF construction plans [24].

The model is divided into four zones: the basement, the main floor, the second floor, and the attic. Each zone has a consistent temperature, humidity ratio, and other properties throughout the zone. Further details on the modeling of the building envelope are presented in Leyde [23].

Figure 1. (a) Google SketchUp model of NZERTF used in TRNSYS simulation [23] (b) Photograph of the NZERTF [25]

1.1.2 *Infiltration*

The NZERTF infiltration is modeled using the component Type 932 which implements the Sherman-Grimsrud infiltration model as described in the ASHRAE Handbook of Fundamentals, 2005 [26].

$$Q = \left(\frac{A_L}{1000}\right)\sqrt{C_s \Delta T + C_w U^2} \quad \textbf{(1)}$$

where Q is the infiltration airflow rate (m^3/s), A_L is the effective leakage area (cm^2), C_s is the stack coefficient ($(L/s)^2/(cm^4\text{-}K)$), ΔT is the average indoor-outdoor temperature difference for the time interval of calculation (K), C_w is the wind coefficient ($(L/s)^2/(cm^4\text{-}(m/s)^2)$), and U is the average wind speed measured for the time interval of calculation (m/s).

The stack coefficient and wind coefficient used correspond to the values given in the ASHRAE Handbook for a class 2 shelter, which is a “typical shelter for an isolated rural

house" [26] and a building height of two stories. Their values are $C_s = 0.00029$ (L/s)^2/(cm^4-K) and $C_w = 0.000325$ (L/s)^2/(cm^4-(m/s)^2). To calculate the infiltration rate, the effective leakage area is required. The effective leakage area was calculated using the results of the final blower door test, which was performed after the house was fully constructed. This blower door test yielded an air exchange rate of 802 m^3/hr at 50 Pa. The effective leakage area was calculated using equation 33 in Chapter 27 of the ASHRAE Handbook of Fundamentals, 2005 [26].

$$A_L = 10000 Q_r \frac{\sqrt{\rho/2\Delta p_r}}{C_D} \quad \textbf{(2)}$$

where A_L is the effective air leakage area (cm^2), Q_r is the airflow rate at Δp_r (m^3/s), ρ is the air density (kg/m^3), Δp_r is the reference pressure difference (Pa), and C_D is the discharge coefficient.

A discharge coefficient of 1 and an air density of 1.204 kg/m^3 were used, which resulted in an effective leakage area of 244 cm^2. It is assumed that the leakage occurs in Zones 2 and 3 (the first and second floors), but not in Zones 1 and 4 (the basement and attic). The effective leakage area is divided into two effective leakage areas based on the volumes of Zones 2 and 3. These leakage areas, along with the other parameters used by Type 932, are listed in Table A-1 in Appendix A. Using these leakage areas, the resulting monthly average numbers of air changes per hour were calculated. The monthly average predicted infiltration rates ranged from 0.03 h^{-1} in summer to 0.07 h^{-1} in winter, as shown in Figure 2. Typical seasonal average infiltration rates for housing in North America vary greatly, generally ranging from

approximately 0.2 h^{-1} to 2.0 h^{-1} [26]. The NZERTF infiltration rates indicate a very tightly constructed envelope.

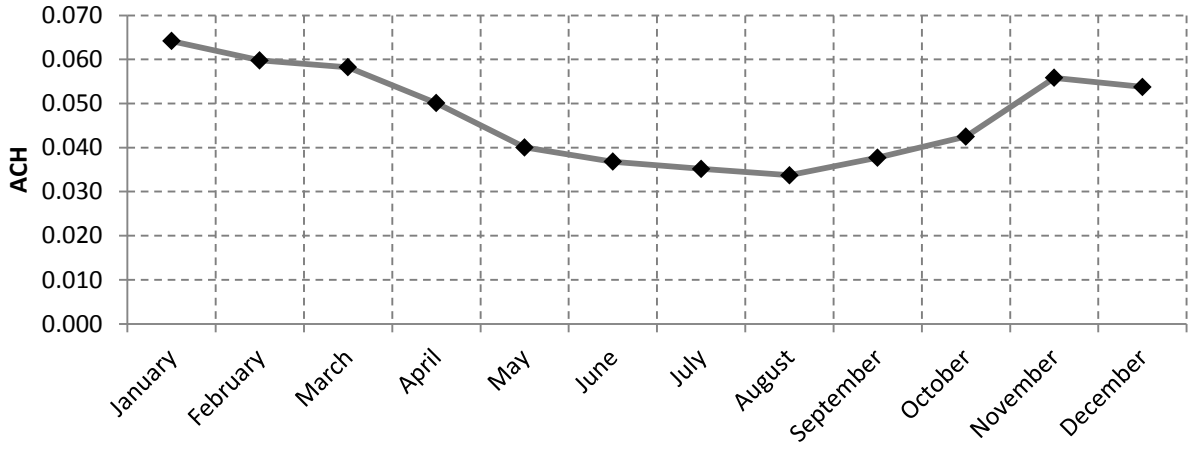

Figure 2. TRNSYS Monthly Average Number of Air Changes per Hour.

1.1.3 *Internal Air Flow*

The fraction of HVAC supply air flow to each zone was determined from as-built drawings [24] for each floor. The flowrates specified on the drawings at each register on each floor were totaled in order to calculate the fraction of flow supplied to each floor. The resulting flow fractions are constant throughout the year and are shown in Table 1.

Table 1. HVAC Air Flow Fractions

Zone	Heat Pump Supply Air Fraction	Heat Pump Return Air Fraction	HRV Supply Air Fraction	HRV Return Air Fraction
Zone 1 (Basement)	0.12	0	0	0
Zone 2 (First Floor)	0.55	0.65	0.27	0.33
Zone 3 (Second Floor)	0.33	0.35	0.73	0.67
Zone 4 (Attic)	0	0	0	0

To estimate the air flow between floors, a mass balance was performed on each zone. Return air vents for the heat pump and HRV are located in Zones 2 and 3. Supply air ducts for the

heat pump are located in Zones 1, 2 and 3, and supply air ducts for the HRV are located in Zones 2 and 3. It was assumed that infiltration only occurs in Zones 2 and 3. Therefore, all of the basement supply air would be forced to enter Zone 1. It is also assumed that there is no air exchange between the attic and the rest of the house. Mass balances are performed in TRYNSYS every time step to find the estimated air flow between zones. Figure 3 shows a schematic of the air flow to and from each zone. The arrows between floors show the air flow between zones.

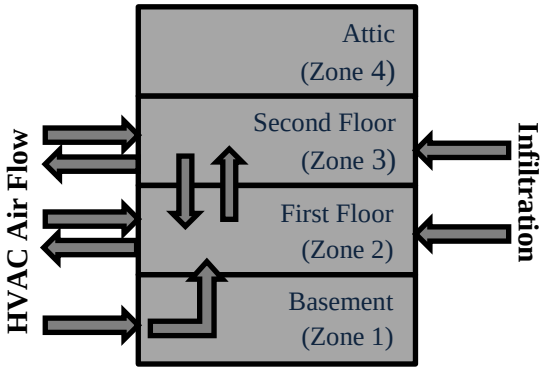

Figure 3. Schematic of Air Flow Between Floors (Zones) in the NZERTF.

1.1.4 *Capacitance*

The ASHRAE Standard 90.2, 2007 [27] provides an estimate of the capacitance of buildings. The standard assumes 5 lb/ft^2 (24.4 kg/m^2) of gypsum board to account for internal structural mass and 8lb/ft^2 (39.1 kg/m^2) of wood to account for furniture and contents. The NZERTF contains no furniture, therefore it is assumed that mass of wood is negligible. The internal capacitance of the first and second floors is estimated as the capacitance of the air and the capacitance of the internal structural mass. The basement contains no internal structural mass other than the staircase, no furniture, and most of the HVAC equipment. The capacitance of the basement was estimated as having the same value as the first floor. The attic contains

only the inverters for the photovoltaic array, so its thermal capacitance was estimated using the thermal capacitance of the air in the attic.

$$C_{zone,i} = A_i c_g \left(24.41 \frac{kg}{m^2}\right) + V_i \rho_a c_{p,a} \quad for\ 1 \leq i \leq 3 \tag{3}$$

$$C_{zone,4} = V_i \rho_a c_{p,a} \tag{4}$$

where i is the zone number, $C_{zone,i}$ is the capacitance of each zone. $A_i$is the floor area of the zone, c_g is the heat capacity of gypsum board $\left(1.09 \frac{kJ}{kgC}\right)$, V_i is the volume of the zone, $\rho_a$is the density of air $\left(1.204 \frac{kg}{m^3}\right)$, and $c_{p,a}$ is the heat capacity of air $\left(1.005 \frac{kJ}{kg\ K}\right)$. The floor area, volume, and capacitances of each zone are shown in Table 2.

Table 2. Interior Thermal Capacitance for Each Zone.

Zone	Floor Area (m^2)	Volume (m^3)	Interior Thermal Capacitance [kJ/K]
Zone 1 (Basement)	142	432	4299
Zone 2 (First Floor)	142	447	4317
Zone 3 (Second Floor)	114	360	3467
Zone 4 (Attic)	114	122	147

1.1.5 *Humidity Capacitance Ratio*

To model the dynamic effect of humidity in the house, a humidity capacitance ratio must be specified. The humidity capacitance ratio is the ratio of the mass of the water in the air and the mass of the water in other materials in the zone to the mass of the water in the air.

$$Humidity\ capacitance\ ratio = \frac{m_{H_2O,air} + m_{H_2O,material}}{m_{H_2O,air}} \tag{5}$$

The mass of moisture in the air was calculated for each zone using the following equation:

$$m_{H_2O,air,i} = V_i \rho \omega \quad \textbf{(6)}$$

where V_i is the volume of the zone, ρ is the density of dry air, and ω is the typical humidity ratio. The typical humidity ratio was evaluated at the integrated average yearly temperature and relative humidity of Zone 2, which are 22^0C and 40% RH, respectively.

Because there is no furniture and very few contents in the NZERTF, the mass of materials in the zone is assumed to be the internal structural mass, which was estimated when calculating the capacitance of each zone. It is assumed that the internal structural mass of the house consists of gypsum board. The mass of water in other materials, $m_{H_2O,material}$, is therefore assumed to be the mass of water that is stored in gypsum board.

$$m_{H_2O,material} = m_{H_2O,gypsum\ board} = u(m_{gypsum\ board}) \quad \textbf{(7)}$$

where u is the mass of water found in gypsum board to the mass of the gypsum board for a given relative humidity, or the sorption isotherm, and $m_{gypsum\ board}$ is the mass of gypsum board in each zone. The sorption isotherm of gypsum board at 40% RH is approximately 0.003 kg/kg [28].

Using these three equations, the humidity capacitance ratio for each zone was calculated and is shown below in Table 3.

Table 3. Humidity Capacitance Ratio for Each Zone.

Zone	Humidity Capacitance Ratio
Zone 1 (Basement)	2.2
Zone 2 (First Floor)	2.2
Zone 3 (Second Floor)	2.2
Zone 4 (Attic)	1

1.2 TRNSYS Model Drivers

Although the NZERTF is unoccupied, the activities of a family of four are emulated by activating appliances, plug loads, lights, water draws, and devices that are designed to represent the sensible and latent loads of each virtual occupant. These loads are activated according to a weekly schedule specified in Omar and Bushby [10]. As noted in Omar and Bushby, the activities of the virtual family are largely based on standard user profiles developed for the U.S. Department of Energy (DOE) Building America program [29].

The following sections will discuss each of the drivers that are used as inputs to the model during a year. These inputs include the occupancy, plug loads, lighting loads, appliance loads, moisture input, water draws, weather data, ground temperature, and time step. Because these drivers are considered inputs to the model and to the house, the measured power for each appliance and the daily water volumes were used as inputs to the model rather than the predicted power and water volumes. Similarly, measured weather data was used. The input of accurate load and weather data allows for a more accurate prediction of the behavior of the HVAC and DHW systems.

1.2.1 *Occupancy Schedule*

The schedules for the four virtual occupants in the NZERTF are based on the Building America profiles [10]. Each occupant is assumed to generate a constant 70 W of sensible heat and 45 W of latent heat, which is the adjusted load per person for seated and very light work [30]. The occupants' sensible load is emulated using resistance heaters situated on the first and second floors. The occupants' latent load was converted from 45 W to 0.07 L/hr using the latent heat of vaporization [10]. The total volume of water generated by the occupants each day was then calculated and is emulated using ultrasonic humidifiers. The volume of water generated by the NZERTF occupants is discussed in Section 1.2.5.

1.2.2 *Plug Load Schedule*

The electric plug loads selected for the NZERTF were assumed to be used or owned by at least 50% of households [10]. The electric plug loads used in the NZERTF follow a weekly schedule, the details of which may be found in Omar and Bushby [10]. Each plug load is represented either by the actual appliance (discussed in the next section) or by an electric resistance heater box. The sensible and latent load fractions for the actual appliances are assumed to be 0.734 and 0.20, respectively [29].

1.2.3 *Lighting Schedule*

The lighting schedule is based on the movements of the virtual occupants, turning on when an occupant enters a room and turning off when the occupant leaves the room. Because the basement and attic are unoccupied, only lights on the first and second floors are activated according to the weekly schedule. All of the lighting contributes to the sensible load.

1.2.4 *Appliance Schedule*

The appliances in the NZERTF include a washing machine, clothes dryer, dishwasher, oven, cooktop range, refrigerator, and a microwave, all of which are located on the first floor. The appliance power is both simulated and measured separately from the plug load. The sensible and latent load fractions differ for each appliance, and each of these fractions, except for the oven and cooktop range latent loads, are obtained from Table 21 in Hendron and Engebrecht [29]. The latent load generated during typical daily cooking events was estimated and this equivalent volume of water is released in the NZERTF each day by ultrasonic humidifiers [10], as will be discussed in greater detail in the next section.

1.2.5 *Moisture Schedule*

The moisture generated by a family of four's occupancy and cooking is emulated in the NZERTF using ultrasonic humidifiers. The volume of water varies from day to day depending on the occupancy schedule and the number of cooking events. Table 4 lists the daily volume of water introduced to the NZERTF through humidifiers located in the kitchen. This volume of water is introduced to Zone 2 in the TRNSYS model at a constant rate during hours in which the house is occupied each day.

Table 4. Daily Moisture Generated by Cooking Events and Occupants.

Day	Moisture from Cooking (liters/gallons)	Moisture from People (liters/gallons)	Total Moisture (liters/gallons)
Monday	0.99/0.26	5.83/1.54	6.83/1.80
Tuesday	0.74/0.20	3.87/1.02	4.61/1.22
Wednesday	0.74/0.20	4.00/1.06	4.74/1.25
Thursday	0.74/0.20	3.87/1.02	4.61/1.22
Friday	0.74/0.20	4.00/1.06	4.74/1.25
Saturday	0.74/0.20	3.87/1.02	4.61/1.22
Sunday	0.99/0.26	5.63/1.49	6.22/1.75

1.2.6 *Water Draw Schedule*

There are five types of water draws in the NZERTF: sink draws, baths, showers, clothes washer cycles, and dishwasher cycles. The showers, the baths, and some of the sink water draw events occur in the master bedroom on the second floor. The other sink events occur in the kitchen on the first floor. The total water volume used in a week is approximately 2,229 L (589 gal) [10]. The sensible and latent heat gains for each type of water draw event were estimated using Table 9 in Hendron and Engelbrecht [29] and were scaled according to the scheduled water volume draw at NZERTF. The sensible and latent heat gain caused be each type of event, as well as other details about each type of event, are found in Table 5.

Table 5. Water Draw Events

	Water Draw per Event (L)	**Length of Water Draw (min)**	**Number of events per week**	**Water Temperature (^{0}C)**	**Sensible Gain [kJ/event]**	**Latent Gain [kg/event]**
Sinks	1.78	1	280	40.56	12.28	0.002
Bath	116.55	11	2	43.33	1713.2	0
Short Shower	39.42	10	21	43.33	581.05	0.226
Long Shower	59.13	15	5	43.33	871.58	0.367
Clothes Washer	56.7	5	6	48.9	-	-
Dishwasher	7	3	5	48.9	-	-

1.2.6 *Weather*

The measured outdoor dry-bulb temperature, outdoor wet-bulb temperature, irradiation on the plane of the solar panel array, and water mains temperatures were used as inputs in the model. The irradiation on the plane of the solar panel array was converted to beam radiation, sky diffuse radiation, and ground diffuse radiation on the collector plane using Type 546.

Weather data collected at the Montgomery County Airpark (KGAI) from July 1, 2013 to June 30, 2014 supplied the other weather inputs used in the TRNSYS simulation. The distance between this airport and the NIST campus is about four miles. The weather file from the KGAI airport includes the data listed in Table 6 on an hourly basis. The NZERTF and KGAI data were converted into a TMY3 weather data file to be read by Type 15, a weather data processor, in TRNSYS.

Table 6. Weather Data Inputs.

Data from the NZERTF	Data from KGAI
Dry Bulb Temperature [^{0}C]	Atmospheric Pressure [Pa]
Dew Point Temperature [^{0}C]	Extraterrestrial Horizontal Radiation [W/m^2]
Irradiation on Plane of Array [W/m^2]	Extraterrestrial Direct Normal Radiation [W/m^2]
Water Mains Temperature [^{0}C]	Wind Direction [deg]
	Wind Speed [m/s]
	Total Sky Cover [tenths]
	Liquid Precipitation Depth [mm]

Three of the most important weather parameters are the outdoor dry-bulb temperature, the outdoor humidity ratio, and the solar irradiation on the plane of the solar array. The outdoor temperature and humidity affect the thermal load, which consequently affects the HVAC system's electrical consumption. The irradiation affects the solar fraction of the domestic hot water system as well as the energy generation of the photovoltaic system. Figure 4 and Figure 5 show the monthly average values for these three weather parameters.

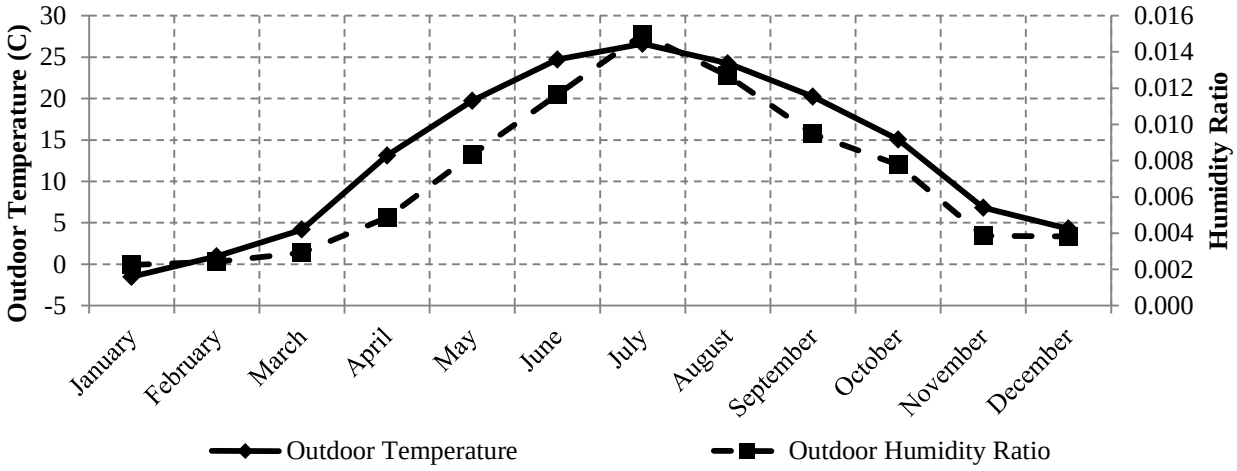

Figure 4. Monthly Average Outdoor Dry-Bulb Temperature and Humidity Ratio.

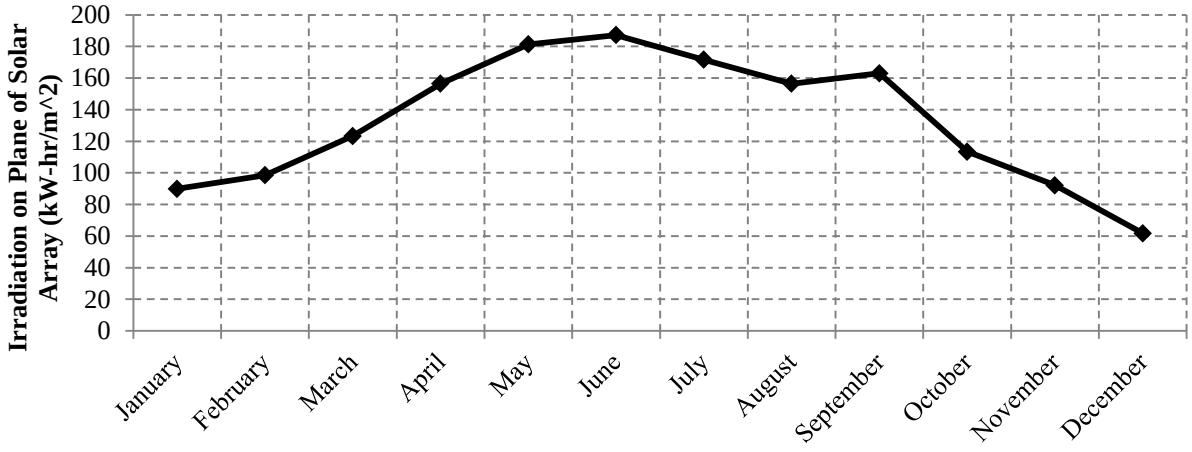

Figure 5. Monthly Average Irradiation on Plane of Solar Array.

1.2.7 *Ground Temperature*

The ground temperature was estimated using Type 1244, a soil model. This type requires soil properties, the deep earth temperature, the amplitude of the soil surface temperature over a year, and the day of the minimum soil surface temperature. The soil property values were provided by MatWeb [31] and the soil temperature data was gathered using soil temperature data recorded at Powder Mills, MD and published by the Natural Resources Conservation Service [32]. The type also requires node position data files, which were created using the

basement dimensions specified on the NZERTF building plans. Using this type, the average ground temperatures at the basement walls and floor were estimated. It is assumed that the predicted ground temperature should be approximately equal to the measured water mains temperature, so these two were compared and were found to differ by only a few degrees. Figure 6 compares the monthly average measured water mains temperature to the basement wall temperature predicted by TRNSYS.

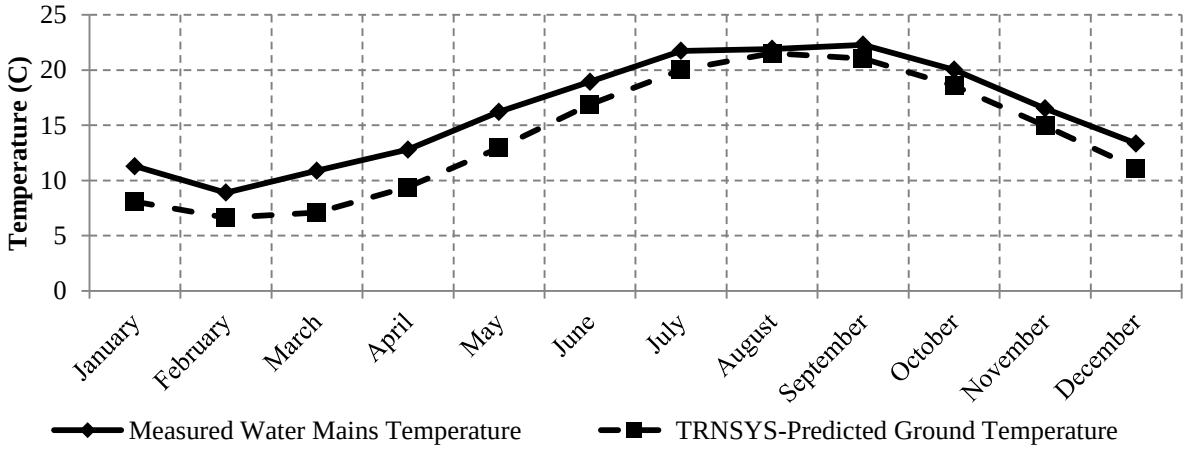

Figure 6. Monthly Average Measured Water Mains Temperature vs. TRNSYS-Predicted Basement Wall Temperature.

1.2.8 *Time Step*

Although the weather data is reported on an hourly basis, the equipment within the house requires a smaller time step. For example, the heat pump triggers a higher stage of operation after running in the lower stage for ten minutes, and the defrost cycle on the HRV causes the fan to run in recirculation mode for seven minutes. Because of the short time periods used by these pieces of equipment, among others, a time step of one minute was chosen.

1.3 Subsystems

There are three main subsystems in the NZERTF: the HVAC system, the DHW system, and the PV system. In this section, each of these subsystems and the models of the subsystems are described.

1.3.1 *HVAC System*

The HVAC system consists of an air source heat pump and a heat recovery ventilator (HRV). The HRV provides the required ventilation for the building while the heat pump provides the space conditioning required to maintain the temperature and relative humidity setpoints.

1.3.1.2 Heat Recovery Ventilation

To bring fresh air into the NZERTF, a Venmar AVS HRV EKO 1.5 was used, which acts as a sensible heat exchanger between the supply of fresh air from the outdoors and the exhaust air from the indoors. ASHRAE Standard 62.2 [33] requires at least 137 m^3/hr (80.6 cfm) of fresh air to be provided to the NZERTF. To meet this requirement, the lowest speed on the HRV that exceeded 137 m^3/hr was selected [34]. According to the manufacturer's specifications [35], this speed setting provides approximately 171 m^3/hr (100 cfm) of air.

The NZERTF also has an exhaust system used to vent the dryer and the kitchen range above the cooktop. When these appliances are on, a motorized damper in the attic is opened to allow makeup air to enter if the pressure differential between outdoors and indoors is greater than 10 Pa. This capability is not modeled in the TRNSYS simulation.

An air source heat recovery model, Type 667, was used to model the HRV. The sensible effectiveness was assumed to be the same for heating and cooling and to vary only with air

speed. The coefficients for the correlation between the air flow and the effectiveness were determined from the data provided in the manufacturer's specifications. The latent effectiveness of the HRV was specified as 0.01 by the manufacturer specifications. The return and supply air flow is split between the first and second floors based on the total air flow at all of the vents on each floor as specified in the as-builts [24]. The HRV runs continuously, but has a defrost mode during which it recirculates the indoor air. According to the manufacturer's specifications, the defrost mode is triggered when the outdoor air temperature falls below -5 ^{0}C. During defrost, the unit recirculates air for seven minutes, then returns to normal operation for 25 minutes. After the 25 minutes, it tests the outdoor air temperature again and repeats the defrost cycle if the temperature is still below -5 ^{0}C. Controls were created in TRNSYS to trigger this defrost cycle. The sensible efficiency and power consumption of the HRV is based on the air flow rate and was listed in the manufacturer specifications. All parameters associated with the HRV are listed in Table A-3 in Appendix A.

1.3.1.1 Air Source Heat Pump

The air source heat pump in the NZERTF is an AAON, Inc. split-system, heat pump with a two-step scroll compressor and a variable speed air handler fan [36][37]. It is controlled by a Robertshaw 9825i2 programmable thermostat [38]. The heat pump has three heating stages, two cooling stages, and a dedicated dehumidification mode. In the third stage of heating, the heat pump activates a 10 kW electric resistance heater. According to AHRI Certificate of Product Ratings [39], the rated heating capacity is 7796 W (26600 Btu/hr) with a heating seasonal performance factor (HSPF) of 9.30. The rated cooling capacity is 7619 W (26000

Btu/hr) with an energy efficiency ratio (EER) of 13.05 and a seasonal energy efficiency ratio (SEER) of 15.80.

The heat pump operation is both temperature- and time-triggered. The setpoints and deadbands are all adjustable within a range defined by the thermostat manufacturer [38]. The temperature setpoint in heating mode is 21.11 ^{0}C (70 ^{0}F) and the setpoint in cooling mode is 23.89 ^{0}C (75 ^{0}F). The first stage in heating mode turns on when the thermostat, located in the living room, reads a temperature 0.56 ^{0}C below the setpoint. The second stage turns on when the first stage has been running for 10 minutes or the temperature drops 1.1 ^{0}C below the setpoint. The third stage uses an electric resistance heater and turns on when the second stage has been running for 40 minutes or the temperature drops 3.3 ^{0}C below the setpoint. The first stage in cooling mode turns on when the thermostat reads a living room temperature 1.1 ^{0}C above the setpoint. The second stage cooling turns on when the first stage has been running for 40 minutes or the thermostat reads a temperature 2.8 ^{0}C above the setpoint. The dedicated dehumidification mode activates only if the cooling mode is not in operation and the relative humidity in the living room is greater than 50%. The second stage of dehumidification, which involves a hot gas reheat of the supply air, turns on when the first stage has been running for 10 minutes. These control logic values are listed in Table A-2 of Appendix A.

The heat pump senses that it is in heating mode when the temperature drops 1.67 ^{0}C below the cooling setpoint, and switches to cooling mode when the temperature rises 1.67 ^{0}C above the heating setpoint. This control logic was programmed in the TRNSYS simulation by creating a new, simple type that reads the zone temperature, heating setpoint, and cooling

setpoint each time step and determines which mode the heat pump is operating in based on this information, the specified deadbands, and the previous time-step's mode.

The heat pump is modeled using two instances of Type 922, a two-speed air-source, split-system heat pump model. One of these instances simulates the heating and cooling modes while the other simulates the dedicated dehumidification mode. These two heat pump models are controlled by multiple stage differential controllers with time delays (Type 974) and equation blocks. The heat pump return and supply air flows to each of the three conditioned floors were determined by summing the total air flow at each of the heat pump air vents on each floor as specified in the as-builts [24].

The rated heating and cooling capacities for second stage heating and cooling mode were set as the rated capacities stated on the AHRI Certificate of Product Ratings [39]. The power, capacity, and sensible capacity at conditions differing from the rated conditions are interpolated using default TRNSYS performance maps. The rated conditions specified by AHRI standards [40] and used in the TRNSYS performance maps for heating performance are at an outdoor dry-bulb temperature of 8.33 ^{0}C and an indoor dry-bulb temperature of 21.1 ^{0}C. The rated conditions for cooling performance are at an outdoor dry-bulb temperature of 35 ^{0}C, indoor dry-bulb temperature of 26.7 ^{0}C, and indoor wet-bulb temperature of 19.4 ^{0}C (50 % RH). The TRNSYS default sensible heat ratio of 0.77 was assumed for the second stage cooling mode. According to the condensing unit's engineering catalog [37], the compressor provides two stages of capacity, 67% and 100%. The rated capacities for first stage heating and cooling were therefore set as 67% of the rated second stage capacities. The sensible heat ratio for the first stage cooling mode was also assumed to be 0.77. The re-

evaporation of condensate on the indoor coil when the unit cycles off was not considered in the model. To find the rated total heat pump power, the HSPF and SEER were converted to second stage heating and cooling mode COPs of 2.65 and 4.63, respectively [41]. For lack of other information, the first and second stage COPs were assumed to be equal for both heating and cooling modes.

The manufacturer's data did not specify the capacity or COP of the dehumidification mode, but it did specify that the first stage dehumidification uses the same fan speed as first stage cooling. The first stage dehumidification was assumed to have the same capacity and power as first stage cooling. According to the manufacturer's data, the second stage dehumidification has a fan speed of 45% of the maximum speed and the air is reheated using hot refrigerant. The dehumidification total cooling capacity and COP before reheat was assumed be equal to the first stage cooling mode capacity and COP. The estimated load introduced to the cooled, dehumidified air by the hot refrigerant during reheat was calculated assuming the return air was at 24 ^{0}C and 52 % relative humidity and assuming that the air was reheated to the cooling setpoint of 23.89 ^{0}C. Under these assumptions, the total cooling capacity after reheat was calculated as 1724 W, the sensible capacity was 24 W, and the power required was 1103 W. Figure 7 shows a simple schematic of the air flow through the heat pump during the dedicated dehumidification mode and labels three points in the flow. Those three points are shown on a psychometric chart in Figure 8.

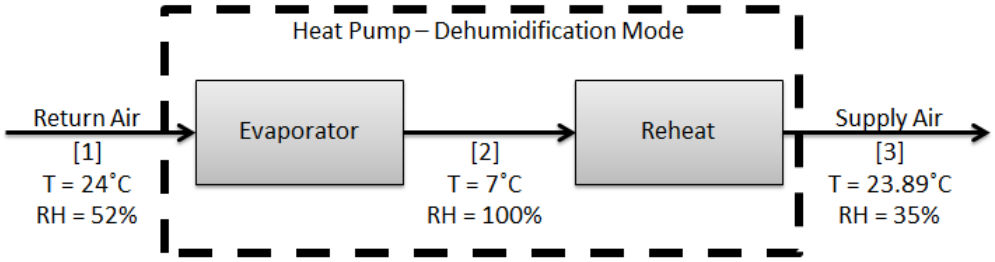

Figure 7. Schematic of Air Flow Through the Air-Source Heat Pump During Dedicated Dehumidification Mode.

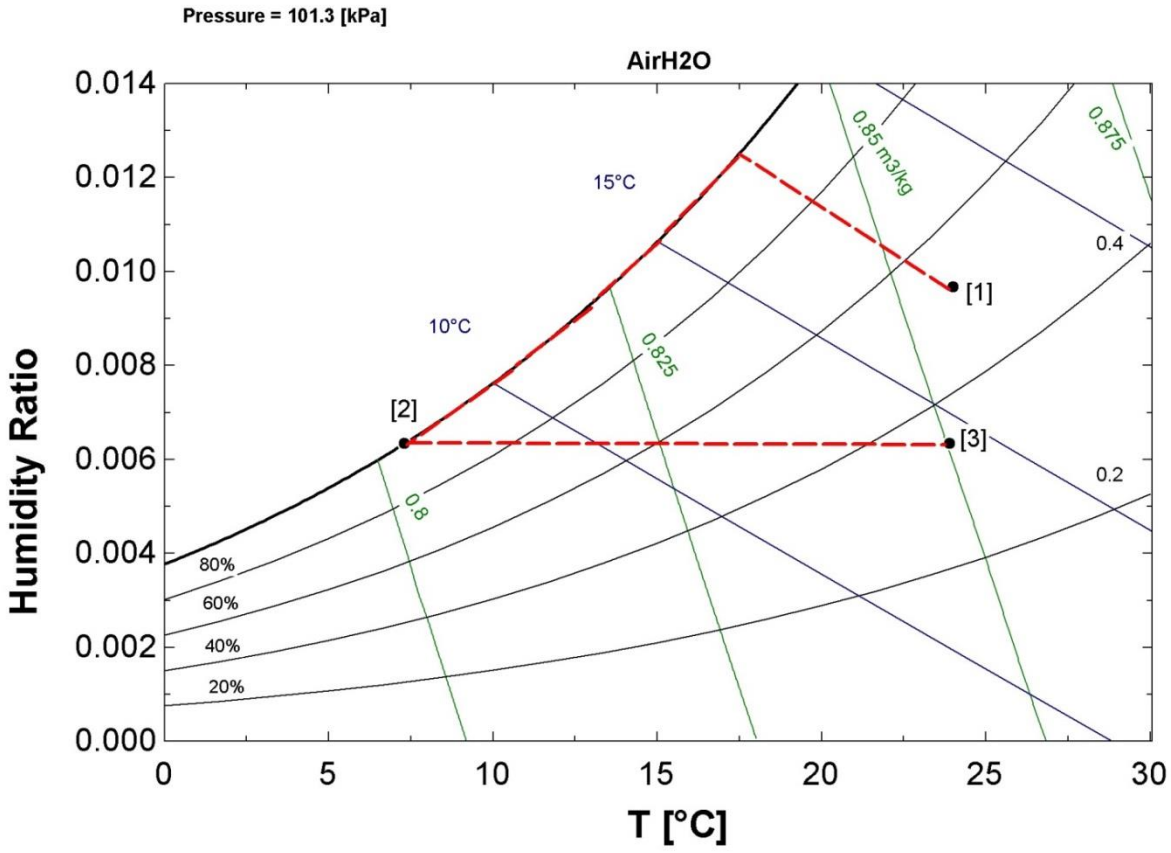

Figure 8. Psychometric Chart Showing Air Properties Corresponding to Points in Figure 7 Schematic.

For lack of data on the air flow rate during first stage operation, the air flow rate was assumed to decrease to 67% of the maximum air flow rate, which was assumed to be the factory preset speed of 800 cfm [37]. The heat pump's indoor and outdoor fan power parameters were assumed to be equal to the fan power measured during the AAON system

balances [42] for second and third stages. All of the parameters for the heat pump models are shown in Table A-4 in Appendix A.

1.3.2 *Domestic Hot Water*

The domestic hot water (DHW) system consists of a solar hot water (SHW) system and a heat pump hot water (HPWH) system. The solar hot water system preheats the water, which is then heated to the setpoint by the heat pump, if necessary, before going to its end use. A schematic of the system is shown in Figure 9.

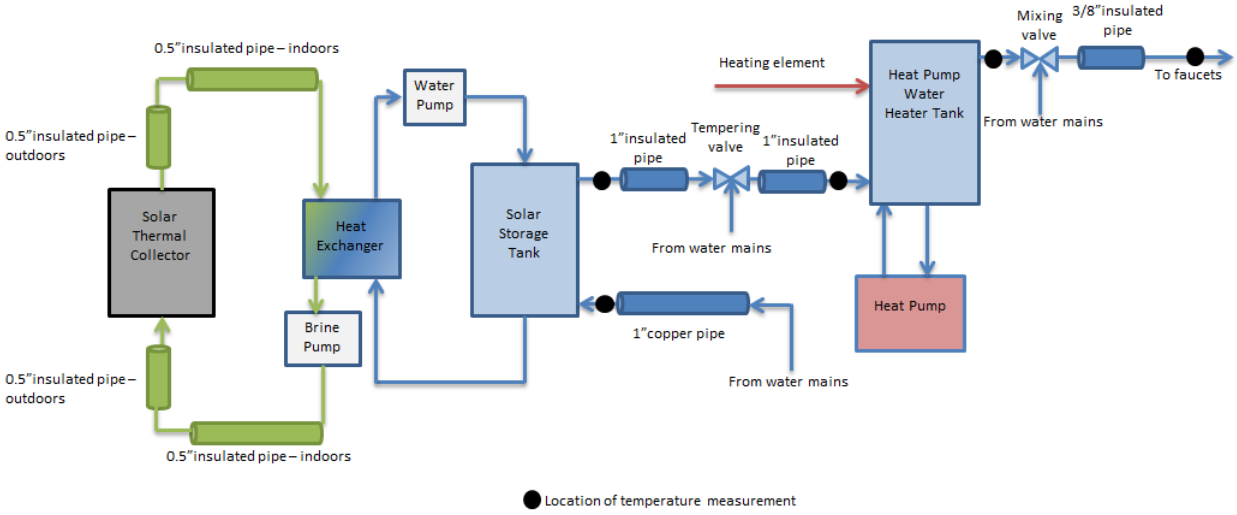

Figure 9. Schematic of the DHW System.

1.3.2.1 Solar Hot Water System

The NZERTF has two separate SHW systems. The system in use during the first year of operation uses a Heliodyne HPAK 303 L (80 gal) storage tank [43], while the system not in use employs a 454 L (120 gal) storage tank. Both systems use two Heliodyne GOBI 406 001 single-glazed, flat plate solar collectors [44] with each collector having an aperture area of 2.1 m^2 facing south at an 18.4 ^{0} tilt. The solar collectors use a 50% by volume propylene

glycol solution. Both systems also use a Heliodyne HPAK cross-flow heat exchanger and two pumps to circulate the fluids through the heat exchanger. The pumps turn on when the temperature difference between the fluid exiting the solar collector and the temperature of the water at the bottom of the storage tank exceeds 10 ^{0}C and turn off when the difference is less than 3 ^{0}C. The pumps also turn off when the temperature at the bottom of the storage tank exceeds 71 ^{0}C. There is a total of 42.7 m (140 ft) of piping wrapped in insulation with an R-value of 0.7 m^2-K/W (4 ft^2-^{0}F/Btu) connecting the heat exchanger to the solar collectors, with 30.5 m (100 ft) of this length indoors and 12.2 m (40 ft) outdoors. The indoor piping to and from the collectors is 1.9 cm (3/4 in) corrugated steel pipe and the outdoor piping is 1.3 cm (1/2 in) copper pipe. Water exits from the top of the tank to enter a thermostatic mixing valve, which tempers the water to 49 ^{0}C before it enters the heat pump water heater tank. The pipe from the tank to the mixing valve is a 0.95 m (3.1 ft) length of 2.5 cm (1 in) copping pipe wrapped in 1.9 cm (3/4 in) polyethylene foam insulation with an R-value of 0.5 m^2-K/W (3 ft^2-^{0}F/Btu). The water entering the house through the basement wall runs through 7.4 m (24.3 ft) of 2.5 cm (1 in) Type L copper tubing before reaching the SHW tank.

TRNSYS component Type 1b was used to model the solar collectors. The efficiency coefficients, the incidence angle modifier coefficients, and the water flow rate at the test conditions were given by the Solar Collector Certification and Rating [45]. Each of the parameters used in Type 1b may be found listed in Table A-5 in Appendix A.

TRNSYS component Type 534, a cylindrical storage tank with immersed heat exchangers, was used to model the solar hot water storage tank. The number of immersed heat exchangers was specified as zero. The tank volume, height, and the location of inlets and outlets were

specified by the manufacturer [43]. The tank was not assumed to be fully mixed; seven nodes were used to model the stratification. The loss coefficients were assumed to be the same as the loss coefficients for the heat pump hot water tank, discussed in the next section.

TRNSYS component Type 91, a heat exchanger with constant effectiveness, was used to model the SHW heat exchanger. A heat exchanger effectiveness of 0.8 was chosen as a reasonable value based on expectations for a high performance solar hot water system. The brine and water pumps were modeled using TRNSYS component Type 114, a single speed pump. The rated flow rate and power were set as the recommended flow rates and the corresponding power given in the manufacturer specifications [43]. Finally, Type 31, a pipe/duct, was used to model the insulated piping to and from the solar collectors as well as the piping carrying the water from the water mains to the SHW tank. The parameters for each of these components can be found in Table A-5 in Appendix A.

1.3.2.2 HPWH System

The HPWH system uses a Hubbell PBX50SL integrated heat pump water heater and tank [46]. After the water from the SHW tank passes through the tempering valve it enters the HPWH tank, where the heat pump heats the water to the set point if necessary. Between the tempering valve and the HPWH tank is a length of 2.5 cm (1 in) copper piping wrapped in 1.9 cm (3/4 in) polyethylene foam insulation with an R-value of 0.5 m^2-K/W (3 ft^2-^{0}F/Btu). The length of this pipe was originally 7.2 m (23.5 ft), but on September 26, 2013, it was shortened to 2.2 m (7.3 ft). In the un-tuned model, this length of pipe is specified as 2.2 m for the entire year. The tank also has two 3,800 W heating elements, although only the upper element is activated in the heat pump heating mode selected to be used during the first year

of NZERTF operation. The heat pump temperature sensor is located near the bottom heating element and a second temperature sensor is located near the upper heating element. The setpoint for the HPWH tank was set as 49 ^{0}C (120 ^{0}F) and according to the manufacturer the deadband is 8.33 ^{0}C. The deadband is assumed to be centered on the setpoint, so the heat pump is activated when the heat pump temperature sensor reads a temperature below the setpoint minus half of the deadband and is deactivated when the temperature sensor reads a temperature above the setpoint plus half of the deadband. According to the manufacturer, if the temperature sensor at the upper heating element reads a temperature 16.8 ^{0}C (30 ^{0}F) below the setpoint, the heat pump turns off and that heating element turns on until that sensor indicates that the temperature has again reached the setpoint. The heat pump then turns on to heat the remainder of the tank. In the NZERTF, after exiting the HPWH tank, the water flows through a manifold distribution system in the basement through which it is directed to the correct faucet, showerhead, or appliance. The water flows from the manifold to the end use through 1 cm (3/8 in) cross-linked polyethylene tubing. The insulation around the tubing is assumed to have the same R-value as the insulation on the pipe between the SHW and HPWH tanks. This manifold distribution system is simplified and modeled in TRNSYS as two pipes. The water exiting the HPWH tank in TRNSYS is directed through one of the pipes, depending on which floor the water is being drawn from. The length of each of these two pipes is the average of the lengths of piping from the manifold to the end uses on each floor, weighted by the volume of water drawn through each length of pipe.

The pipe between the SHW tempering valve and the HPWH tank was modeled the same way that the pipe between the SHW tank and the tempering valve was modeled, using Type 31.

The two pipes leading from the HPWH tanks were also modeled using Type 31. The losses from these two pipes modeled as gains to Zone 2. To model the HPWH integrated heat pump and tank, Type 534, Type 938, and Type 1226 were used. Type 938, a heat pump water heater, was connected to Type 534, a cylindrical storage tank with an immersed heat exchanger. The heat pump water heater, like the air to air heat pump, uses normalized performance data maps to interpolate the performance of the heat pump at conditions differing from the rated conditions. TRNSYS default performance maps were used with rated conditions at 43.5 ^{0}C water temperature, 21.1 ^{0}C dry-bulb temperature, and 50 % RH for the ambient air. The rated heat pump capacity, power, and air flow rate were given by the manufacturer specifications [46]. In addition to modeling the water heating rate, this type also models the heat pump's effect on the ambient air. From the manufacturer specified heat pump capacity and power, the air cooling capacity was predicted. The sensible heat ratio of the air was assumed to be 0.95, which is similar to the sensible heat ratio for similar integrated heat pump water heaters [47]. Additional information from the manufacturer specified the fan power and the standby power. The heating capacity of the heating element was listed in the manufacturer specifications as 3800 W [46]. The thermal efficiency of the heating element is 1.0. The flow rate of the water through the heat pump was not measured by the manufacturer, so a value of 454 kg/hr (2 gpm) was chosen as the flow rate between the Type 938 heat pump and the Type 534 tank. Two Type 2 aquastats were used to control the heat pump and the heating element. After exiting the HPWH tank, the hot water enters a tempering valve in TRNSYS, where it is tempered to the temperature required based on its end use. Sinks and showers require a temperature of 41 ^{0}C, baths require a temperature of 43 ^{0}C, and the dishwasher and clothes washer require a temperature of 49 ^{0}C.

The HPWH tank height, volume, and the inlet and outlet positions are specified by the manufacturer [46]. Because the heat pump water heater's supply water is preheated by the SHW system and because the heat pump both draws and discharges at a position near the bottom of the tank, the heat pump water heater tank was assumed to have little stratification. For this reason, only five nodes were used when modeling the tank. The tank's skin loss coefficient was estimated using the standby heat loss of the tank specified by the manufacturer. The standby heat loss was used to calculate the energy loss rate, Q.

$$Q = V\rho c(\Delta T) \quad \textbf{(8)}$$

where Q is the energy loss rate, V is the volume of the tank, ρ is the density of water, c is the specific heat of water, and ΔT is the standby heat loss specified by the manufacturer (0.2 ^{0}C/hr).

The standby heat loss was then used to calculate the uniform skin loss coefficient.

$$USL = \frac{Q}{A_{surface}(T_{tank} - T_{ambient})} \quad \textbf{(9)}$$

where USL is the uniform skin loss coefficient, $A_{surface}$ is the surface area of the tank, T_{tank} is the temperature of the water in the tank, and $T_{ambient}$ is the temperature of the ambient air. T_{tank} and $T_{ambient}$ are specified as 57.2 ^{0}C (135 ^{0}F) and 19.7 ^{0}C (67.5 ^{0}F), respectively, by the test method for measuring the energy consumption of water heaters [48]. The calculated uniform skin loss coefficient was 0.59 W/m^2-K. All parameter values for each of the HPWH types discussed may be found in Table A-6 in Appendix A.

1.3.3 *Photovoltaic System*

The NZERTF uses thirty-two 320 W positively-grounded SunPower E19 photovoltaic (PV) modules with maximum power point tracking [49]. These modules are mounted approximately 14 cm above the surface of the roof, facing south at an angle of 18.4 ^{0}, and are arranged in four rows of eight. The maximum power of the modules at standard test conditions is 10.24 kW [49]. Two SunPower inverters with an efficiency of 95.5 % are used to convert the direct current from the PV modules to 60 Hz alternating current [50].

The PV system is modeled using two instances of Type 194b, a photovoltaic array and inverter model. This type is based on the 5-Parameter model presented by De Soto [51]. These five parameters were calculated using PV Reference Parameter Determination, an Engineering Equation Solver (EES) program developed for this purpose [52]. A tau-alpha product for normal incidence of 0.95 was assumed and the TRNSYS extinction coefficient-thickness product of the cover default was used. The other parameters required by this type were given by the manufacturing specifications. These parameters are found in Table A-7 in Appendix A.

Snow covered at least part of the photovoltaic array on 39 days during the first year of NZERTF operation, limiting the array's energy production. The snow cover is partially accounted for in the TRNYS model because the solar irradiation measured at the NZERTF is used in the TRNSYS model. On days of snow accumulation, less solar irradiation was recorded because the pyranometer was also covered with snow. However, the snow tended to melt off of the pyranometer before the rest of the PV array was uncovered, so on days

following heavy snowfall the pyranometer often recorded solar irradiation while the PV array remained covered in snow.

1.4 Un-tuned Subsystem Results

The un-tuned NZERTF model was simulated for a period of 13 months with a one minute time step. The first month was used for pre-conditioning and was not included in the analyzed results. The TRNSYS-predicted results are discussed in this section and compared to the measured data.

1.4.1 *Overall Heat Transfer Coefficient of the House*

After the building envelope and HVAC subsystem were modeled, the overall heat transfer coefficient (*UA*) of the house (also known as the overall conductance) was compared to the measured *UA*. The total thermal energy provided by the HVAC system each day was plotted against the difference between the outdoor and indoor temperature. Note that this is not a strict definition of *UA* since the HVAC load is not exclusively related to heat transfer through the envelope. The *UA* calculated here is also affected by air exchange through the HRV, occupant and plug loads, and solar heat gains. The slope of this line is the *UA* of the house. Figure 10 shows both the measured data and the TRNSYS results. Overall, the measured *UA* and TRNSYS *UA* agree fairly well.

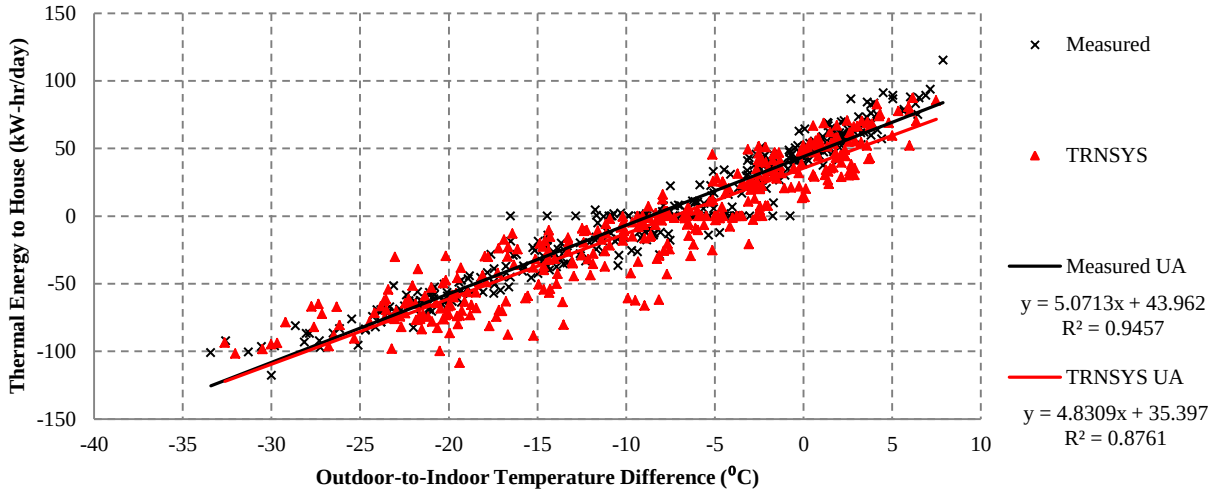

Figure 10. Measured vs. TRNSYS Overall Heat Transfer Coefficient

1.4.1 *HVAC System Results*

1.4.1.1 Heat Recovery Ventilation Results

The HRV affects the heat pump operation because it introduces both sensible and latent loads that must be met by the heat pump. Figure 11 shows the TRNSYS latent and sensible loads compared to the measured loads. The sensible loads agree well in the summer and in the winter are under-predicted by TRNSYS by about 35 %. The latent loads agree well.

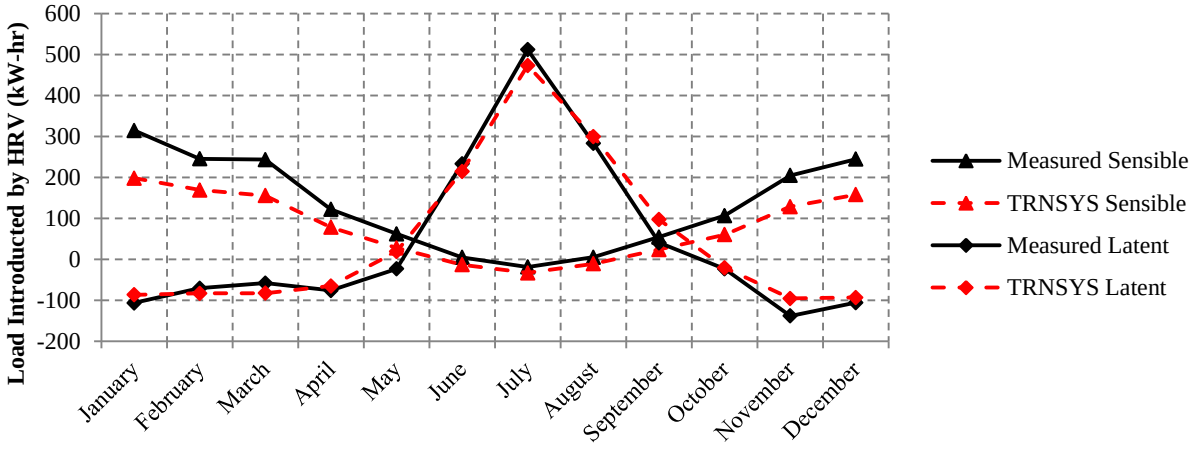

Figure 11. Measured vs. TRNSYS Loads Introduced by HRV.

Although the measured and TRNSYS loads appear to agree well, TRNSYS supplied less ventilation to the house than was measured. The TRNSYS average flow rate was less than the measured average flow rate by 12%. An increase in the flow rate would cause an increase in the loads, so after the TRNSYS flow rate is tuned the loads are expected to increase. Also, the annual energy consumption of the HRV was under-predicted by 31% and the average effectiveness was over-predicted by 4%. The TRNSYS and measured annual energy consumption, average effectiveness, and average flow rate are listed in Table 7.

Table 7. HRV Performance Data

	Energy Consumption (kW-hr)	Effectiveness	Average Flow Rate (m^3/hr)
Measured	514.4	0.72	195.1
TRNSYS	354.6	0.75	171.0
Percent Error	-31 %	4 %	-12 %

1.4.1.2 Air Source Heat Pump Results

Next, the monthly integrated average thermal loads met by the air source heat pump were compared. Figure 12 shows this comparison, and the values of the monthly integrated thermal energy are found in Table B-1 in Appendix B. TRNSYS over-predicts the heating load by 11% and under-predicts the cooling load by 15% when compared to the measured values. This discrepancy may be caused by a number of various factors, including measurement error and to differences in modeled and actual thermostat control logic, infiltration, *UA* of the building, air flow rates within the house, and the loads introduced by the devices, equipment, water draws, and occupants.

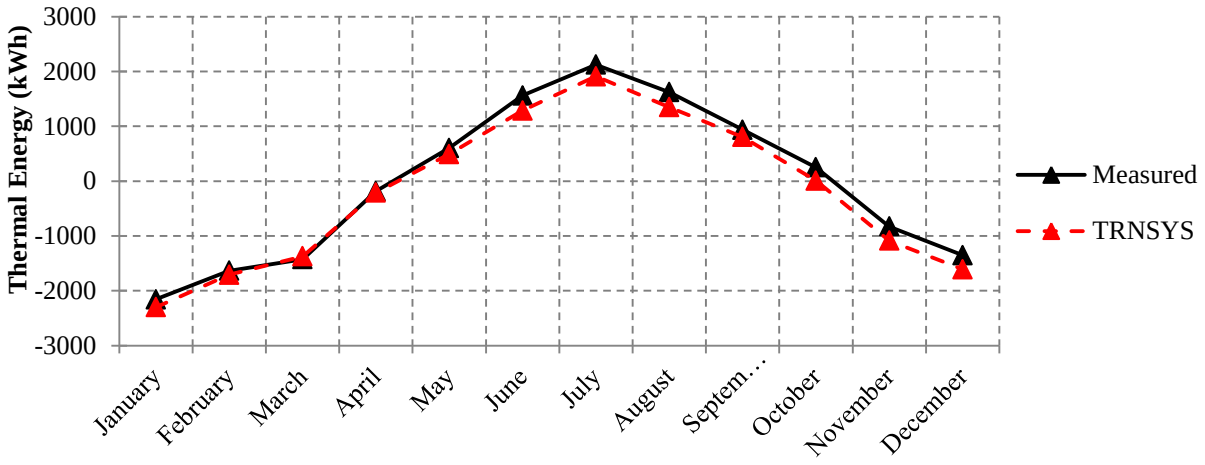

Figure 12. Measured vs. TRNSYS Thermal Energy.

The electrical energy required to operate the air source heat pump depends on the thermal load as well as the stage in which the heat pump is operating and the performance of the heat pump at that stage. During the heating season, the third stage resistive heating has a much lower COP than the first or second stage COPs. During the cooling season, the supply air is reheated while in second stage dehumidification mode, causing this stage to have a much lower COP than first stage dehumidification mode and the cooling modes.

Figure 13 shows the heat pump electrical energy required in TRNSYS compared to the measured heat pump electrical energy consumed by the NZERTF. TRNSYS under-predicts the total energy required in the cooling season by 34%. The TRNSYS-predicted total energy required in the heating season matches the measured value closely; TRNSYS under-predicts the energy consumption by 4 %. However, TRNSYS over-predicts the energy used by the first and second stages of heating by 15% and does not predict the 423 kWh of energy used by the heat pump for defrost cycles. These two discrepancies canceled out, resulting in a prediction of total heating season electrical energy that nearly matches the measurements.

Figure 14 compares the measured and predicted energy used by different heat pump stages and functions. The monthly total energy consumption for each stage is listed in Table B-2 in Appendix B. When comparing the TRNSYS and measured electrical data, a number of causes for the discrepancy in electrical energies were found. These causes for error and the strategies used to improve the fidelity of the model are discussed in Section 2.1.

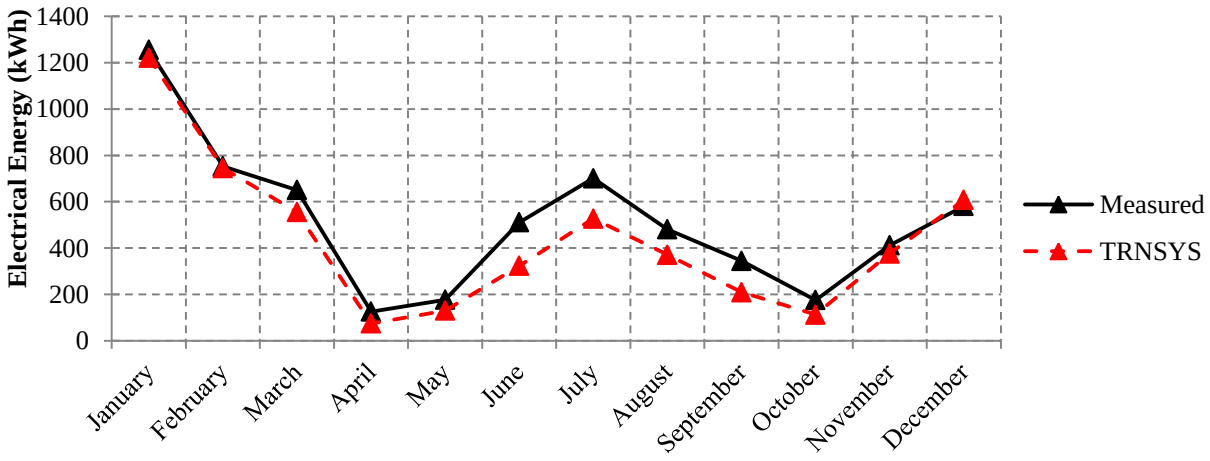

Figure 13. Measured vs. TRNSYS Heat Pump Electrical Energy.

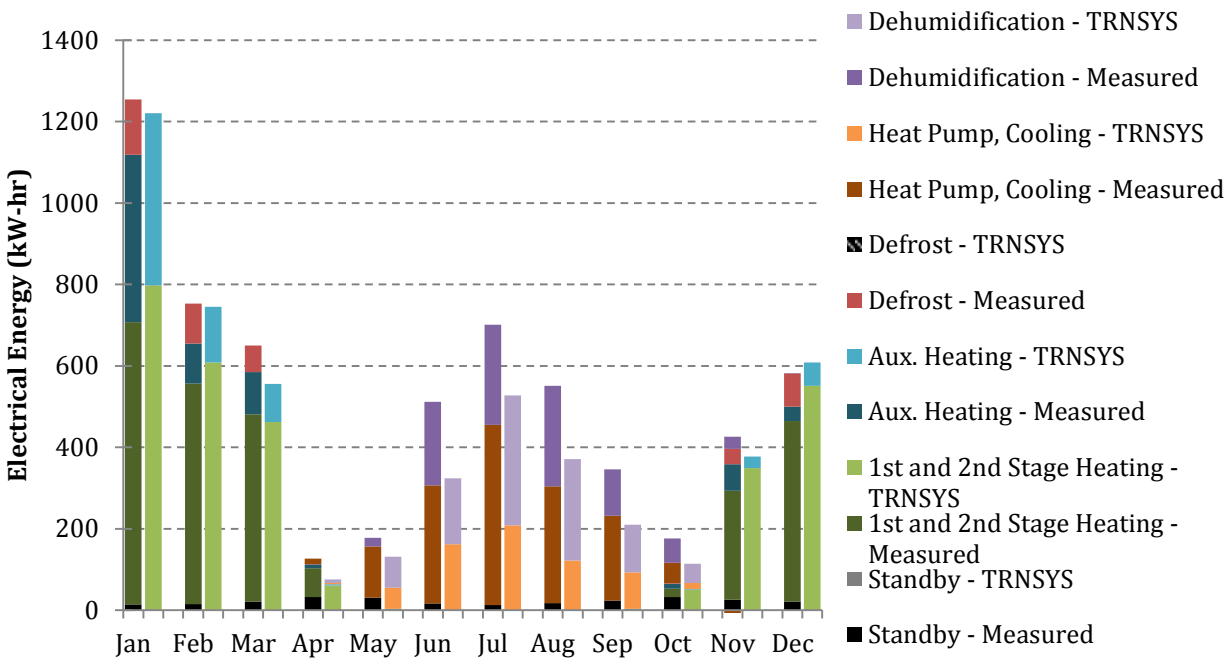

Figure 14. Measured vs. TRNSYS Monthly Electrical Energy.

1.4.2 *DHW System Results*

1.4.2.1 SHW Results

The temperature of the water entering the SHW tank, exiting the SHW tank, and exiting the tempering valve are recorded in the NZERTF every 3 s, and the monthly average temperatures are calculated for the periods the water is flowing. A comparison of these measured temperature and the TRNSYS predicted monthly integrated average temperatures for periods when the water is flowing are shown below in Figure 15 and in Table B-5 of Appendix B.

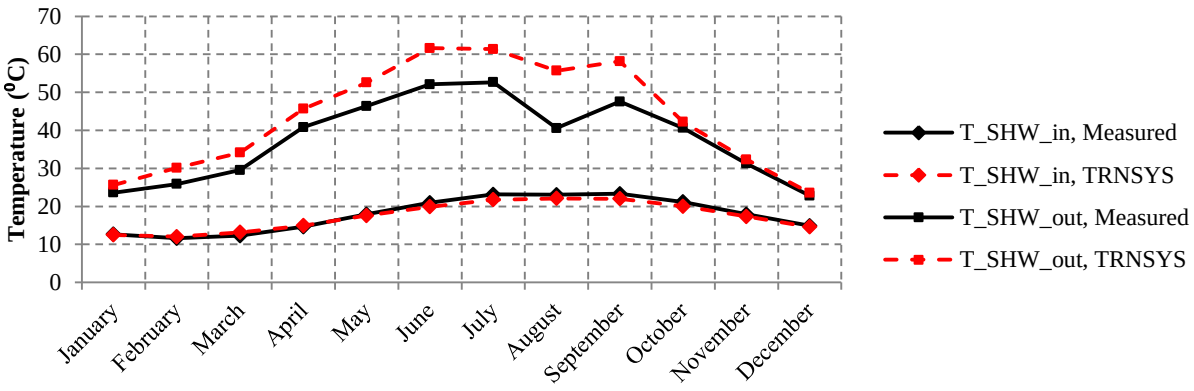

Figure 15. Measured vs. TRNSYS SHW Temperatures.

The water entering the SHW tank in TRNSYS is approximately equal to the measured temperature of the water entering the SHW tank. Measured water mains temperatures were used as an input to the model and the model accurately predicted the heat gained by the water in the piping from the water mains to the SHW tank. TRNSYS over-predicts the performance of the SHW system, as can be seen by the higher TRNSYS-predicted water temperature leaving the SHW system than the measured leaving water temperature. The dip in the temperature of the water exiting the SHW tank occurring in August was caused by the SHW system pumps not being operational from August 24, 2013 through September 3, 2013 which resulted in the water in the solar tank not being heated by the solar collectors before it is drawn into the HPWH tank. Also, from July 1 through September 26, 2013, the length of pipe between the tempering valve and the HPWH tank was 7.2 m and the tempering valve did not operate. After September 26, the length of pipe was shortened to 2.2 m and the tempering valve controlled the entering water temperature to the setpoint. The energy delivered by the SHW system is calculated according to the following equation:

$$Q_{del,SHW} = \int \dot{m}_{SHW}\, c(T_{SHW,out} - T_{SHW,in}) \qquad \textbf{(10)}$$

where $Q_{del,SHW}$ is the energy delivered by the SHW system, $\dot{m}_{SHW}$ is the mass flow rate of the water leaving the SHW system, c is the specific heat of water, $T_{SHW,out}$ is the temperature of the water leaving the SHW tank, and $T_{SHW,in}$ is the temperature of the water entering the SHW tank. Table 8 compares the TRNSYS-predicted to the measured $Q_{del,SHW}$ as well as the electrical energy consumed by the SHW pumps.

Table 8. SHW Performance.

Month	Measured $Q_{del,SHW}$ [kWh]	TRNSYS $Q_{del,SHW}$ [kWh]	*Percent Difference [%]*	Measured SHW Pump Energy Consumption [kWh]	TRNSYS SHW Pump Energy Consumption [kWh]	*Percent Difference [%]*	Measured SHW Water Delivered [L]	TRNSYS SHW Water Delivered [L]	*Percent Difference [%]*
Jan-14	102	121	*19 %*	20.4	12.5	*-39 %*	7722	7368	*-5 %*
Feb-14	124	150	*21 %*	19.8	13.9	*-30 %*	7113	6694	*-6 %*
Mar-14	158	186	*18 %*	22.6	16.8	*-25 %*	7430	7318	*-2 %*
Apr-14	227	247	*9 %*	29	20.7	*-29 %*	7118	6835	*-4 %*
May-14	237	263	*11 %*	34.3	25.1	*-27 %*	7169	6533	*-9 %*
Jun-14	239	250	*4 %*	34.8	25.0	*-28 %*	6634	5318	*-20 %*
Jul-13	239	231	*-3 %*	35.7	23.8	*-33 %*	6710	5281	*-21 %*
Aug-13	131	217	*65 %*	27.1	22.8	*-16 %*	6833	5815	*-15 %*
Sep-13	204	218	*7 %*	31.4	21.8	*-31 %*	7794	5375	*-31 %*
Oct-13	173	173	*0 %*	24.2	16.9	*-30 %*	8140	6702	*-18 %*
Nov-13	117	118	*1 %*	22	13.3	*-39 %*	7637	6636	*-13 %*
Dec-13	78	82	*5 %*	18.2	10.0	*-45 %*	7790	7231	*-7 %*
Total	**2029**	**2254**	***11%***	**319.5**	**222.8**	***-30%***	**88089**	**77106**	***-12%***

The water exiting the SHW system is predicted to be warmer than the measured temperature. A number of potential reasons for this discrepancy. Likely causes include the assumed heat exchanger effectiveness being too large or the SHW tank's assumed skin loss coefficient being too low. As mentioned in Section 1.3.2.1, both of these parameters were not specified by the manufacturer and were chosen by engineering judgement. The higher predicted difference between entering and exiting water temperature lead to 11 % over-prediction in

the total energy delivered by the system. The water in the tank being warmer also does not allow the SHW circulation pumps to be triggered as often, lending to the 30 % under-prediction in annual pump energy consumption. Finally, the over-prediction of the exiting water temperature means that during the summer months, when the temperature is over 49 ^{0}C, more water from the water mains must be used to temper the exiting water, so the total volume of water delivered by the SHW system is under-predicted by 12 %.

1.4.2.2 Heat Pump Hot Water Results

Like the water temperatures in the SHW system, the temperature of the water entering the HPWH tank, exiting the HPWH tank, and exiting the tempering valve are recorded in the NZERTF every 3 s, and monthly average temperatures are calculated for the periods the water is flowing. A comparison of these measured temperatures and the TRNSYS predicted monthly integrated average temperatures for when the water is flowing are shown below in Figure 16 and in Table B-6 of Appendix B.

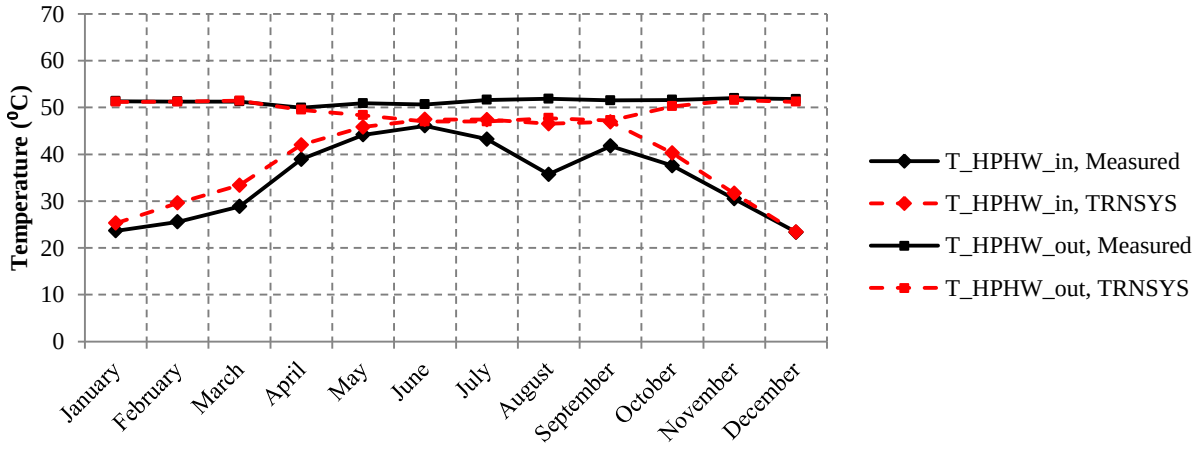

Figure 16. Measured vs. TRNSYS HPWH Temperatures.

The discrepancy between the temperatures of the water entering the SHW tank is largely caused by the TRNSYS-predicted temperature of the water exiting the SHW system being warmer than the measured temperature of the water exiting the SHW system. The measured and TRNSYS-predicted temperature exiting the HPWH tank agree well, especially during the winter months when the heat pump operates more frequently. During the summer months, the HPWH is predicted to operate much less frequently than measured, allowing the temperature of the water in the tank to drop to the lower end of the deadband range. A likely cause for this is the predicted entering water temperatures are higher, so the heat pump control is not triggered.

Similar to the energy delivered by the SHW system, the energy delivered by the HPWH system is calculated according to the following equation:

$$Q_{del,HPHW} = \int \dot{m}_{HPHW} c (T_{HPWH,out} - T_{HPWH,in}) \quad \textbf{(11)}$$

where $Q_{del,HPHW}$ is the energy delivered by the HPWH system, $\dot{m}_{HPHW}$ is the mass flow rate of the water leaving the HPWH system, $T_{HPHW,out}$ is the temperature of the water leaving the HPWH tank, and $T_{HPHW,in}$ is the temperature of the water entering the SHW tank. Table 9 compares the TRNSYS to the measured $Q_{del,HPHW}$ as well as the electrical energy consumed by the heat pump.

Table 9. HPWH Performance.

Month	Measured $Q_{del,HPHW}$ [kWh]	TRNSYS $Q_{del,HPHW}$ [kWh]	*Percent Difference [%]*	Measured Total Energy Used by HPWH [kWh]	TRNSYS Total Energy Used by HPWH [kWh]	*Percent Difference [%]*	Measured HPWH Heating Element [kWh]	TRNSYS HPWH Heating Element [kWh]	*Percent Difference [%]*
Jan-14	240.2	220.1	*-8 %*	142.8	111.6	*-22 %*	13.9	0.0	*-100%*
Feb-14	207.7	165.0	*-21 %*	125	86.0	*-31 %*	14.2	0.0	*-100%*
Mar-14	187.3	149.4	*-20 %*	120.7	81.4	*-33 %*	12.8	0.0	*-100%*
Apr-14	84.4	54.4	*-36 %*	72.7	35.3	*-52 %*	3.3	0.0	*-100%*
May-14	54.7	16.1	*-71 %*	55.2	18.0	*-67 %*	0.6	0.0	*-100%*
Jun-14	35.3	-8.1	*-123 %*	46.1	5.5	*-88 %*	0.0	0.0	*0%*
Jul-13	42.1	-8.3	*-120 %*	53.3	5.9	*-89 %*	0.0	0.0	*0%*
Aug-13	107.9	3.8	*-97 %*	70.8	11.7	*-83 %*	5.8	0.0	*-100%*
Sep-13	68.3	-3.3	*-105 %*	57	8.4	*-85 %*	3.2	0.0	*-100%*
Oct-13	118.7	73.8	*-38 %*	82.5	44.1	*-47 %*	3.2	0.0	*-100%*
Nov-13	172	151.1	*-12 %*	129.8	80.7	*-38 %*	44.3	0.0	*-100%*
Dec-13	244	232.0	*-5 %*	156.3	115.3	*-26 %*	36.1	0.0	*-100%*
Total	**1562.6**	**1045.9**	***-33%***	**1112.2**	**603.8**	***-46%***	**137.4**	**0.0**	***-100%***

TRNSYS under-predicts the amount of energy supplied by the HPWH system by 33 %. This occurs because TRNSYS over-predicts the temperature of the water exiting the SHW system throughout the year and under-predicts the temperature of the water exiting the HPWH tank during the summer months. The electrical consumption predicted by TRNSYS is 46 % less than the measured electrical consumption. This can largely be attributed to the under-prediction of the thermal load. Another contributing factor to this discrepancy is the lack of resistance heat predicted by TRNSYS. The HPWH heating element was used in the NZERTF every month except for June 2014 and July 2013, but the node in which the heating element is located never reaches a temperature low enough to trigger the heating element in TRNSYS. Note that from November 25, 2013 through December 5, 2013, the heat pump was not operational, so during that time period only the heating element was used to heat the

water in the HPWH system. It is for this reason that the measured heating element energy is greatest in November and December.

The energy delivered by the entire DHW system is calculated in the same manner as the SHW and HPWH loads, but uses the SHW inlet temperature and the HPWH outlet temperatures.

$$Q_{load} = \int \dot{m}_{HPHW} c (T_{HPWH,out} - T_{SHW,in}) \quad \textbf{(12)}$$

where Q_{load} is the total energy provided by the SHW and HPWH systems. Table 10 compares TRNSYS and measured total energy and water volume delivered by the DHW system each month.

Table 10. Energy Delivered by DHW System.

Month	Measured Total Hot Water Load Q_{load} [kWh]	TRNSYS Total Hot Water Load Q_{load} [kWh]	Percent Difference [%]	Measured Total Hot Water Delivered [L]	TRNSYS Total Hot Water Delivered [L]	Percent Difference [%]
Jan-14	343.1	319.9	-7%	7738	7368	-5%
Feb-14	330	312.2	-5%	7113	6694	-6%
Mar-14	340.5	331.9	-3%	7430	7320	-1%
Apr-14	300.3	296.1	-1%	7118	7282	2%
May-14	276.9	272.4	-2%	7169	7513	5%
Jun-14	250.6	234.5	-6%	7215	7367	2%
Jul-13	252.4	215.9	-14%	6710*	7357	10%
Aug-13	217.8	213.6	-2%	6833*	7226	6%
Sep-13	238.2	207.6	-13%	7872	7140	-9%
Oct-13	268.5	241.3	-10%	8180	6899	-16%
Nov-13	283.2	265.7	-6%	7663	6635	-13%
Dec-13	325.9	312.7	-4%	7790	7231	-7%
Total	**3427.4**	**3223.8**	**-6%**	**75287**	**71451**	**-5%**

*Missing data 7/1-7/2 and 8/2-8/6 inclusive. These months are not included in total.

Both the total volume of hot water delivered and the total annual energy delivered by the TRNSYS DHW system match the measured data fairly closely. The annual energy delivered by the TRNSYS DHW system is 6 % less than the measured annual energy delivered. The total volume of hot water delivered by the HPWH from September 2013 through Jun 2014 is under-predicted by 5%. Note that water volume data was missing for seven days, so these months are not included in the totals. This delivered hot water then travels through pipes to either the first or second floor, where it is mixed with cold water to reach its setpoint before arriving at its end use. Note that there are days of missing water volume data in July and August 2013. Because of this these months are not included in the total compared water volume.

1.4.3 *Photovoltaic System Results*

Of all of the systems in the un-tuned model, the PV system's predicted results matched most closely with the measured data. Figure 17 compares the TRNSYS AC energy generated by the PV system to the measured AC energy generated. Also shown in Figure 17 for reference is the total solar insolation measured at the NZERTF each month.

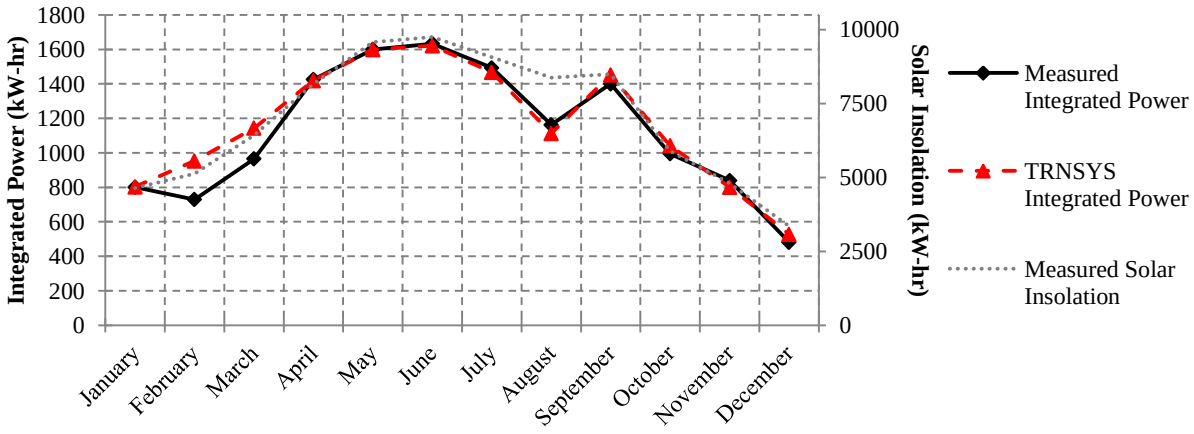

Figure 17. Measured vs. TRNSYS PV Power and Solar Insolation

Overall, the TRNSYS annual PV energy generated agrees well with the measured PV energy generated. The percent error between the TRNSYS and measured annual totals is only 3.1 %, and the average absolute value of the percent error in the monthly totals is 6.6 %. These monthly and annual totals are found in Table 11. The largest percent errors occur in February, March, and December, which are also the months with the greatest number of days during which snow covered at least part of the PV array.

Table 11. PV Performance.

Month	Measured Solar Power (kW-hr)	TRNSYS Solar Power (kW-hr)	Percent Error (%)
Jan-14	801	802	0.1%
Feb-14	729	953	30.7%
Mar-14	965	1143	18.5%
Apr-14	1425	1418	-0.5%
May-14	1600	1599	-0.1%
Jun-14	1633	1621	-0.8%
Jul-13	1493	1467	-1.7%
Aug-13	1162	1112	-4.3%
Sep-13	1400	1452	3.7%
Oct-13	994	1041	4.7%
Nov-13	839	801	-4.6%
Dec-13	481	528	9.7%
Total	13523	13937	3.1%

1.5 Overall Un-tuned Model Results and Discussion

One of the purposes of the NZERTF is to prove that it is possible to achieve net-zero energy operation with a home that is similar to a typical Maryland house. This goal was achieved; during the first year of operation the NZERTF produced 484 kW-hr more than it consumed. The un-tuned TRNSYS model predicted an annual energy consumption of 13.8 % less than

measured. As discussed in Section 1.4.3, TRNSYS predicted an annual PV generation 3.1 % more than measured. This resulted in 2697 kW-hr of surplus energy.

Table 12 shows the predicted and measured annual electrical energy generation and consumption as well as the annual consumption for each subsystem. Note that the electrical consumption of each individual subsystem was measured by meters separate from the total energy consumption meter, so the sum of the energy consumed by each of the subsystems does not exactly equal the value stated as the total consumed electrical energy. An uncertainty analysis was performed on the energy consumed and generated on a day with high electrical usage, January 4, 2014. This analysis showed that the uncertainty in the PV generation was 1.0 % and the uncertainty in the total energy consumed was 1.1 % [41].

Table 12. Measured and Predicted Annual Electrical Energy Generation and Consumption.

	Measured (kW-hr)	**TRNSYS - Un-tuned (kW-hr)**	***Percent Difference***
Lighting	435	442	*1.4 %*
Plug Loads	2440	2462	*0.9 %*
Appliances	1867	1898	*1.6 %*
Air Source Heat Pump	6241	5258	*-15.7 %*
HRV	514	355	*-31.1 %*
DHW	1432	827	*-42.3 %*
Total Consumed	13039	11241	*-13.8 %*
PV	13523	13937	*3.1 %*
Net Generation	484	2697	

The un-tuned model's total electrical consumption and generation prediction is reasonably close to the measured value. The predicted energy consumption of the lighting, plug loads, and appliances match the measured energy consumption very well, as they should because the power for each of these were directly input to the model and their operation in the

NZERTF was carefully controlled according to a weekly schedule However, when individual subsystems are compared, the model does not agree with the measured data as well. This discrepancy may be caused by some of the assumptions made when modeling being incorrect or the equipment not performing as the manufacturer's specifications predict. To create a more accurate model, the model described in this chapter was tuned using data collected at the NZERTF during the first year of operation. Chapter 2 will discuss the tuning process and the results predicted by the tuned model.

Chapter 2: Tuning the NZERTF Model

The un-tuned model predicted a total energy consumption 13.8 % less than the measured energy consumption. This discrepancy was caused by a number of factors, which will be discussed in this chapter. Each of the subsystems of the NZERTF are carefully monitored and measured, as described in Davis et al [41]. Using this data, the model described in Chapter 1 was tuned. The tuning process and the results of the simulation using the tuned model are discussed in this chapter.

2.1 Tuning the HVAC Subsystem

The error between the TRNSYS-predicted and the measured HVAC electrical energy consumption was caused by a number of factors, which include inaccurate thermal capacitance of the house, no heat pump defrost cycle modeled, incorrect heat pump capacity and power information as a function of operating conditions, the thermostat in the NZERTF deviating from its expected behavior, and an incorrect flow rate and sensible effectiveness for the HRV. All of these factors were addressed in the tuned model, leading to a more accurate model with less discrepancy between the measured and TRNSYS data.

2.1.1 *Interior Thermal Capacitance*

The capacitance of the floors, roof, and external walls are fixed by the properties library in TRNBuild, which was used when specifying the materials used in the construction of the NZERTF. However, the capacitance of the internal furnishings and the internal structural mass is a required parameter for each zone. This capacitance was estimated for the un-tuned model using ASHRAE standard 90.2 [27], as discussed in Section 1.1.4. Due to the control strategy used for the heat pump, which included time-out limits, adjusting this capacitance

can have a significant effect on the HVAC system's electrical usage. If the capacitance is large, the time constant of the house is increased and more time will be required for the heat pump to bring the temperature of the house to the setpoint. Because the second and third stages of conditioning are triggered after a specified amount of operating time, these higher stages may be triggered more often as the capacitance of the house increases. The third stage of heating, which uses an electric resistance heater, has a COP of 1, so the heat pump may become less energy efficient as the capacitance of the house increases and the third stage of heating is triggered more often. To tune the capacitance of the house, temperature data at 1 minute intervals were analyzed for two different periods of time when the heat pump was not running. These periods of time were selected to be during the night so that solar radiation would not affect the building temperature and were 6 to 7 hours long. The TRNSYS simulation was run for approximately the same length of time, on the same day of the week, and at the same time of day. The measured outdoor dry-bulb temperatures for that time period were used in the TRNSYS simulation and the TRNSYS heat pump was turned off. The un-tuned TRNSYS model's predicted Zone 2 temperature was then compared to the measured living room temperature over time and was found to drop more quickly than measurements. The internal capacitance of conditioned living area was subsequently increased until the TRNSYS-predicted rate of change in temperature closely matched the measured rate of change in temperature. Figure 18 shows the measured, un-tuned model, and tuned model temperature over time.

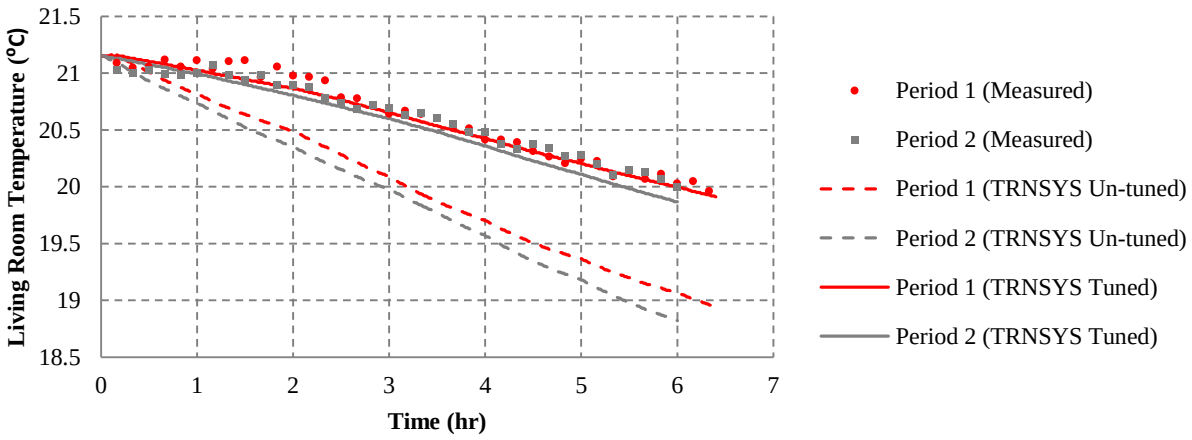

Figure 18. Living Room Temperature with Heat Pump Off.

The adjusted capacitance of the house is shown in Table 13. Also shown are the capacitance of the house according ASHRAE Standard 90.2 if there are no internal furnishings and the capacitance of the house according ASHRAE Standard 90.2 if the house was fully furnished. Although the NZERTF is not furnished, the tuned interior thermal capacitance approaches the total interior thermal capacitance as estimated using ASHRAE 90.2 [27].

Table 13. Thermal Capacitance

	Un-tuned Interior Thermal Capacitance [kJ/K]	Tuned Interior Thermal Capacitance [kJ/K]	Fully Furnished Interior Thermal Capacitance [kJ/K]
Zone 1	4299	11951	13357
Zone 2	4317	12000	13375
Zone 3	3467	9638	10739
Zone 4	147	147	10452

2.1.2 *HRV Performance*

In the un-tuned model, the air flow rate was under-predicted, and the fan energy consumption was also under-predicted, and the HRV effectiveness was over predicted. The average air flow rate through the HRV over the course of the year was measured to be 195 m^3/hr, the

average power consumption was measured to be 59 W, and the average sensible effectiveness was measured to be 0.72. These TRNSYS parameters were adjusted to reflect these measured values and the power and sensible effectiveness versus mass flow rate curves were adjusted accordingly. Furthermore, the defrost cycle control settings were adjusted to reflect the observed behavior. Instead of being triggered at an outdoor air temperature of -5 ^{0}C, as specified in the manufacturer's specifications [35], it is triggered at a temperature of -10 ^{0}C. It then runs in recirculation mode for 7 minutes, then cycles on again for 22 minutes before sampling the air temperature again and repeating the cycle if the temperature is still below -10^{0}C. These updated parameters can be found in Table A-9 in Appendix A.

2.1.3 *Heat Pump Defrost Cycle*

One aspect of the heat pump operation that is neglected by the Type 922 TRNSYS model is the defrost cycle. During normal operation frost can build up on the outdoor coil, reducing the heat pump's capacity. To melt the frost from the coil, the AAON, Inc. heat pump operates in reverse and reheats the air entering the house with an electric resistance heater. This defrost cycle is activated after 90 minutes of accumulated compressor runtime if the outdoor temperature is below 1.7 ^{0}C (35 ^{0}F). To model the defrost cycle, the heat pump's measured electrical energy during defrost time periods was linearly correlated to the outdoor dry bulb temperature. Figure 19 shows the measured electrical energy per defrost cycle as a function of outdoor temperature. This correlation was used in TRNSYS to predict the electrical energy used each time a defrost cycle is activated. Although the defrost cycle on the physical heat pump often runs for more than one minute, it is modeled in TRNSYS as a single event occupying only one time step that uses an equivalent amount of electrical energy.

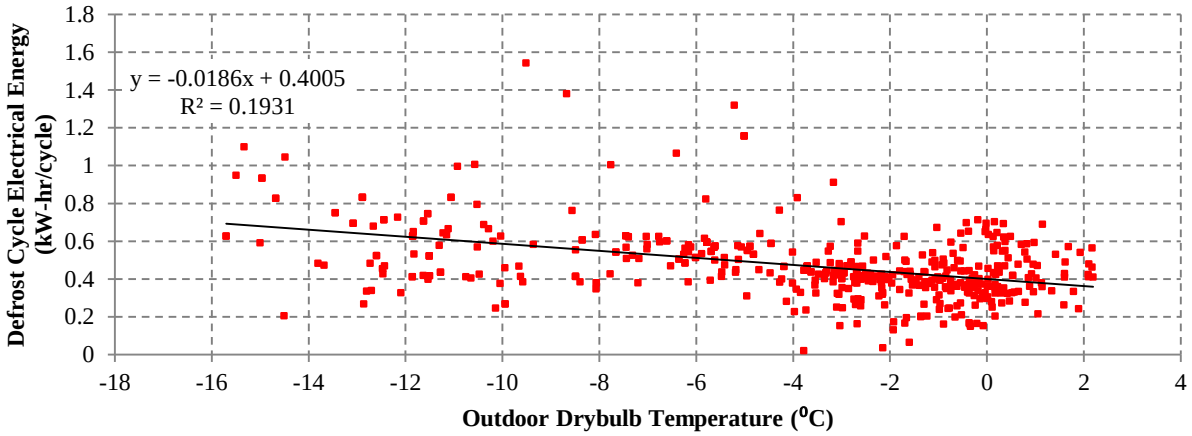

Figure 19. Measured Defrost Cycle Electrical Energy.

2.1.4 *Air Source Heat Pump Performance*

The un-tuned heat pump model inaccurately simulates the physical heat pump because not all of the information necessary for modeling each stage of the heat pump was provided in the manufacturer specifications and the physical heat pump may not perform exactly as the manufacturer specifications predict. To tune the heat pump, the rated capacity, power, air flow rate, and performance maps were revised using measured data. The performance maps for the heat pump were modified using heat pump performance versus outdoor dry bulb temperature provided by NIST. The performance map modification is discussed in Leyde [23]. The rated performance and air flow rate at each stage of heating, cooling, and dehumidification were then tuned using minutely heat pump data provided by NIST. Minute data for period from February 23 through 28, when the outdoor temperature ranged from about 13^{0}C to about -13.5^{0}C, were analyzed for heating performance. Minute data for August 22 through 26, when the outdoor temperature ranged from about 14^{0}C to 29^{0}C, and for September 9 through 11, when the outdoor temperature ranged from about 16^{0}C to 35^{0}C, were analyzed for cooling and dehumidification performance. Average measured capacities

and power for periods of heat pump operation in each stage were converted to rated capacities and power using the updated performance maps. These rated capacities and power were then averaged for each heat pump stage to find new rated capacities and power. The measured data show that the third stage of heat pump operation in heating mode used a higher air flow rate than the first or second stages. Because Type 922 only allows for two air speeds, another instance of Type 922 was added to the TRNSYS model to simulate the third stage in heating mode. The measured data also show that the heat pump standby power was approximately 50 W. This standby energy was added to the TRNSYS model. Table A-10 in Appendix A shows the tuned heat pump parameters.

2.1.5 *Thermostat Setpoint and Deadbands*

There were a number of problems related to the thermostat in matching the model to the measurements. The indoor dry bulb temperature and relative humidity are measured in five rooms in the house, including in the middle of the living room. Because the thermostat is located in the living room, the temperature and humidity measurements from the living room were used to study the thermostat control logic. While analyzing living room temperature data on a minute basis, it was noticed that the heating setpoint and both the heating and cooling deadbands do not match the specified setpoint and deadbands, which are described in Table A-8 in Appendix A. Figure 20 shows the measured living room temperature and the living room temperature predicted by the un-tuned TRNSYS model from February 23 – 28. The Zone 2 temperature predicted by TRNSYS, shown in red, followed the specified thermostat control logic of a setpoint of 21.1 ^{0}C and a deadband of 0.56 ^{0}C. The peaks in temperature seen in the middle of the days are caused by solar irradiation warming the living

room. The measured temperature in the living room did not meet the specified setpoint for the majority of the time and appeared to be meeting a setpoint of approximately 20.5 ^{0}C instead. Although the deadband for first stage heating was specified as 0.56 ^{0}C, the measured data showed the heat pump turning on after the temperature fell only approximately 0.1 ^{0}C. Because the deadband used in the un-tuned TRNSYS model is larger than what is observed in the data, the heat pump in the model stays on for long periods of time that exceed the time-out limits, which triggers the second and sometimes the third stages of heating. The NZERTF heat pump, however, cycles on and off rapidly because of the tight deadband. The thermostat control logic does not appear to follow the specified setpoints and deadbands, and it also appears to be inconsistent. The temperature is shown to drop down to 20 ^{0}C in the early morning hours of February 23rd and 24th, but is maintained around 20.5 ^{0}C the other nights. Also, even though the temperature reaches 21 ^{0}C during the middle of the day on February 24th, the minutely heat pump power data still shows the heat pump cycling on and off.

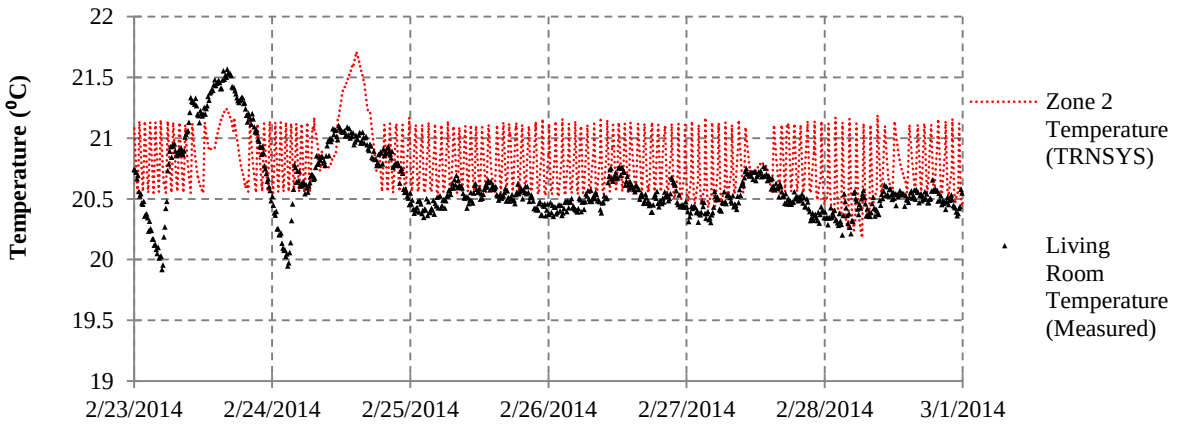

Figure 20. Living Room Temperature during Heating Mode – Un-tuned Thermostat.

The measured data during the cooling season did not show a noticeable discrepancy relative to the setpoint used in the un-tuned model. However, the measured deadband during cooling appeared to be approximately 0.2˚C, as opposed to the specified deadband of 1.1˚C in the un-tuned model. The measured data also show that the second stage dehumidification mode acted to keep the relative humidity between approximately 48 % and 50 %. The relative humidity deadband was not specified by the manufacturer and the dehumidification mode had been assumed to be triggered at a relative humidity of 51 % in the un-tuned TRNSYS model. Figure 21 shows the TRNSYS Zone 2 temperature and relative humidity compared to the measured living room temperature and humidity for five days in August.

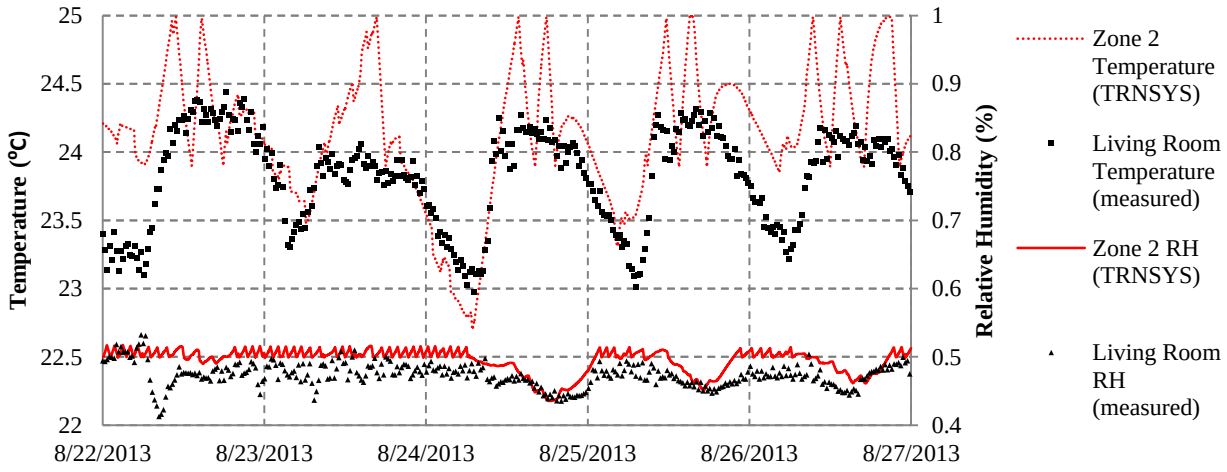

Figure 21. Living Room Temperature during Cooling Mode – Un-tuned Thermostat.

Two other inconsistencies were noticed during cooling season operation. The first stage of the dehumidification mode is observed to last approximately six minutes rather than the specified ten minutes. Also, it was observed that the second stage cooling does not consistently turn on after 40 minutes (as it should according to the thermostat program). Data for a time period in August showed the heat pump rarely switching to second stage even after

more than 40 minutes of operation in first stage. However, minute data collected for a time period in September showed the heat pump operating as-programmed; that is, it consistently switched to second stage after 40 minutes. This unpredictable behavior could not be replicated in the model.

The thermostat is programmed to have a specified set of setpoints, deadbands, and run-times, yet the data clearly show that the heat pump is not following this control logic consistently. A test was performed by NIST in which the temperature at the location of the thermostat and the temperature in the middle of the living room (where the instruments that measure the room's dry-bulb temperature and relative humidity are located) were simultaneously measured. That test concluded that there was virtually no difference between the temperature at the thermostat and the temperature in the middle of the living room. However an internal fault may affect the thermostat's internal temperature measurements. At this time the cause of the thermostat malfunction is unknown. These differences between the programmed logic and the actual behavior cause discrepancies in the predicted power, efficiency, and runtime of the heat pump, even in the tuned model. To better predict the actual behavior of the NZERTF the heating mode setpoint, the dehumidification setpoint, and the heating mode, cooling mode, and dehumidification mode deadbands were adjusted in TRNSYS, as shown in Table 14.Figure 22 compares the tuned TRNSYS Zone 2 temperature versus the measured living room temperature in heating mode while Figure 23 compares the tuned TRNSYS Zone 2 temperature and relative humidity versus the measured values in cooling mode.

Table 14. Air source heat pump control logic.

Mode	Setpoint		*Turn-on Trigger*						
				First Stage		Second Stage		Third Stage	
	Un-tuned	*Tuned*		*Un-tuned*	*Tuned*	*Un-tuned*	*Tuned*	*Un-tuned*	*Tuned*
Heating	21.1 ˚C	20.5 ˚C	Deadband (˚C)	0.56	0.1	1.1	1.1	3.3	3.3
			Time Delay (min)	N/A	N/A	10	10	40	40
Cooling	23.9 ˚C	23.9 ˚C	Deadband (˚C)	1.1	0.2	2.8	2.8	N/A	N/A
			Time Delay (min)	N/A	N/A	40	40	N/A	N/A
Dehumid.	50 %	48 %	Deadband (%)	1	2	N/A	N/A	N/A	N/A
			Time Delay (min)	N/A	N/A	10	6	N/A	N/A

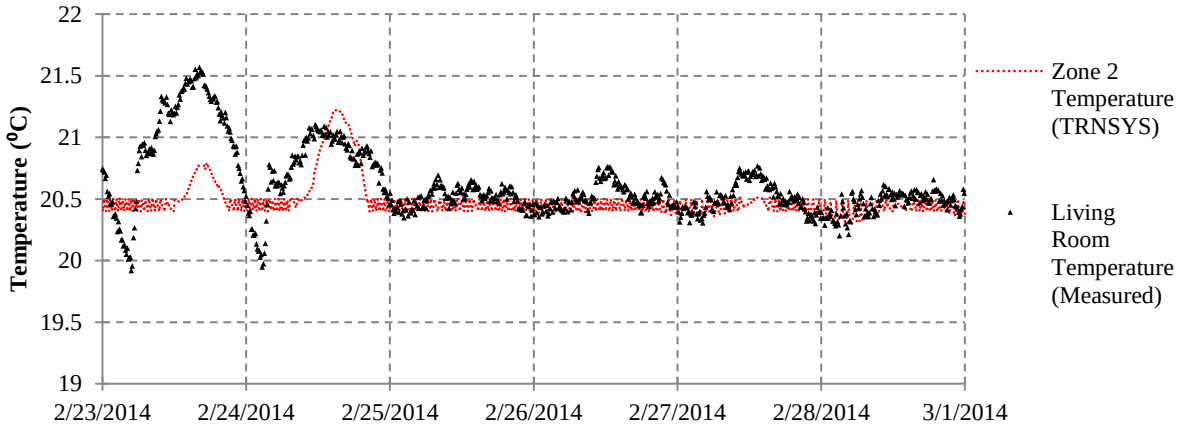

Figure 22. Living Room Temperature during Heating Mode – Tuned Thermostat.

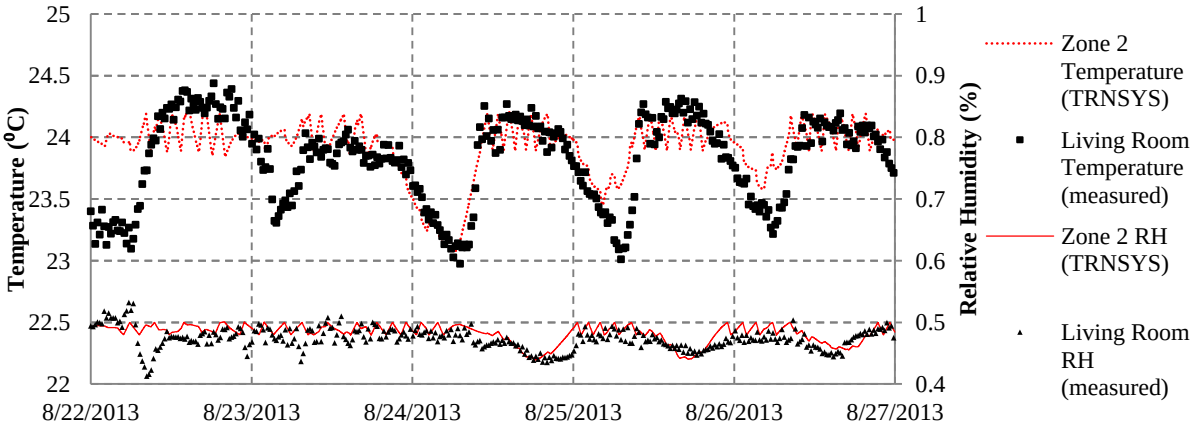

Figure 23. Living Room Temperature during Cooling Mode – Tuned Thermostat.

2.2 Tuning the DHW System

In order to tune the DHW system it was necessary to examine the flow rates, the heat exchanger effectiveness, the tank heat loss coefficient, the control logic, and the power draws. Tuning these parameters improved the agreement between the measured and predicted energy consumption and the water temperatures.

2.2.1 *SHW System*

To tune the SHW system, the circulating pumps' power and flow rates, the heat exchanger effectiveness, and the solar hot water tank heat loss coefficient were adjusted so as to better match experimental data. The combined power draw for both circulating pumps was measured to be between 160 and 165 W, so each pump's rated power was increased from 55 W to 80 W in the tuned model. The water flow rate through the heat exchanger was updated to match the measured flow rate of 4.4 gpm. The propylene glycol flow rate was measured to be 0.83 gpm, which is only a slight modification of the un-tuned flow rate of 0.85 gpm. The effectiveness of the heat exchanger was measured to be 0.44, which is a significant reduction relative to the effectiveness of 0.8 that is assumed in the un-tuned model. To achieve a better match between the predicted and measured water temperature leaving the solar hot water system, the SHW tank skin loss coefficient was increased from 0.6 W/m^2-K to 1.0 W/m^2-K.

2.2.2 *HPWH System*

To tune the HPWH, measured power data was analyzed to find the actual power draw for the heat pump and the heating element in a similar way the air-source heat pump was tuned. The heat pump's measured standby power of 6.92 W was included in the tuned model. While the air-source heat pump was sufficiently instrumented to allow in-situ measurements to be used

for this process, the HPWH was not and therefore results from tests performed by NIST on the same HPWH model (but a different piece of hardware) were used to tune the control logic and the COP. The test results indicated a larger deadband on the HPWH's heating element, changing it from +0 ^{0}C/-16.8 ^{0}C to +4.4 ^{0}C/-16.8 ^{0}C. A test was also performed to determine the heat pump COP given a range of tank water temperatures. The TRNSYS heat pump performance map rated conditions were set to an inlet water temperature of 32.22^{0}C, ambient air temperature of 21.67^{0}C, and ambient air relative humidity of 40%, which are conditions similar to those found in the NZERTF. The test results were then used to modify the rated power and capacity relative to the value at these conditions. As a result, the TRNSYS predicted COP agrees well with the COP values found in the test, especially at water temperatures greater than 25^{0}C. The TRNSYS-predicted vs. measured COP is shown in Figure 24. Note that for the measured data, the water temperature is the average tank water temperature and for TRNSYS, it is the water temperature entering the heat pump. However, during the testing it was noted that there was very little stratification in the HPWH tank, so the measured average water temperature is not much warmer than the temperature of the water entering the heat pump. Also, because there is little stratification, the temperature of the water drawn by the heat pump will rarely reach temperatures as low as 25 ^{0}C, so the discrepancy between the measured and predicted COP at these lower water temperatures is of little concern.

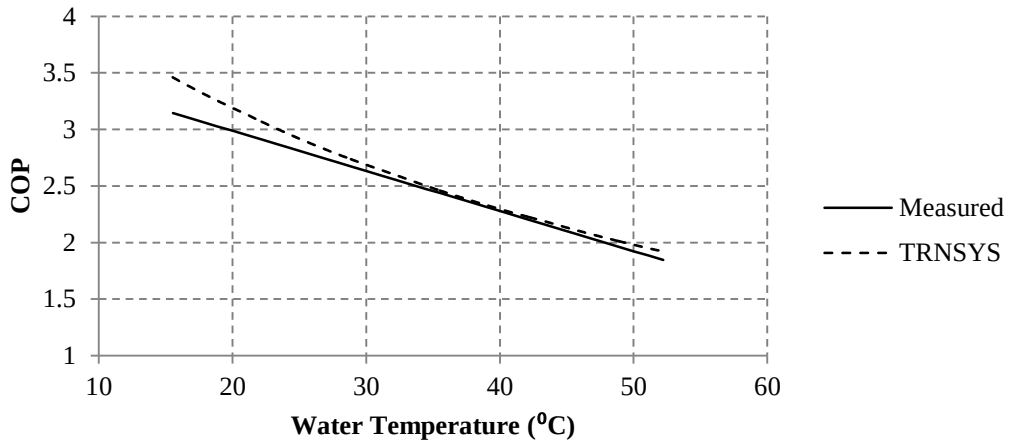

Figure 24. Measured vs. TRNSYS HPWH COP.

2.3 Tuned Subsystem Results

2.3.1 *Overall Heat Transfer Coefficient of the House*

Tuning the air exchange through the HRV affected the *UA* of the house. The un-tuned model predicted a *UA* of 4.83 kW·hr/day·K whereas the measured *UA* was 5.07 kW·hr/day·K. Tuning the model resulted in slightly better agreement between the predicted and measured *UA*, with the tuned model's *UA* predicted as 5.14 kW·hr/day·K. The measured and predicted thermal energy per day versus the difference between the outdoor and indoor temperatures is shown in Figure 25.

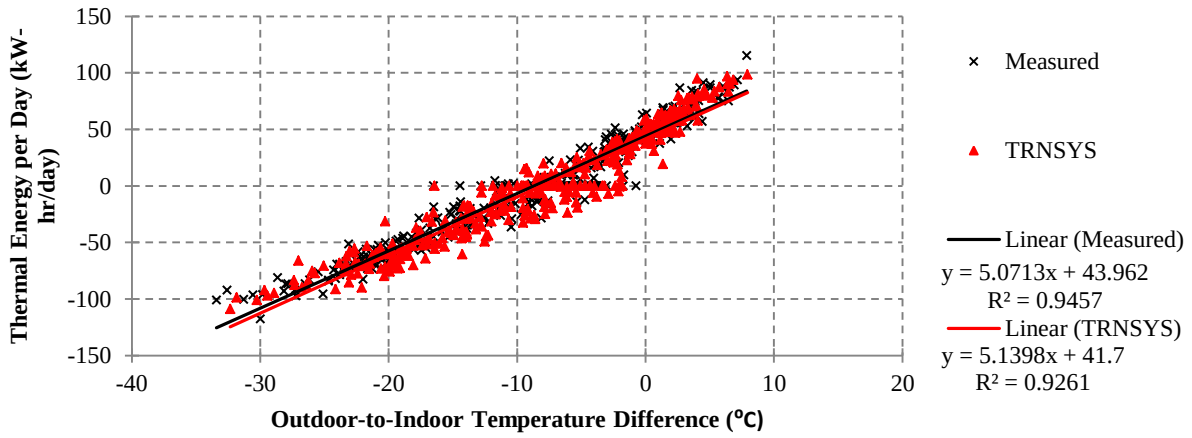

Figure 25. Measured vs. Tuned TRNSYS Overall Heat Transfer Coefficient

2.3.2 *HVAC System Results*

2.3.2.1 Heat Recovery Ventilation Results

Tuning the HRV resulted in an increase in the loads introduced to the house by the HRV, which was seen in the previous section with the tuned *UA* being greater than the un-tuned *UA*. The monthly loads introduced by the HRV in the un-tuned model are less than the loads introduced by the HRV in the tuned model because the predicted average flow rate in the un-tuned TRNSYS model was 12 % less than the measured average flow rate. Figure 26 shows the un-tuned and tuned TRNSYS latent and sensible loads introduced by the HRV compared to the measured loads with associated uncertainty.

Overall, the tuned TRNSYS model under-predicts the sensible load and over-predicts the latent load. The difference in the loads may be caused by measurement uncertainty and variation in the apparent sensible effectiveness and the air flow rate of the physical HRV, as well as small differences between the measured and predicted temperature and humidity ratio of the return air. The error bars in Figure 26 show a representative uncertainty in the loads of

25 %, which is the minimum combined uncertainty of the HRV sensible and latent loads [53].

The tuned TRNSYS results and the measured annual energy consumption, average HRV effectiveness, and average flow rate are listed in Table 15. Also listed are the percent differences between the model's predicted values and the measured values.

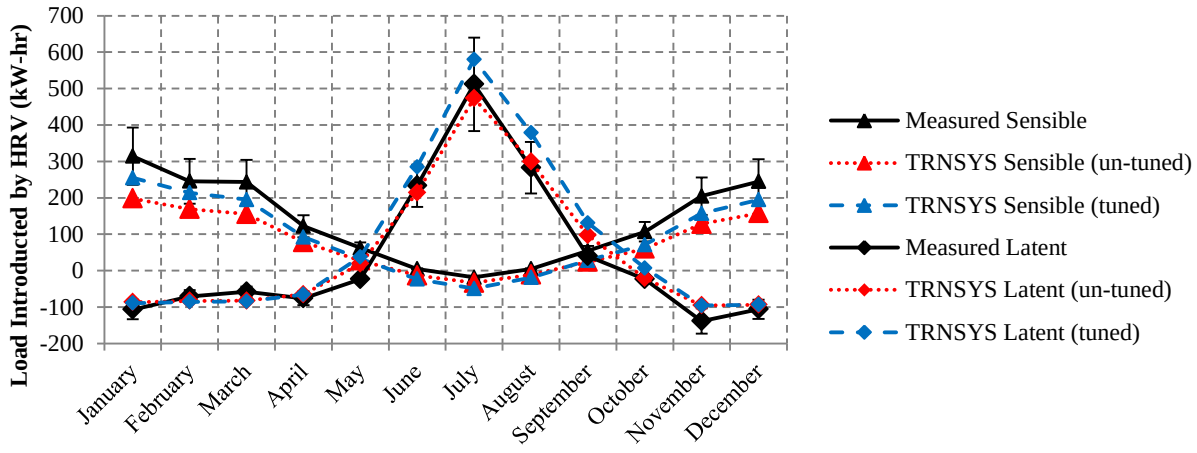

Figure 26. Measured vs. TRNSYS Monthly Loads Introduced by HRV – Tuned and Un-tuned Model.

Table 15. HRV Performance Data

	Energy Consumption (kW-hr)	Effectiveness	Average Flow Rate (m^3/hr)
Measured	514	0.72	195
TRNSYS	524	0.71	196
Percent Error	2 %	-1 %	1 %

2.3.2.2 Air Source Heat Pump Results

The monthly integrated average thermal load met by the air-source heat pump predicted by the models are compared with measured values. The tuned model over-predicts the heating load by 4 % and under-predicts the cooling load by 5 % when compared to the measured

values. The remaining discrepancy in the thermal loads predicted by the tuned model may be caused by a combination of factors including measurement error as well as inaccuracy of the modeled infiltration, *UA* of the building, solar gains, and loads introduced by ventilation, equipment, appliances, plug loads, and occupants. A representative uncertainty of the total capacity of the heat pump is estimated to be between 8.3 % and 9.4 % while in cooling mode and between 4.2 % and 5.9 % while in heating mode [41]. Figure 27 shows the thermal load that was measured and predicted by the tuned TRNSYS model and the un-tuned TRNSYS model. These values of the monthly integrated thermal energy are compared and the percent difference between the TRNSYS and measured values are shown in Table 16. Note that the highest percent differences occur during months of small total thermal loads.

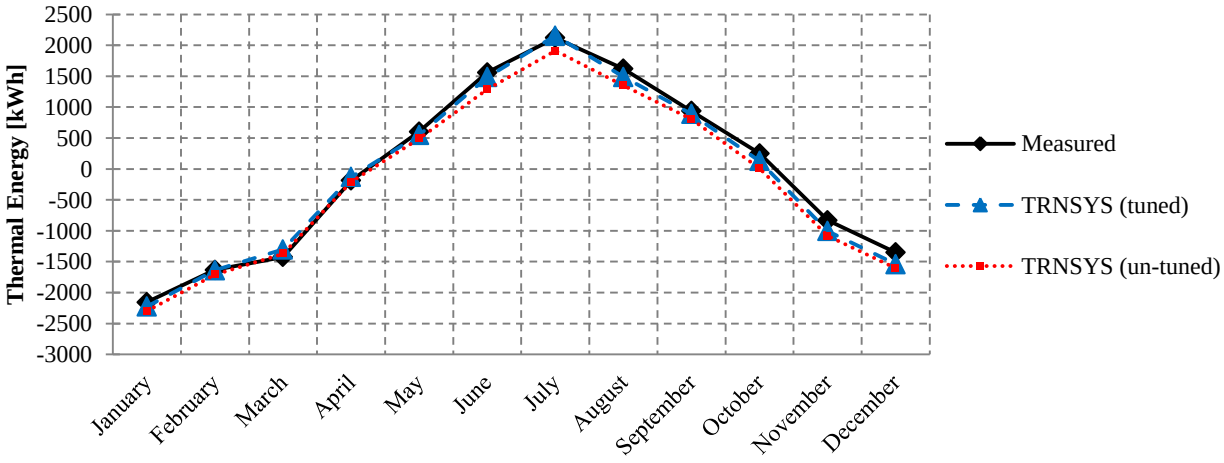

Figure 27. Measured vs. TRNSYS Thermal Energy.

Table 16. Measured vs. TRNSYS Monthly Thermal Energy.

Month	Measured Energy [kW-hr]	Un-tuned TRNSYS Energy [kW-hr]	*Percent Difference [%]*	Tuned TRNSYS Energy [kW-hr]	*Percent Difference [%]*
Jan-14	-2157	-2299	*7%*	-2226	*3%*
Feb-14	-1635	-1709	*5%*	-1638	*0%*
Mar-14	-1424	-1371	*-4%*	-1304	*-8%*
Apr-14	-186	-211	*14%*	-131	*-30%*
May-14	603	492	*-18%*	549	*-9%*
Jun-14	1560	1285	*-18%*	1485	*-5%*
Jul-13	2123	1912	*-10%*	2157	*2%*
Aug-13	1621	1348	*-17%*	1489	*-8%*
Sep-13	937	805	*-14%*	890	*-5%*
Oct-13	250	7	*-97%*	128	*-49%*
Nov-13	-830	-1086	*31%*	-1005	*21%*
Dec-13	-1351	-1608	*19%*	-1542	*14%*

The electrical energy required to operate the air source heat pump depends on the thermal load as well as the heat pump operating stage and the performance of the heat pump when operating in that stage. Figure 29 and Figure 29 compare total heat pump electrical consumption measurements to the predictions from the un-tuned and tuned TRNSYS models, divided into the cooling/heating stages, defrost, and standby. The data values can be found in Table B-4 in Appendix B.

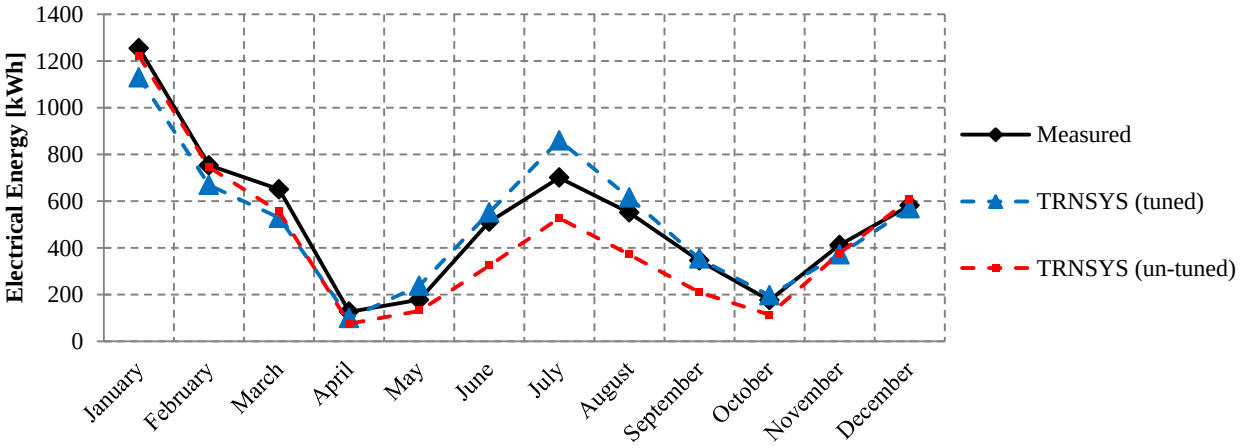

Figure 28. Measured vs. TRNSYS Total Heat Pump Electrical Energy – Tuned and Un-tuned Model.

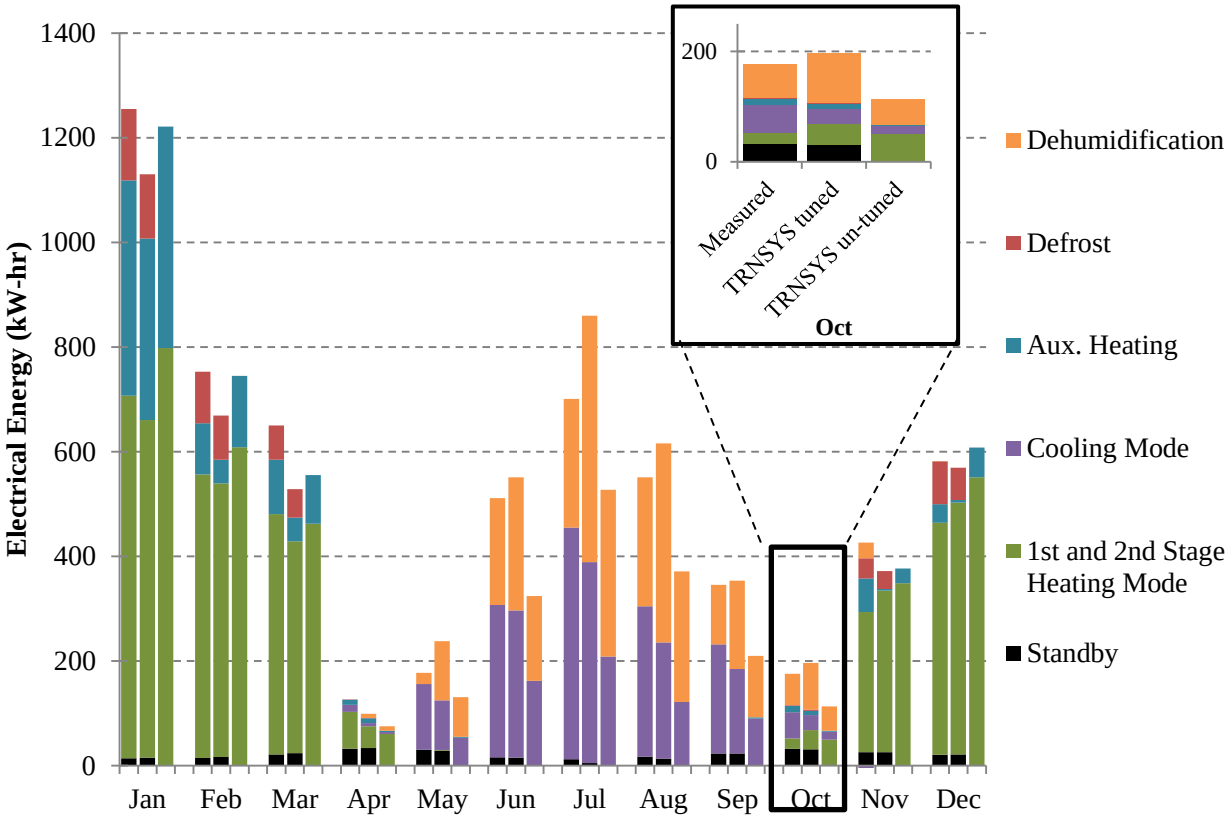

Figure 29. Measured vs. TRNSYS Heat Pump Electrical Energy by Stage – Tuned and Un-tuned Model.

Tuning the model decreased the percent difference in the total predicted cooling mode electrical energy with respect to the measured energy from -32 % (for the un-tuned model) to

13 % (for the tuned model). The previously mentioned tuned parameters, including the HRV airflow, the heat pump performance, and the smaller deadband, resulted in the increase of the electrical energy consumption. While the prediction of total cooling energy improved with the tuned model, there is still a large discrepancy occurring in July primarily caused by the second stage dehumidification mode running more frequently in the model than it does in the actual NZERTF. The heat pump COP is relatively low in second stage dehumidification mode (compared to the cooling modes) because the supply air is reheated, effectively reducing capacity. Over-predicting 2nd stage dehumidification in the model therefore resulted in significantly over-predicted energy use.

In heating, the tuned model somewhat increased the percent difference between the predicted and measured total heat pump electrical energy from 4 % (for the un-tuned model) to 10 % (for the tuned model). Although the un-tuned model's heating energy matched the measured data more closely, the tuned model better matched the energy consumed by the first and second stages, defrost, and standby. The exception to the improved prediction with the tuned model was the third stage resistance heater energy. The resistance heater ran less often in the tuned model because the deadband was smaller, causing the heat pump to run for a shorter period of time and the third stage to be triggered less often.

The thermostat is a likely contributor to the discrepancy in the amount of time that the system spends in second stage dehumidification mode and third stage heat pump mode. Although the setpoints and deadbands were tuned, the model does not reproduce the actual thermostat behavior consistently because the thermostat itself does not seem to operate consistently, as discussed in the "Thermostat Setpoints and Deadbands" section. Another contributor to the

discrepancy between the measured data and TRNSYS predictions is the assumption that each floor behaves as one zone. In reality, rooms on the same floor are often at slightly different temperatures and relative humidity. The humidifiers simulating the occupant latent load in the test facility are located in the kitchen, so the relative humidity is often higher in the kitchen than in the living room. However, because the entire first floor is modeled as a single zone in TRNSYS, the added moisture impacts the relative humidity throughout the floor equally. The humidity measurement at the thermostat will subsequently be higher in the model, which could increase the frequency of the activation of heat pump second stage dehumidification. Thirdly, the air flow between each floor in TRNSYS may not correspond perfectly to the air movement within the actual NZERTF. The total HVAC return and supply air flow to each floor was modeled using the measured flow rates specified in the as-builts, but the air flows between different floors of the house have not been determined. A final consideration is that although the loads introduced by the HRV are within measurement error, the uncertainty of the measurements is rather large, so these modeled introduced loads may differ somewhat from the actual introduced loads, contributing to the discrepancy in the second stage dehumidification mode and third stage heat pump mode.

2.3.2 *DHW System Results*

2.3.2.1 SHW Results

Tuning the SHW system, incorporating the changes made to the length of the pipe between the tanks and to the tempering valve, and turning off the SHW circulation pumps for the period during which they were not being operations from August 24, 2013 through September 3, 2013 resulted in better agreement between the predicted results and the

measured data. The outlet SHW tank temperatures in the tuned model match the measured temperatures more closely than in the un-tuned model, as seen in Figure 30. The absolute value of the percent error between the predicted and measured pump energy consumption decreased from 30 % to 4 %. The tuned model's predicted volume of water delivered by the SHW system also agrees more closely with the measured data. The monthly energy delivered, water delivered, and energy consumed by the SHW system are listed in Table 17.

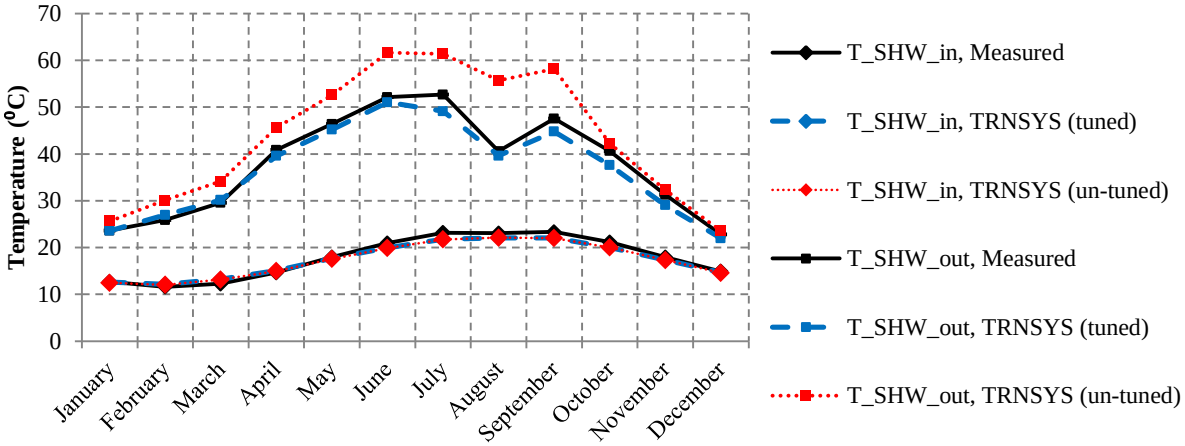

Figure 30. Measured vs. TRNSYS SHW Temperatures – Tuned and Un-Tuned Model.

Table 17. SHW Performance – Tuned Model.

Month	Measured $Q_{del,SHW}$ [kWh]	TRNSYS $Q_{del,SHW}$ [kWh]	*Percent Difference [%]*	Measured SHW Pump Energy Consumption [kWh]	TRNSYS SHW Pump Energy Consumption [kWh]	*Percent Difference [%]*	Measured SHW Water Delivered [L]	TRNSYS SHW Water Delivered [L]	*Percent Difference [%]*
Jan-14	102	99	*-3%*	20.4	18.8	*-8%*	7722	7305	*-5%*
Feb-14	124	118	*-5%*	19.8	20.8	*5%*	7113	6570	*-8%*
Mar-14	158	146	*-8%*	22.6	25.3	*12%*	7430	7200	*-3%*
Apr-14	227	194	*-14%*	29	31.1	*7%*	7118	6807	*-4%*
May-14	237	215	*-9%*	34.3	37.7	*10%*	7169	6840	*-5%*
Jun-14	239	223	*-7%*	34.8	38.1	*10%*	6634	6396	*-4%*
Jul-13	239	215	*-10%*	35.7	38.4	*7%*	6710	6796	*1%*
Aug-13	131	138	*6%*	27.1	26.5	*-2%*	6833	6776	*-1%*
Sep-13	204	176	*-14%*	31.4	30.9	*-1%*	7794	6656	*-15%*

Oct-13	173	137	*-21%*	24.2	26.3	*9%*	8140	6818	*-16%*
Nov-13	117	94	*-19%*	22	20.7	*-6%*	7637	6918	*-9%*
Dec-13	78	67	*-14%*	18.2	16.7	*-8%*	7790	7392	*-5%*
Total	**2029**	**1823**	*-10%*	**319.5**	**331.3**	***4%***	**88089**	**82475**	*-6%*

2.3.2.2 HPWH Results

The improved prediction of SHW outlet temperatures in the tuned model resulted in better prediction of the HPWH inlet temperatures, as shown in Figure 31. Incorporating the heat pump 11 day down-time into the tuned model and tuning the HPWH model caused significant improvement in the comparison between the predicted and measured HPWH tank outlet temperature, annual HPHW energy delivered, and energy consumption. However, as with the un-tuned model, the heating element was never triggered in the tuned model except for the period of time that the heat pump itself was not operational. Because TRNSYS inlet and outlet temperatures, the hot water volumes, and the HPWH loads agree closely with the measured values, the cause of the discrepancy in heating element energy may be that the physical heating element is actually triggered at a higher temperature than what is specified by the manufacturer. Table 18 compares the monthly energy delivered ($Q_{del,HPWH}$) and energy consumed by the HPHW system.

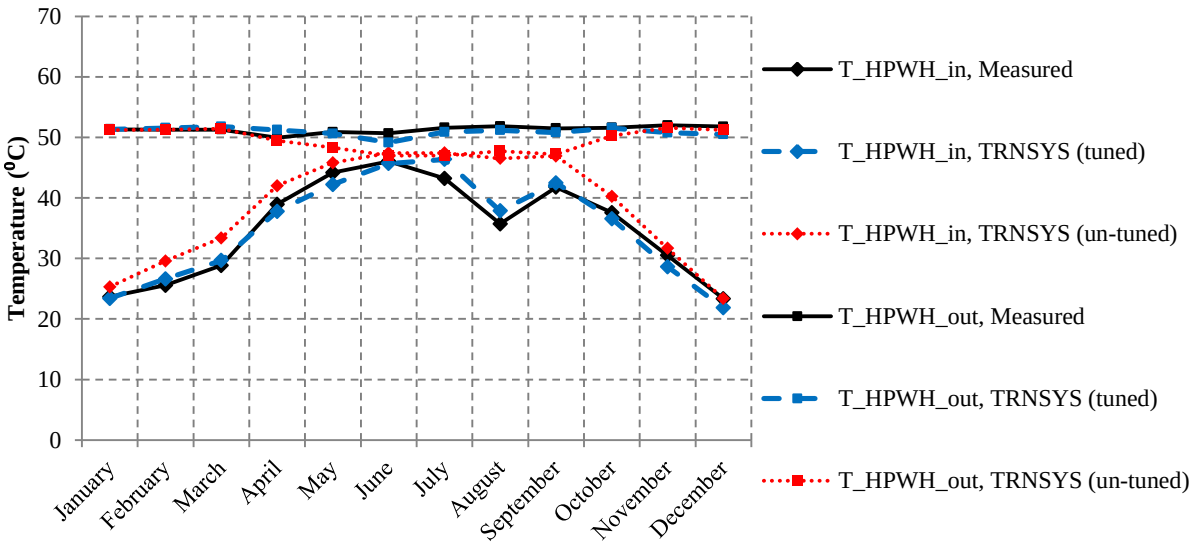

Figure 31. Measured vs. TRNSYS HPWH Temperatures – Tuned and Un-tuned Model.

Table 18. HPWH Performance – Tuned Model.

Month	Measured $Q_{del,HPHW}$ [kWh]	TRNSYS $Q_{del,HPHW}$ [kWh]	*Percent Difference [%]*	Measured Total Energy Used by HPWH [kWh]	TRNSYS Total Energy Used by HPWH [kWh]	*Percent Difference [%]*	Measured HPWH Heating Element [kWh]	TRNSYS HPWH Heating Element [kWh]	*Percent Difference [%]*
Jan-14	240.2	234.6	*-2%*	142.8	133.3	*-7%*	13.9	1.5	*-89 %*
Feb-14	207.7	188.1	*-9%*	125	109.2	*-13%*	14.2	0.0	*-100 %*
Mar-14	187.3	182.7	*-2%*	120.7	109.6	*-9%*	12.8	0.0	*-100 %*
Apr-14	84.4	105.2	*25%*	72.7	69.3	*-5%*	3.3	0.0	*-100 %*
May-14	54.7	66.5	*22%*	55.2	51.2	*-7%*	0.6	0.0	*-100 %*
Jun-14	35.3	24.4	*-31%*	46.1	28.2	*-39%*	0	0.0	*0 %*
Jul-13	42.1	30.4	*-28%*	53.3	32.2	*-40%*	0	0.0	*0 %*
Aug-13	107.9	100.3	*-7%*	70.8	65.9	*-7%*	5.8	0.0	*-100 %*
Sep-13	68.3	58.0	*-15%*	57	45.2	*-21%*	3.2	0.0	*-100 %*
Oct-13	118.7	117.0	*-1%*	82.5	75.7	*-8%*	3.2	0.0	*-100 %*
Nov-13	172	174.1	*1%*	129.8	122.4	*-6%*	44.3	40.1	*-10 %*
Dec-13	244	238.8	*-2%*	156.3	148.3	*-5%*	36.1	33.8	*-6 %*
Total	**1562.6**	**1520.0**	***-3%***	**1112.2**	**990.5**	***-11%***	**137.4**	**75.4**	***-45%***

The total hot water load and volume delivered by the DHW system changed varied little between the un-tuned and tuned models. The total hot water load improved from a -6 % difference compared to measured data to a -4 % percent difference while the percent difference between the predicted and measured total volume increased from -5 % to -7 %. The monthly totals for these values are found in Table 19.

Table 19. Energy Delivered by DHW System – Tuned Model.

Month	Measured Total Hot Water Load Q_{load} [kWh]	TRNSYS Total Hot Water Load Q_{load} [kWh]	*Percent Difference [%]*	Measured Total Hot Water Delivered [L]	TRNSYS Total Hot Water Delivered [L]	*Percent Difference [%]*
Jan-14	343.1	324.0	*-6%*	7738	7305	*-6%*
Feb-14	330	306.0	*-7%*	7113	6570	*-8%*
Mar-14	340.5	327.1	*-4%*	7430	7202	*-3%*
Apr-14	300.3	295.9	*-1%*	7118	6959	*-2%*
May-14	276.9	276.8	*0%*	7169	7177	*0%*
Jun-14	250.6	241.8	*-4%*	7215	7091	*-2%*
Jul-13	252.4	230.2	*-9%*	6710*	6795	*1%*
Aug-13	217.8	229.0	*5%*	6833*	6776	*-1%*
Sep-13	238.2	221.8	*-7%*	7872	6689	*-15%*
Oct-13	268.5	251.1	*-6%*	8180	6881	*-16%*
Nov-13	283.2	267.1	*-6%*	7663	6918	*-10%*
Dec-13	325.9	306.9	*-6%*	7790	7392	*-5%*
Total	**3427.4**	**3277.7**	***-4%***	**75287**	**70185**	***-7%***

*Missing data 7/1-7/2 and 8/2-8/6 inclusive. These months are not included in total.

2.4 Overall Tuned Model Results and Discussion

Tuning the model resulted in a reduction in the difference between the predicted and measured total annual energy consumption as well as in the difference for each subsystem. The absolute value of the percent difference between the predicted and measured annual energy consumed was reduced to 1.6 % for the tuned model. Table 20 shows the predicted

and measured annual electrical energy generation and consumption as well as the annual consumption for each subsystem. As noted in Section 1.5, the sum of the energy consumed by each of the subsystems does not exactly equal the value stated as the total consumed electrical energy and an uncertainty analysis showed that the uncertainty in the PV generation was 1.0% and the uncertainty in the total energy consumed was 1.1% [41].

Table 20. Measured and Predicted Annual Electrical Energy Generation and Consumption.

	Measured (kW-hr)	**TRNSYS – Un-tuned (kW-hr)**	***Percent Difference***	**TRNSYS - Tuned (kW-hr)**	***Percent Difference***
Lighting	435	442	*1.4%*	442	*1.4%*
Plug Loads	2440	2462	*0.9%*	2462	*0.9%*
Appliances	1867	1898	*1.6%*	1898	*1.6%*
Air Source Heat Pump	6241	5258	*-15.7%*	6184	*-0.9%*
HRV	514	355	*-31.1%*	524	*1.8%*
DHW	1432	827	*-42.3%*	1322	*-7.7%*
Total Consumed	13039	11241	*-13.8%*	12831	*-1.6%*
PV	13523	13937	*3.1%*	13937	*3.1%*
Net Generation	484	2697		1106	

When considering the percentage that the energy consumption of each subsystem contributed to the total energy consumed, the TRNSYS results were nearly identical to the measured data. Space conditioning used the largest portion of the consumed energy, accounting for 47 % of the total energy consumed. The plug loads and appliances follow as the next largest contributors, using 19 % and 15 % of the total energy consumed, respectively. Figure 32 illustrates the TRNSYS-predicted and the measured percentage of total electrical energy consumed by each subsystem.

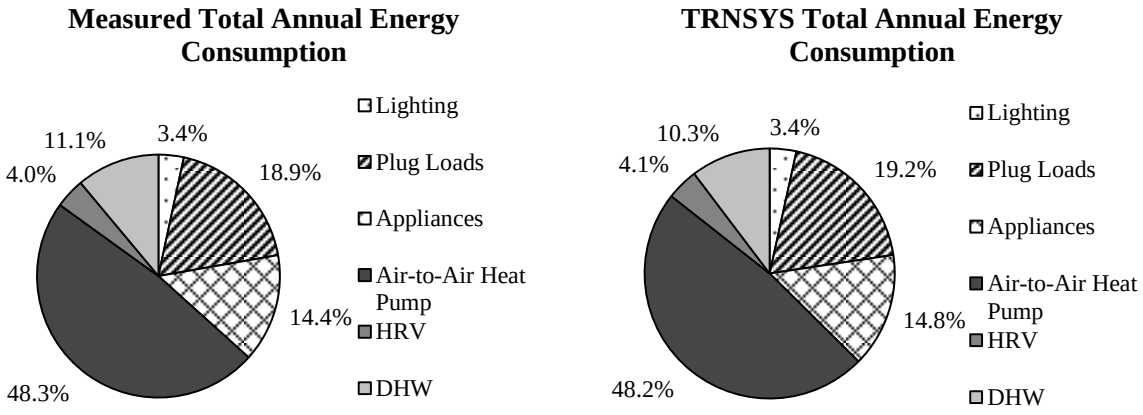

Figure 32. Percentage of Total Electrical Energy Consumed by Each Subsystem.

Tuning the TRNSYS model resulted in a more accurate model, and also revealed a number of discrepancies between the predicted and actual behavior of the equipment and the building envelope. It emphasized the importance of certain subsystem parameters and controls.

The thermostat had a large effect on the thermal load, the heat pump run time, and the electrical energy. The electrical energy used by the heat pump may be strongly impacted by the thermostat behavior because the heat pump stages are triggered by both temperature and time. The thermostat did not behave as expected; the setpoint was not met during the heating season and the dead-bands were much smaller than specified throughout the year. This resulted in the heat pump cycling on and off frequently, which may negatively impact the life of the compressor. Furthermore, the cause of the thermostat's deviation from its expected behavior is unknown at this time. For this reason, although the modeled thermostat was adjusted to more closely match the observed thermostat behavior, it cannot highly accurately predict the faulty thermostat's behavior.

The TRNSYS model showed the large effect the latent energy introduced to the house during the cooling season has on the electrical consumption of the heat pump. The relative humidity in Zone 2 in TRNSYS was slightly higher than that in the living room of the NZERTF, where the thermostat is located, for reasons discussed in Section 2.3.2. This caused the dedicated dehumidification cycle to run more in the TRNSYS simulation than in the NZERTF. The dedicated dehumidification cycle has a low COP because it requires the supply air to be reheated after cooling it to remove moisture from the air. Although TRNSYS under-predicted the thermal load required during cooling mode by 5 %, the electrical energy required was over-predicted by 13 % because the dedicated dehumidification ran more in TRNSYS. Because the operation of the dedicated dehumidification mode can have such a large effect on the energy consumption of the HVAC system, finding ways to decrease the latent load during the cooling season could result in significant energy savings.

The measured electrical consumption allows one to see which subsystems use the greatest amount of energy, which can be used to determine which subsystems may be modified and improved in order to find the greatest energy savings. It was found that the space-conditioning system is by far the largest electricity consumer, followed by the plug loads and the appliances. Although the HRV itself only accounted for 4 % of the electrical consumption, the HRV also introduced sensible and latent loads that had to be met by the heat pump. The hot water system accounts for 10 % of the electrical consumption, but this system also increases the amount of energy required by the heat pump in order to meet the loads introduced by the DHW system. The HPWH is the primary water heater during the heating season, and the HPWH cools the space while operating. The SHW system is the

primary water heater during the cooling season, and the tank skin and pipe losses from this system heat the space.

The lack of actual occupants in the NZERTF, the regularly scheduled plug load activation and water draws, and the careful monitoring of the NZERTF make it an unusual and ideal situation for comparing modeled results with physical residential house behavior. The NZERTF's occupancy, plug, appliance, and lighting loads, and water draws were carefully controlled, and the model developed to simulate the NZERTF is detailed. Even so, the TRNSYS model developed using information that was available before the NZERTF's first year of operation was not able to accurately predict some aspects of the residence operation. This type of model is representative of the ability of typical building models to predict loads and electrical consumption. After tuning this model using the measured data collected at the NZERTF, most the differences between the predicted and measured results decreased. However, discrepancies between the results of the tuned model and the measurements of the air-source heat pump's dehumidification mode and auxiliary heating mode and the HPHW system's heating element use persisted. Precisely modeling even a highly controlled, accurately measured facility proves challenging.

2.5 Future Work

There remains a significant discrepancy between the predicted and measured electrical energy associated with the heat pump's third stage resistive heater and second stage dehumidification mode. These discrepancies are largely driven by differences in the gradient and dynamic behavior of temperature and humidity in the house, as well as differences between the modeled and actual control system. Therefore, to make the model more accurate,

the house can be further subdivided into more zones, and a better model of the infiltration and the movement of air between zones can be included. Furthermore, a thermostat that behaves more consistently should be used in the NZERTF.

A number of interesting simulations may be performed using the tuned TRNSYS model of the NZERTF in order to gain a deeper understanding of net-zero energy houses. For example, the simulation could be run using weather data from a different climate to determine how well the house performs under different conditions. The house orientation, size, geometry, and number of windows could varied to find the impact those parameters have on the ability of the house to meet the net-zero goal. The occupancy, hot water load, plug loads, and appliance schedule could also be varied to find how well the house performs when occupied by a family that deviates from average family behavior.

Chapter 3: Evaluation of Domestic Hot Water Systems

DHW systems consume a significant portion of the total electrical energy use in residential homes. In the NZERTF, the DHW system accounted for 11 % of the total energy consumption. The NZERTF's system uses a solar thermal system to preheat the water and a heat pump water heater to further heat the water, if needed. This dual tank system is more expensive than a solar thermal water heating system (SWH) or a heat pump water heater (HPWH) used exclusively. Furthermore, the use of a solar preheating system lowers the efficiency of the HPWH. For these reasons, other DHW systems were modeled and compared to the model of the NZERTF's DHW system, described in Section 1.3.2. In total, eight DHW systems were evaluated, including the original NZERTF DHW system. The individual systems comprising the tuned model of the dual tank DHW system used during the first year of operation of the NZERTF (a SHW system and a HPWH) were modeled and compared to the NZERTF's DHW system. In addition, different sizes of the SHW system, the HPWH, and the SHW plus HPWH system as well as a SHW plus tankless water heater (TWH) system modeled. As a baseline for comparison, a 189 L (50 gal.) electric resistance water heater was also modeled. These eight DHW systems are listed below in Table 21.

Table 21. Modeled DHW Systems.

System Number	Description
1	189 L (50 gal.) electric resistance water heater with two 3800 W heating elements
2	303 L (80 gal.) SWH with one 4500 W heating element
3	454 L (120 gal.) SHW with one 4500 W heating element
4	189 L (50 gal.) HPWH with one 3800 W heating element
5	303 L (80 gal.) HPWH with one 3800 W heating element
6	303 L (80 gal.) SHW with heating element disabled and 189 L (50 gal.) HPWH with one 3600 W heating element
7	454 L (120 gal.) SHW with heating element disabled and 189 L (50 gal.) HPWH with one 3600 W heating element
8	303 L (80 gal.) SHW with heating element disabled and 25 kW electric TWH

3.1 Model Drivers

Hourly average measured basement temperatures and relative humidity were used as inputs for the models. TMY3 weather data collected at the Dulles International Airport, which is approximately 18 miles away from the NZERTF, were used in the simulation. The water mains temperature was assumed to be the ground temperature, which was estimated using a TRNSYS soil model type and soil temperature data recorded by the Natural Resources Conservation Service [32], as was discussed in Section 1.2.7. The water draw schedule used while evaluating the various hot water systems was the same water draw schedule used in the whole house model and discussed in Section 1.2.6. Each simulation used a one minute timestep and was run for a 13 month period, with the first month being a pre-conditioning month which was disregarded during the analysis of the simulation results.

3.2 Number of Tank Nodes

A sensitivity analysis was performed on the 120 gallon SHW system for the month of January to determine the number of nodes needed to model the tanks. The monthly thermal load and electrical energy consumed were recorded for various numbers of nodes. The thermal load is defined in a manner similar to Equation 12. These data can be seen in Figure 33. The thermal load remained approximately constant while the electrical energy decreased slightly as the number of nodes increased from 3 to 13 nodes, but remained approximately constant for 13 or more nodes. Slight changes in the thermal load occurred because changing the number of nodes affected the temperature of the water at the outlet and thereby required the tempering valve to adjust the volume of water drawn from the tank. The electrical energy required decreased as the node sizes decreased. Because the 120 gallon tank is the largest

tank in the simulations, it is the most likely to be stratified, and it was therefore assumed that the number of nodes used to model the 120 gallon tank would suffice for the other tanks as well. Fifteen nodes were used to model each tank in the configurations.

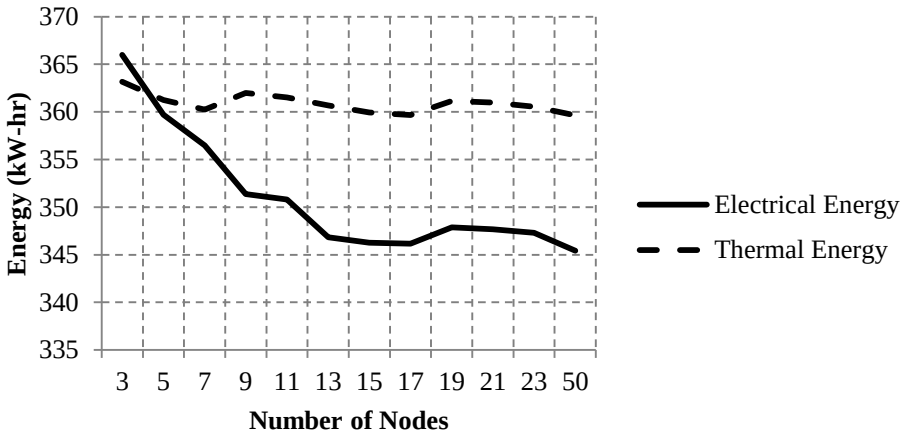

Figure 33. Tank Node Sensitivity Analysis.

3.3 DHW System Models

The nodes in which the inlets, outlets, and heating elements were located in each tank were determined from the schematics found in the manufacturer specifications. The height at which some of the inlets, outlets, and heating elements were located were specified, while the location of others had to be estimated using the drawings in the specifications. In addition to the storage tanks, the solar thermal panels, the SHW external heat exchanger, and the heat pump, the systems' piping from the water mains to the system outlet was also considered in this analysis. This piping includes the uninsulated copper pipe carrying the water from the water mains to the tank, the pipe between tanks in the dual tank systems, and the pipes between the heat exchanger and the solar thermal arrays in the SHW systems.

3.3.1 *System 1: Electric Resistance Water Heater*

The water from the mains enters the tank in node 14 (second from the bottom) and leaves the tank from node 3 (third from the top). The standard electric water heater used two 3800 W heating elements, located in nodes 5 and 13. The setpoint for each element was set to 49^0C. The deadband for the top element was estimated as ±2.8 ^{0}C and the deadband for the bottom element was estimated as ±8.3 ^{0}C. To estimate the skin loss coefficient, the manufacturer specified R-value of 16 was converted to a metric U-value. Note that this skin loss coefficient estimate is likely to be low because it does not account for losses due to piping connections. A schematic of this tank as well as a table of the parameters used in this model can be found in Appendix C.

3.3.2 *Systems 2 and 3: SHW Systems*

The SHW system for Systems 2 and 3 were modeled in the same way the SHW system was modeled for the whole house simulation, described in Section 1.3.2.1 and Section 2.2.1, except that the heating element within the tank was activated and the number of nodes were increased. The water from the mains enters both the 303 L (80 gal.) SHW tank and the 454 L (120 gal.) tanks in node 15 (bottom node) and the heated water exits from the top node. The inlet from the heat exchanger is located in node 2 (second from top) and the outlet to the heat exchanger is located in node 14 (second from bottom). The heating elements in both tanks have a capacity of 4500 W and are set to 49 ^{0}C ± 2.8 ^{0}C. In the 303 L tank the heating element is located in node 7 while in the 454 L tank it is located in node 6. The circulating pumps will turn on when the temperature differential between node 14 (near the bottom) and the solar panel outlet temperature is 10 ^{0}C or greater and will turn off when the differential is

3 ^{0}C or less. The pumps will not run if the temperature at node 14 reaches 71 ^{0}C, the shutoff temperature. When a water draw occurs, the water exiting the solar storage tank is tempered to 49 ^{0}C, if needed, using water from the water mains. The skin loss coefficient for the SHW tank was determined while tuning the DHW system in the whole house simulation, as discussed in Section 2.2.1. A tank schematic, a system schematic, and a table of the parameters used in each of these systems can be found in Appendix C.

3.3.3 *Systems 4 and 5: HPWH Systems*

The HPWH for Systems 4 and 5 were modeled in the same way the HPWH was modeled for the whole house simulation, described in Section 1.3.2.2 and Section 2.2.2, except that the number of nodes were increased. The water from the mains enters the tank in node 13 (third from the bottom) in both the 189 L (50 gal.) and 303 L (80 gal.) HPWH tanks. The heated water exits the tank from the top node. The heat pump both draws and discharges from node 13. The heat pump's temperature sensor is located in node 13. The setpoint for the heat pump temperature sensor is 49 ^{0}C and it had a deadband of ±1.1 ^{0}C. The heat pump standby power is 6.9 W. The backup electric heating element is located in node 5 (fifth from the top). It is activated when the temperature at that location drops to 32.2 ^{0}C and remains on until the temperature at that location reaches 53.4 ^{0}C. When the heating element is activated, the heat pump is shut off. A schematic of the tank, the system, and the parameters used for these systems can be found in Appendix C.

3.3.4 *Systems 6 and 7: SHW Plus HPWH Systems*

The model for system in which the 303 L (80 gal.) SHW system is connected to the 189 L (50 gal.) HPWH system was previously described in Section 1.3.2 and Section 2.2. The

model for the 454 L (120 gal.) SHW plus 189 L (50 gal.) HPWH system is identical to the smaller system except for the SHW tank, which was modeled for System 3 and described in Section 3.3.2. The only difference between the SHW tank in System 7 and System 3 is that the heating element within the tank is deactivated in System 7. The schematic for the SHW plus HPWH system was shown in Figure 9.

3.3.5 *System 8: SHW Plus TWH System*

System 8 is comprised of a 303 L (80 gal.) SHW system plus a 25 kW TWH used to further heat the water if needed. The model for the SHW system is identical to the SHW system modeled in System 6. The TWH was modeled based on a unit tested at NIST. It has two stages of capacity, 12.5 kW and 25 kW, and the standby power is 2 W. The setpoint for the TWH is 48.9^0C ± 2.8^0C. The heat loss coefficient for the TWH was estimated as the heat loss coefficient provided by Glanville et al [54] for a gas TWH with the fan off. The parameters for the TWH are provided in Appendix C.

3.4 Results and Discussion

Using the parameters specified in the previous sections, each DHW system was simulated as if it were operating in the NZERTF for a period of one year. The results were compared on a monthly basis.

The load met by each DHW system was calculated according to Equation **(13)**. The monthly COP for each system is defined as the total energy delivered by the system in the month divided by the total electrical energy required by the DHW system in the month.

$$\boldsymbol{COP = \frac{Q_{del}}{E_{tot}}} \quad \textbf{(13)}$$

Figure 34 plots the monthly COP for each system. The annual load, energy consumed, and COP for each system are listed in Table 22.

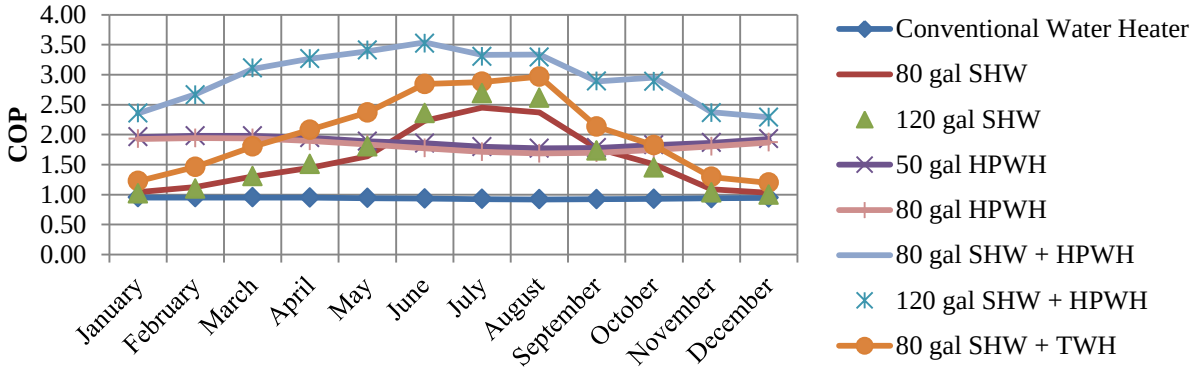

Figure 34. Monthly COP for Each DHW System.

Table 22. Annual Performance of each DHW System.

DHW System	Load, Q_{del} [kWh]	Total Energy Consumed, E_{tot} [kWh]	COP
Conventional Water Heater	3309	3519	0.94
80 gal SHW	3305	2371	1.39
120 gal SHW	3309	2373	1.39
50 gal HPWH	3309	1749	1.89
80 gal HPWH	3310	1808	1.83
80 gal SHW + HPWH	3309	1155	2.86
120 gal SHW + HPWH	3309	1159	2.85
80 gal SHW + TWH	3309	1906	1.74

Each of the systems analyzed was found to have significant energy savings over the conventional water heater. The 80 gal SHW + HPWH system has the highest annual COP, followed closely by the 120 gal SHW + TWH system.

The annual load is fairly consistent across all systems, varying slightly because of differences in water temperatures and flow rates at the system outlet. However, the monthly load is

higher in the winter months than in the summer months. Because the water mains temperature increases in the summer months, the load decreases. Despite the reduction in energy required to meet this load, the decrease in load has a net effect of decreasing the monthly COP for the conventional water heater, the HPWHs, and the SHW + HPWH systems. The annual mass of water delivered by each system and a more detailed analysis of the annual energy delivered by each system is shown in Table 23.

Table 23. Analysis of Annual Energy Delivered by Each DHW System.

DHW System	Average SHW Tank Temp. [C]	$Q_{del,SHW}$ [kWh]	Average HPWH Tank Temp. [C]	$Q_{del,HPWH}$ [kWh]	Load, Q_{del} [kWh]	Mass of Load [kg]	Total Mass Delivered [kg]
Conventional Water Heater	53*				3309	70819	116315
80 gal SHW	48				3305	72185	116317
120 gal SHW	48				3309	72907	116317
50 gal HPWH			46		3309	83838	116317
80 gal HPWH			46		3310	82500	116317
80 gal SHW + HPWH	36	2265	48	1099	3309	83654	116317
120 gal SHW + HPWH	36	2269	48	1094	3309	83628	116315
80 gal SHW + TWH	37	2251		1094[+]	3309	83827	116318

*The conventional water heater's tank temperature is listed in the SHW Tank Temp. column for convenience only. The conventional water heater tank is not a SHW tank.

[+]This value is the load delivered by the TWH and is listed in the load delivered by the HPWH column for convenience only.

$Q_{del,SHW}$ is the energy delivered by the SHW system in the SHW + HPWH systems and the SHW + TWH system, while $Q_{del,HPHW}$ is the energy delivered by the HPWH in those systems. The energy delivered by the SHW system in the 80 gal SHW + TWH system is slightly greater than the energy delivered by the SHW system in the SHW + HPWH systems despite the mass of the load being smaller because the tank temperature is greater. The mass

of the load is the mass used when calculating Q_{del} and is the total hot water delivered by the system before being mixed with cold water to meet the temperature setpoint. This mass will vary system to system, depending on the temperature of the water leaving the tank(s) and therefore the amount of cold water needed to temper the water to the setpoint. The total mass delivered is the mass of water flowing out of the final mixing valve. It should vary minimally from system to system because the total volume of water demand by the hot water schedule for the sink draws, showers, baths, and appliances is constant.

The annual energy consumed by the conventional water heater, which serves as a baseline comparison for each of the other systems, is 3519 kWh. The other DHW systems show a significant reduction in the annual energy consumed, ranging from 1155 kWh to 2373 kWh. A more detailed analysis of the annual power used by each system is shown in Table 24.

Table 24. Analysis of Annual Energy Consumed by Each DHW System.

	Total Energy [kWh]	**Circulating Pump Energy [kWh]**	**Heating Element(s) Energy [kWh]**	**Heat Pump Energy [kWh]**	**TWH Energy [kWh]**	**Standby Energy [kWh]**
Baseline	3519		3519			
80 gal SHW	2371	299	2072			
120 gal SHW	2373	325	2048			
50 gal HPWH	1749		42	1659		48
80 gal HPWH	1808		0	1760		48
80 gal SHW + HPWH	1155	406	2	692		56
120 gal SHW + HPWH	1159	408	2	693		56
80 gal SHW + TWH	1906	397			1509	

The circulating pump power is lower for the stand-alone SHW systems than for the other systems incorporating a SHW system because the upper portion of the stand-alone SHW

system tanks are kept at the setpoint by the heating elements. This causes the pumps, which turn on with a temperature differential between the solar panels and the tank of 10 ^{0}C, to not be triggered as often. The larger SHW tank uses more pump energy and less heating element energy because it allows for more stratification, which causes the solar circulating pumps to run more and the heating element to turn on less than in the smaller SHW tank. Although the heating element for the 80 gal HPWH is never triggered in this simulation, the larger tank uses more power in total because it has larger losses. The 80 gal SHW + HPWH system uses slightly more energy than the 120 gal SHW + HPWH system because the larger SHW tank is able to preheat more of the water entering the HPWH, which outweighs the higher tank losses in the larger system. The SHW + TWH system requires less energy than the stand-alone SHW systems because the tank is not being warmed by the heating elements, allowing the solar panels to meet a larger fraction of the total load, and because the TWH loses less thermal energy than the SHW tank over the course of a year.

Table 25 shows the losses from the tanks, the TWH, the pipe bringing water from the water mains to the DHW system, the pipe between the SHW and HPWH tanks or the SHW tank and the TWH, the indoor piping carrying propylene-glycol between the heat exchanger and the solar collectors, and the heat pump. A positive loss means that thermal energy is added to the surrounding by the DHW system and a negative loss means that thermal energy is extracted from the surroundings by the system.

Table 25. Analysis of Annual Energy Losses From Each DHW System.

DHW System	SHW Tank Losses (kW-hr)	HPWH Tank Losses (kW-hr)	TWH Losses (kW-hr)	Mains Pipe Losses (kW-hr)	Pipe Btw Tanks Losses (kW-hr)	PG Pipe Losses (kW-hr)	Heat Pump Losses (kW-hr)	Overall Losses (kW-hr)
Baseline	207			-146				61
80 gal SHW	599			-149		391		841
120 gal SHW	767			-149		371		989
50 gal HPWH		240		-146			-1880	-1785
80 gal HPWH		339		-146			-1924	-1731
80 gal SHW + HPWH	349	268		-146	55	291	-696	119
120 gal SHW + HPWH	443	269		-146	54	277	-692	205
80 gal SHW + TWH	355		362	-146	55	295		921

The tank losses are smallest for the baseline tank because the skin loss coefficient is smallest for this tank. The skin loss coefficient for the baseline tank is 0.355 W/m^2-K, for the HPWH tank is 0.6 W/m^2-K, for the both of the SHW tanks is 1.0 W/m^2-K, and for the TWH is 9.1 W/m^2-K. Piping losses for each system were calculated for the purpose of comparing each system's effect on space conditioning. The thermal energy added to the water mains pipe varies slightly from system to system, depending on how much water is drawn through the pipe to the tank, the mixing valve, and the tempering valve in the SHW systems. The pipe between the tanks consists of the pipe stretching from the SHW tank to the tempering valve and the pipe between the tempering valve and the HPWH or TWH. The losses from this piping will depend on the temperature of the water leaving the SHW tank. Of the total length of propylene glycol (PG) piping, only the stretch of piping located indoors is considered in this analysis. The variation in these losses depends on the water temperature entering the heat exchanger and the amount of time that the circulating pumps run. The heat pump losses

are negative because the heat pump extracts thermal energy from the ambient air in order to heat the water.

When comparing DHW systems, it is interesting to consider the system's effects on the other systems of the house. The losses from the tanks and the pipe and the thermal energy taken from the air by the HPWH introduce loads which must be met by the HVAC system. Depending on the system and the month of the year, the losses from the DHW system may have a negative or a positive effect on the amount of energy required by the HVAC system. Figure 35 shows the monthly losses for each system, with a positive loss meaning thermal energy was added to the space and a negative loss meaning thermal energy from the space was added to the system. During the first year of operation of the NZERTF, an air-source heat pump was used to heat, cool, and dehumidify the house. To approximate the net effect each of these DHW systems has on the HVAC electrical energy requirements, the measured monthly COP of the HVAC heat pump during the first year of operation was used. During months in which the heat pump ran in both heating and cooling modes, the COP of the mode used most often that month was used. The results of the calculation of the electrical energy required by the HVAC system to meet the loads imposed by the DHW system on the space are shown in Table 26.

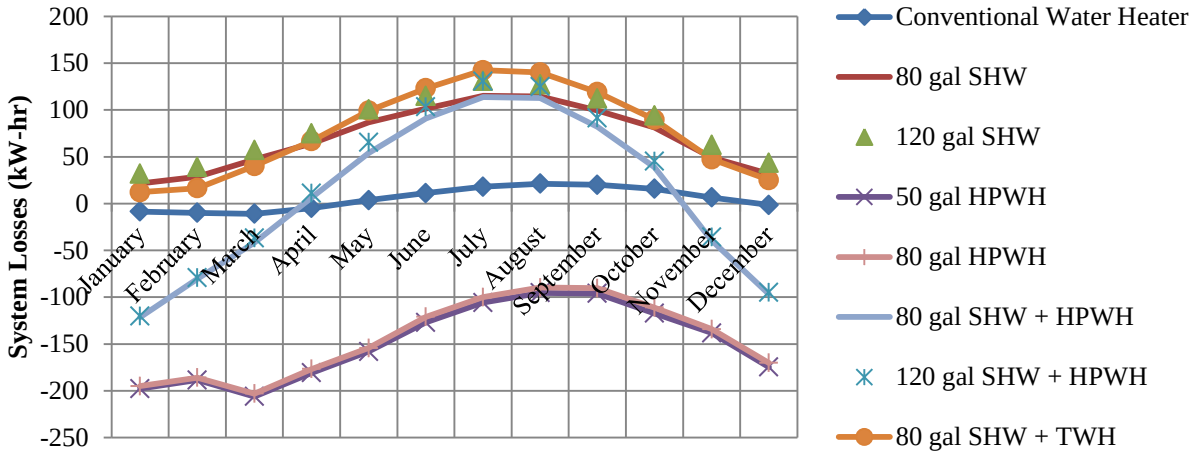

Figure 35. Net Load Imposed on HVAC System by DHW System.

Table 26. Electrical Energy Required by HVAC System Resulting from DHW System Losses.

	HVAC Heat Pump COP	Conv. Water Heater	80 gal SHW	120 gal SHW	50 gal HPWH	80 gal HPWH	80 gal SHW + HPWH	120 gal SHW + HPWH	80gal SHW + Instantaneous
January	1.72	5	-13	-19	115	113	70	70	-7
February	2.17	5	-13	-18	87	86	37	36	-8
March	2.19	5	-22	-26	94	93	19	17	-18
April	2.23	2	-29	-34	81	79	-3	-5	-30
May	3.39	1	26	30	-47	-46	16	19	29
June	3.05	4	33	38	-42	-40	30	34	40
July	3.03	6	38	43	-35	-33	38	43	47
August	2.89	7	40	44	-33	-31	39	43	48
September	2.71	7	37	41	-35	-33	30	34	44
October	2.15	7	38	44	-55	-52	18	21	42
November	2.1	-3	-23	-30	66	64	19	17	-23
December	2.32	1	-14	-19	75	73	42	41	-11
Total		**47**	**98**	**95**	**272**	**274**	**355**	**371**	**154**

*The heat pump is assumed to be in heating mode November through April and in cooling mode May through October.

Each DHW system introduces a thermal load to the house because of its net losses, and Table 26 shows that this thermal load may either reduce or increase the electrical energy required by the HVAC system, depending on the season and the particular DHW system. During the heating season, the stand-alone SHW systems and the SHW + TWH system reduce the

energy required by the HVAC system, while the stand-alone HPWH systems reduce the energy required by the HVAC system in the cooling season. The combined SHW + HPWH systems increase the energy required by the HVAC system every month except for April. This is because during the heating season, the HPWH, which cools the space, meets the majority of the load, while in the cooling season, the SHW system, which heats the space, meets the majority of the load. In April, the heat pump is still considered to be in heating mode in this study, and the overall thermal losses from the DHW system are positive, although they are small. Overall, the conventional water heater requires the least amount of HVAC electrical energy, while the 120 gal SHW + HPWH system requires the most. Considering both the electrical energy required by the DHW system itself as well as the electrical energy required by the HVAC system as an effect of the operation of the DHW system when calculating the annual COP of the system results in a modified COP. Table 27 lists both the traditional and modified annual COP for each system configuration. Modifying the COP to include the HVAC electrical energy required by the DHW system reduces the COP of the combined SHW + HPWH systems by approximately 20%, but only reduces the COP of the stand-alone SHW systems by 4%.

Table 27. Comparison of DHW System COP and Modified COP.

	COP	Modified COP
Baseline	0.94	0.93
80 gal SHW	1.39	1.34
120 gal SHW	1.39	1.34
50 gal HPWH	1.89	1.64
80 gal HPWH	1.83	1.59
80 gal SHW + HPWH	2.86	2.19
120 gal SHW + HPWH	2.85	2.16
80 gal SHW + TWH	1.74	1.61

Chapter 4: Evaluation of Alternate HVAC Systems and Controls

4.1 Evaluation of Ventilation Systems

The amount of ventilation for the house required is specified according to ASHRAE Standard 62.2 [33]. There are multiple options regarding the equipment used to meet this ventilation requirement. In this study, a heat recovery ventilator (HRV) system, an energy recovery ventilation (ERV) system, and a system without heat recovery were compared to a baseline of no ventilation.

4.1.1 *Description of Ventilation Systems*

The ventilation equipment used in the NZERTF during the first year of operation was an HRV. The HRV acts as a sensible heat exchanger, transferring energy between the flow of fresh air coming into the house from the outdoors and the flow of return air exiting the house. An ERV, in contrast, transfers both heat and moisture between the two streams.

The HRV used in the NZERTF and the method used to model the HRV was described in Section 1.3.1.2 and Section 2.1.2. For a more consistent comparison between the ventilation systems, the un-tuned model of the HRV was used, with the exception of the flowrate, which was set to the measured annual average flowrate through the HRV.

The ERV, a Venmar AVS E15 ECM ERV, is very similar to the HRV except for the core. It is manufactured by the same company, is the same size, and uses the same defrost cycle. The ERV core differs from the HRV core in that the ERV core is made of polymerized paper and has two Merv 7 filters, while the HRV core is made of polypropylene and has two Merv 9

filters. Both the ERV's and the HRV's core are crossflow exchangers and have 10.2 m^2 of surface area.

The ERV was modeled in TRNSYS using the same type as the HRV, Type667b. The power, sensible effectiveness, and latent effectiveness coefficients were determined in the same way the un-tuned HRV power and sensible effectiveness coefficients were determined. The manufacturer specifications were used to fit curves correlating the apparent sensible effectiveness, latent recovery, and the power consumed to the air flowrate.

The system without heat recovery simply brings in fresh air from the outdoors. It is assumed that this system uses only one supply fan which uses half of the power required by the HRV.

Table 28 compares the sensible effectiveness, latent effectiveness, air flowrate, and total power for each ventilation system.

Table 28. Annual Average Performance of Ventilation Systems.

Ventilation System	Sensible Efficiency	Latent Efficiency	Flow Rate (cfm)	Power (W)
Measured	0.72	0	115	62.8
HRV	0.73	0.01	115	54
ERV	0.68	0.47	115	60
No Heat Recovery	0.00	0.00	115	27
No Ventilation	0	0	0	0

4.1.2 *Results*

The sensible and latent loads introduced to the house varied depending on the ventilation system used. Figure 36 shows the sensible and latent loads introduced by the HRV, the ERV,

and the system without heat exchange. For comparison, the measured sensible and latent loads from the first year of NZERTF operation are also shown. The system without heat exchange introduces the largest absolute value of the sensible loads in both the winter and the summer. However, in the winter the difference between the average outdoor and indoor temperatures is much greater than in the summer, so the introduced sensible load is much greater in the winter. The latent loads introduced by the system with no heat exchange and the HRV are approximately equal because the only latent heat exchange taking place in the HRV is a small amount of leakage between the two air streams. The sensible load introduced by the HRV is much less than the system with no heat exchange. The ERV introduces the smallest latent load, but the sensible load introduced is slightly greater than the sensible load introduced by the HRV because of its lower sensible effectiveness. The total sensible and latent loads introduced by each system are listed in Table 29.

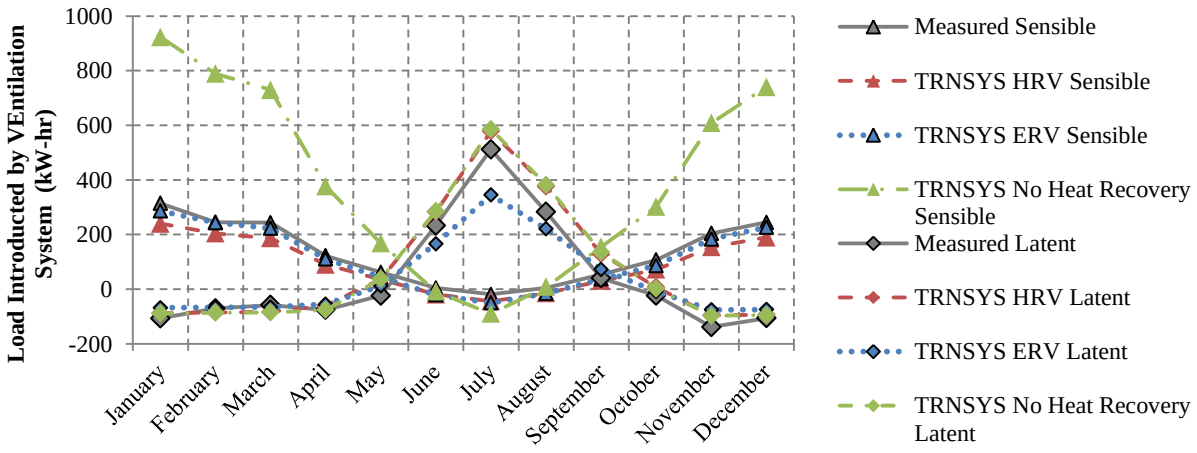

Figure 36. Monthly Sensible and Latent Loads Introduced by Ventilation Systems.

Table 29. Total Annual Sensible and Latent Loads Introduced by Ventilation Systems.

Ventilation System	Sensible Load Introduced (kWh)	Latent Load Introduced (kWh)
HRV	1124	905
ERV	1355	402
No Heat Recovery	4704	899
No Ventilation System	0	0

The loads introduced by the ventilation system must be met by the air-source heat pump. Figure 37 and Table 30 compare the thermal loads of the house using an HRV, ERV, a system with no heat exchange, to a house with no ventilation system. No ventilation significantly reduces the heating and cooling loads. The system with no heat exchange has a similar cooling load to the HRV, but the heating load is much greater. The ERV's heating load is slightly greater than the HRV's heating load, but the cooling load is significantly less.

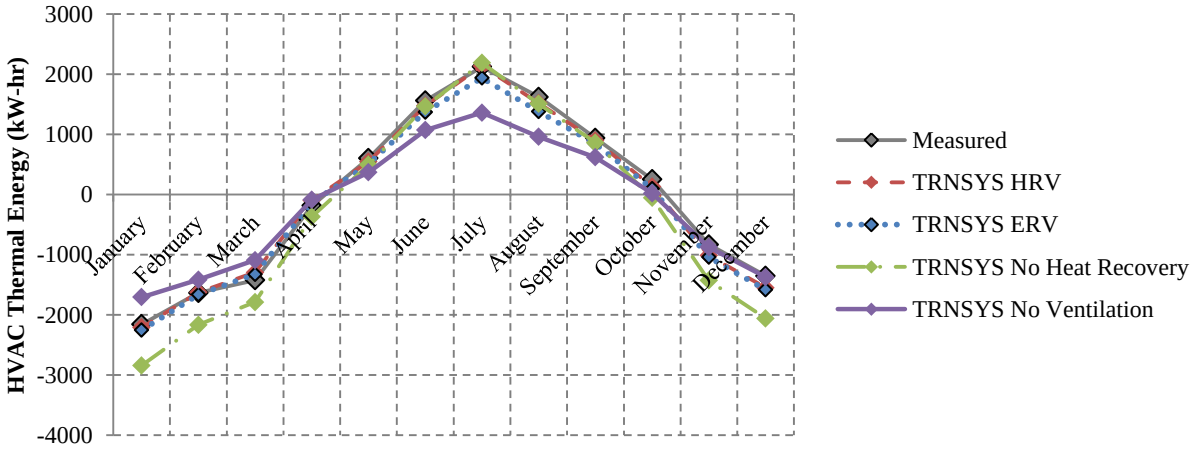

Figure 37. Monthly Thermal Energy Required When Using Each Ventilation System.

Table 30. Annual Total Thermal Load Met by Air-Source Heat Pump When Using Each Ventilation System.

	Heating (kWh)	Cooling (kWh)	Total (kWh)
Measured	-7707	7218	-489
HRV	-7985	6891	-1095
ERV	-8199	6323	-1876
No HX	-10960	6762	-4198
No Vent.	-7037	5561	-2161

The differences in thermal loads result in differences in the electrical energy required by the air-source heat pump. Figure 38 compares the electrical energy consumed by the heat pump each month using each ventilation system to the electrical energy consumed by the heat pump if there were no ventilation system. The ERV's smaller latent load introduced in the summer results in significant energy savings in the cooling season.

Table 31 compares the electrical energy consumed by the heat pump and the ventilation system to the electrical energy consumed by the heat pump if there were no ventilation system. The simple ventilation system with no heat exchange consumes the least amount of energy, but the loads it introduces to the house results in the heat pump requiring over 1000 kWh more energy than the heat pump would require with an HRV or ERV. As shown in Table 28, the manufacturer specified that the ERV requires slightly more electrical energy than the HRV. Also, it introduces a larger sensible load, so the heat pump uses slightly more electrical energy during the heating season using the ERV than the HRV. However, the ERV greatly reduces the latent energy introduced during the cooling season. The heat pump's dedicated dehumidification mode has a low COP, so using the ERV results in significant

energy savings over the HRV during the cooling season. In total, the ERV saves 283 kWh over the HRV, which is 4.3 % of the total HVAC electrical energy using the HRV.

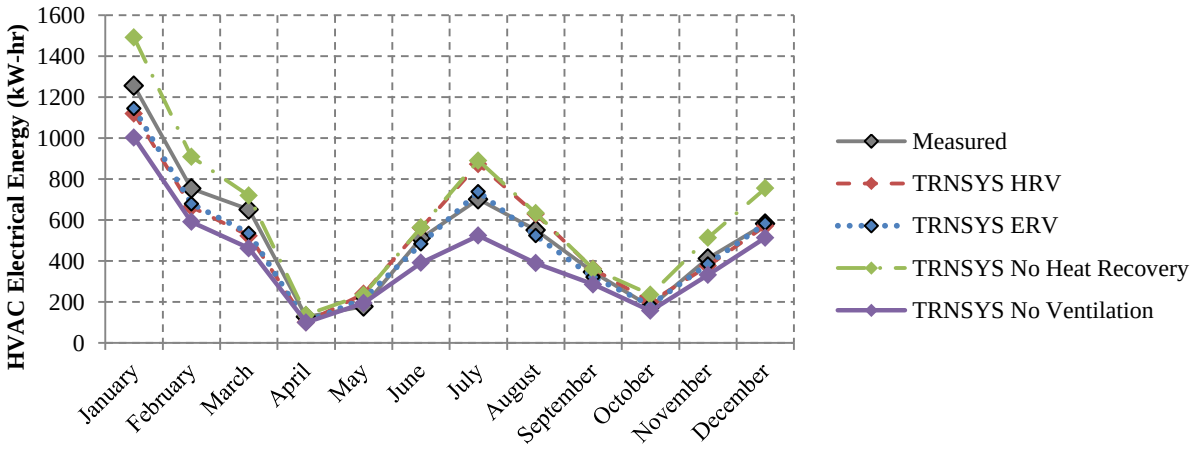

Figure 38. Monthly Electrical Energy Required When Using Each Ventilation System.

Table 31. Annual Total HVAC Electrical Energy Required Using Each Ventilation System.

	Fan Energy Consumption (kWh)	Heating Electrical Energy (kWh)	Cooling Electrical Energy (kWh)	Total Heat Pump Electrical Energy (kWh)	Total Consumption (Heat Pump + Ventilation) (kWh)	Total Consumption Percent Difference (%)
Measured	514	3783	2458	6241	6755	36.9
HRV	439	3380	2832	6212	6651	34.7
ERV	479	3464	2425	5889	6368	29.0
No Heat Recovery	226	4615	2821	7436	7662	55.2
No Ventilation System	0	3008	1928	4936	4936	---

4.1.3 *Discussion and Future Work*

TRNYSYS simulations of ventilation systems show that ventilation increases the total energy consumption of the HVAC system by 29 % to 55 %. This is a significant increase in energy

consumption. Choosing a ventilation system that provides the fresh air required for the health and comfort of the home while minimizing the added cost of the ventilation is desirable. From purely an energy consumption standpoint, the simulations show that the ERV is the best choice in ventilation systems. However, the ERV only reduces the energy consumption of the HVAC system by 4.3 % over the HRV, and ERV systems may have higher initial and maintenance costs. An economic analysis of an HRV versus an ERV is outside of the scope of this thesis.

The results of these simulations are specific to the location of the NZERTF. Gaithersburg, MD has a mixed, humid climate. The relative impact of these ventilation systems on the space conditioning equipment's energy consumption is expected to change if the house were located in a different climate zone.

4.2 Evaluation of Alternate Air-Source Heat Pump Control Logic

The air-source heat pump's (ASHP) thermostat control logic can have a great impact on the energy consumption of the heat pump, as was seen when tuning the thermostat control logic for the whole-house NZERTF model. When using the thermostat control logic specified for the first year of operation, the heat pump would often go into higher stages because the time-out limit for the lower stage would be reached. The higher stages are less efficient, so the time-out limit may have caused the heat pump to use more energy than necessary to stay within the temperature deadband. Also, it was found during the first year of operation that one thermostat on the first floor was not sufficient for maintaining the temperature and humidity setpoints on both floors. During the second year of operation, an alternate thermostat control logic was used that incorporates thermostats on both floors and that does

not include time-out limits for the heating and cooling modes. Other changes were also made to the operation of the NZERTF during the second year of operation, so to isolate the impact that the thermostat change had on energy consumption, a simulation was run using the tuned TRNSYS NZERTF model with the alternate thermostat control logic.

4.2.1 *Description of Alternate Ventilation System*

During the second year of operation of the NZERTF, the space conditioning logic was changed. During the first year of operation, the single thermostat located in the living room on the first floor was used to control the heat pump. For the second year of operation, a second thermostat was installed in the main hallway on the second floor. The temperature and humidity read at each of these locations was averaged, and this averaged temperature and humidity was used to determine the heat pump operation. In addition, during the second year of operation the time-out limits causing the heat pump to switch from a lower stage to a higher stage were removed. The temperature deadbands set during the first year of operation remained for the second year of operation.

4.2.2 *Results*

Other changes were also made to the HVAC system for the second year of operation. To isolate and analyze the effect of the change in the thermostat logic, simulations were run with the old and new control logic and the results were compared. The following plots, Figure 39 and Figure 40, shows thermal energy required to be supplied by the heat pump and the electrical energy consumed by the heat pump using the old and the new thermostat control logic.

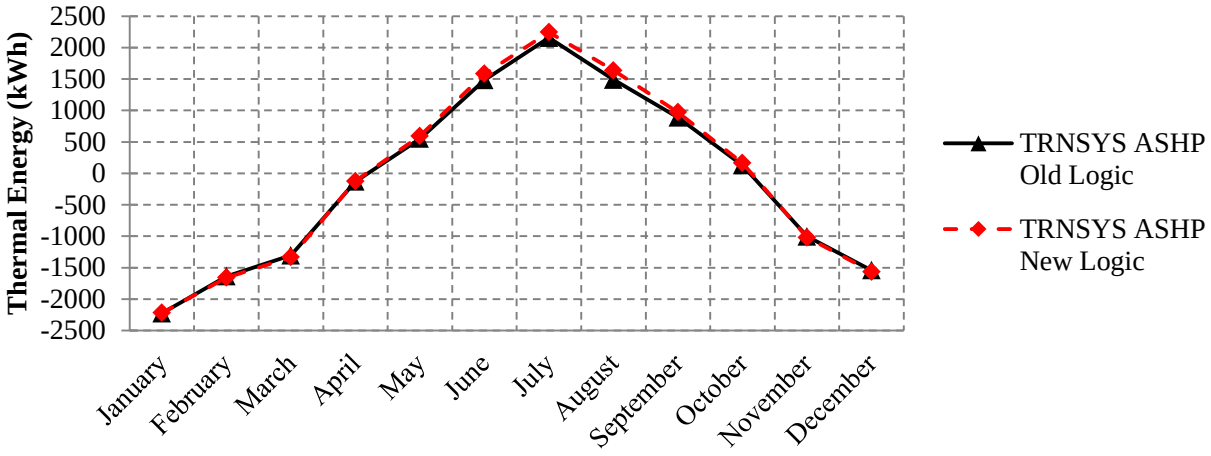

Figure 39. Monthly Average Thermal Energy Using Old Thermostat Control Logic vs. New Thermostat Control Logic.

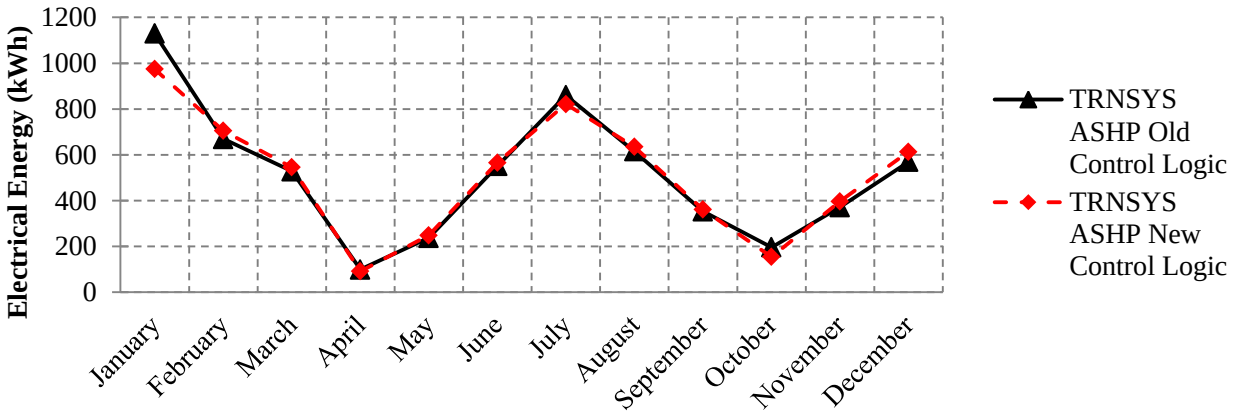

Figure 40. Monthly Average Electrical Energy Using Old Thermostat Control Logic vs. New Thermostat Control Logic.

The plots of the thermal and electrical energy show little difference between the old and new control logic. To understand the effects of the changes in thermostat logic, the heat pump energy for each stage and mode must be analyzed. Table 32 shows the thermal energy for heating and cooling and the electrical energy used by each stage and mode of the heat pump.

Table 32. Thermal Energy and Energy Consumption of ASHP Using Old vs. New Thermostat Control Logic

	Old Thermostat Control Logic	New Thermostat Control Logic	Percent Difference
Heating Thermal Energy	-8026	-8083	1%
Cooling Thermal Energy	6879	7370	7%
1st Stage Heating	1193	2334	96%
2nd Stage Heating	1249	426	-66%
3rd Stage Heating	463	0	-100%
Defrost	360	479	33%
1st Stage Cooling	830	1280	54%
2nd Stage Cooling	363	0	-100%
Dehumidification	1485	1408	-5%
Standby	256	228	-11%
Total Heating Electrical Energy	3402	3315	-3%
Total Cooling Electrical Energy	2780	2801	1%
Total Electrical Energy	6183	6116	-1%

Eliminating the time-out limits caused the second and third heat pump stages in heating mode to run much less frequently using the new control logic. In fact, using the new control logic caused the third stage to never turn on. However, the first stage in heating mode ran much more with the new logic than with the old logic. Because the defrost mode is triggered after 90 min. of compressor runtime if the outdoor temperature is below 1.1 ^{0}C, the longer runtime of the compressor using the new control logic caused the defrost cycle to turn on more often and resulted in a 33 % increase in defrost mode energy consumption. Overall, in heating mode, the new control logic caused a decrease in the second and third stage electrical

consumption but an increase in the electrical consumption of the first stage and defrost modes, resulting in only a 3% decrease in total heating electrical consumption.

As with the heating mode, the first stage in cooling mode also ran more frequently and the second stage ran less frequently with the new control logic than with the old logic. The dehumidification mode consumed slightly less energy, which is likely caused by the cooling mode running for longer periods of time. Overall, using the new control logic demanded more cooling thermal energy, but the more efficient first stage ran more often, resulting in an increase in the cooling electrical energy consumption of only 1 %.

Averaging the first and second stage temperatures and relative humidities caused a 1 % increase in the heating thermal energy and a 7 % increase in the cooling thermal energy. The averaging of the first and second floor temperatures resulted in cooler temperatures on both first and second floors using the new control logic, as can be seen in Figure 41. The new control logic allowed the monthly average relative humidity on both floors to increase by 0.1 % to 1.2 %. The slightly higher relative humidity is likely caused by the lower zone temperatures and the longer heat pump runtimes using the new control logic. The monthly average relative humidity for each zone can be seen in Figure 42.

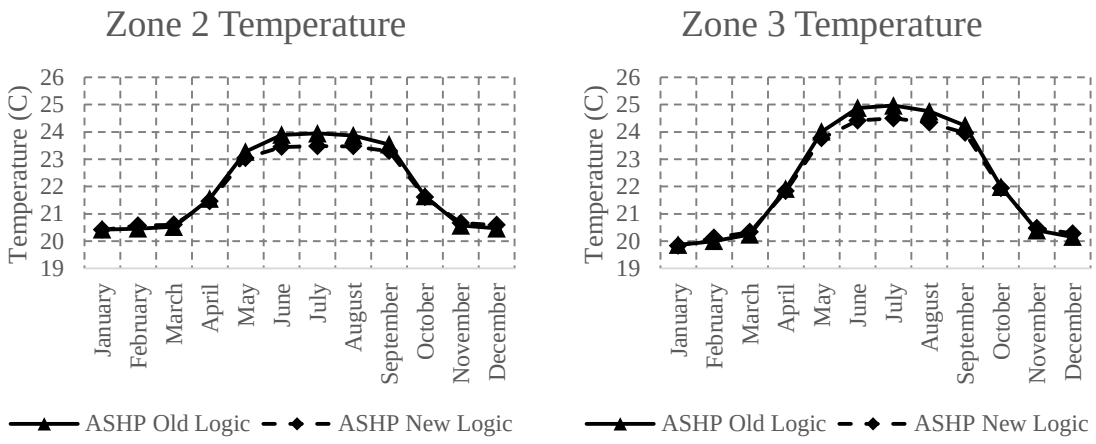

Figure 41. Zone 2 and Zone 3 Air Temperature with ASHP Old Thermostat Control Logic vs. New Thermostat Control Logic.

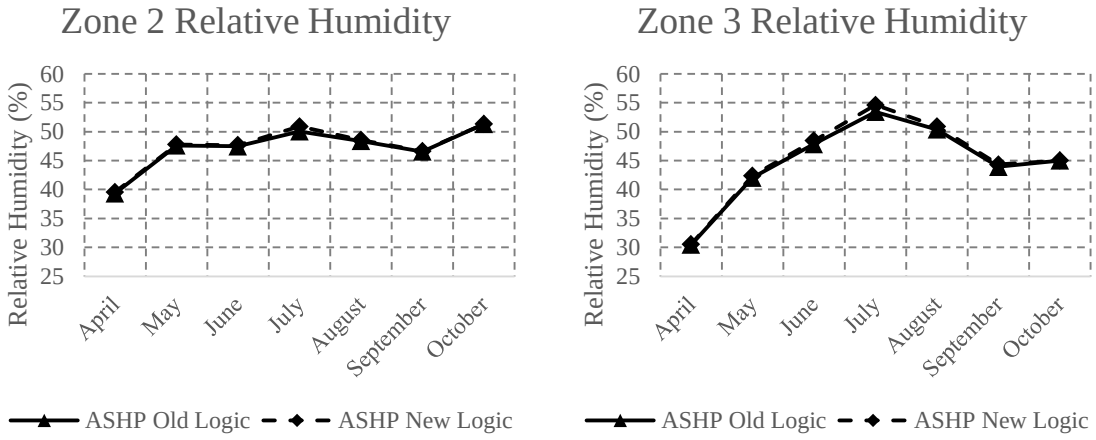

Figure 42. Zone 2 and Zone 3 Relative Humidity with ASHP Old Thermostat Control Logic vs. New Thermostat Control Logic.

4.2.3 *Discussion and Future Work*

According to the simulation results, the new thermostat logic slightly reduces the temperature and slightly increases the relative humidity on both the first and second floors during the summer months. The change in temperature during the winter is minute. This reduction in temperature during the summer results in a small increase in the thermal load. The larger thermal load requires the heat pump to run more, but removing the time-out limit prevents

the heat pump from unnecessarily going into the less efficient second stage, so overall the energy consumption during the cooling season differs by only 1 %. The thermal load during the heating season is approximately equal between the old and new logic. However, the removal of the time-out limits results in the heat pump never going into the less efficient higher stages less often. However, the first stage has a lower capacity than the higher stages and much run for more time than it had using the old logic. In addition to longer runtimes requiring more energy, it also triggers the defrost cycle more often. Overall, the simulation predicted that the new thermostat logic reduced the energy consumption during the heating season by only 87 kWh, which is a 3 % difference.

Future work on alternate thermostat control logic should consider varying the setpoint and increasing the deadbands. Other climates should also be considered for a more robust study on alternate control logics.

4.3 Evaluation of Ground-Source Heat Pump vs. Air-Source Heat Pump

Although an air-source heat pump (ASHP) has been used for the first two years of operation, the NZERTF has the capability of using a ground-source heat pump (GSHP) instead of the air-source heat pump. Three types of boreholes have been installed at the NZERTF: vertical boreholes, horizontal boreholes, and slinky boreholes. Simulations were run to predict the performance of a GSHP using the vertical boreholes compared to the ASHP.

4.3.1 *Description of the Energy Equipment*

No GSHP has been installed in the NZERTF, so a two speed, two ton WaterFurnace 3 Series - 300A11 geothermal heat pump was chosen as the piece of equipment on which to base the model of the heat pump. The cooling capacity of this heat pump at full load is rated as 6770

W with an EER of 4.6, and the heating capacity at full load is rated as 5539 W with a COP of 3.8 [55]. The rated conditions are specified by AHRI/ISO 13256-1 GLHP standards [56]. The GSHP was modeled using Type 919, a water-source heat pump model with normalized performance. The manufacturer specifications give the rated heating and cooling capacities at full as well as at part loads. The auxiliary heater that is activated when the heat pump is in third stage in heating mode is rated at 4800 W. The blower is a 5-speed ECM motor. The manufacturer specifications give the airflow rate for each blower motor speed at various external static pressures, which was assumed to be 0.2 inches water gauge. The manufacturer specifications also give performance corrections for using various antifreeze solutions, for air flows differing from nominal at full load and part load, for a range of entering air temperatures, and for a range of entering water temperatures. These performance corrections were used to create new performance maps for the ground-source heat pump.

During the second year of operation of the NZERTF, the dedicated dehumidification mode on the air-source heat pump was deactivated and a separate dehumidifier was used. The dehumidifier, an UltraAire 70H model, was installed in the basement of the house and was connected to the existing heat pump ductwork [57]. The humidistat, an UltraAire DEH 3000 [58], uses control logic similar to that used for the dedicated dehumidification mode in the air-source heat pump. The dehumidifier turns on at a relative humidity above 50% when the heat pump is not in operation. The deadband was specified as 3 % by the manufacturer specifications. Unlike the ASHP, the GSHP does not have a dedicated dehumidification mode. To meet the latent cooling load, the UltraAire dehumidifier was added to the GSHP HVAC system model. To model the dehumidifier, Type 921, a residential/commercial air

conditioner was used. Measured power and capacity data from two days during which the dehumidifier ran for substantial amounts of time were used to determine the performance of the unit. The performance maps were created using the measured data and were changed so that the capacity and power were a function of only the relative humidity. When in operation, the airflow through the dehumidifier was specified at a constant 115 cfm, which was the average measured airflow.

According to the measured data, the air exiting the dehumidifier was warmer than it was entering the dehumidifier. The dehumidifier model, Type 921, is unable to both dehumidify and heat the air, so the dehumidifier was modeled as having only latent capacity (no sensible capacity) and Type121b, an auxiliary air heater, was used to add heat to the dry air exiting the dehumidifier. The load added to the dry air by the auxiliary air heater was calculated each time step according to the following energy balance.

$$\dot{\boldsymbol{Q}}_{\boldsymbol{sens}} = \dot{\boldsymbol{W}} + \dot{\boldsymbol{Q}}_{\boldsymbol{lat}} \quad \textbf{(14)}$$

where $\dot{Q}_{sens}$ is the sensible heat added to the dry air exiting the dehumidifier, $\dot{W}$ is the work done by the compressor, and $\dot{Q}_{lat}$ is the latent heat removed from the air entering the dehumidifier. Although the total electrical energy consumed by the dehumidifier is measured, the electrical energy consumed by the dehumidifier's compressor and blower individually is not measured. The relation delineated in Equation 14 was used to determine the compressor power; the measured latent heat removed from the air was subtracted from the sensible heat added to the air at a relative humidity of 50 %. The blower power was then determined by subtracting the calculated compressor power from the total measured power at

a relative humidity of 50 %. The blower power was calculated to be approximately 200 W and was assumed to be constant when the dehumidifier was in operation. The compressor power at other relative humidities at each time step was then determined by subtracting this blower power from the total power interpolated from the performance maps. The values for the parameters required by the GSHP, the dehumidifier, and the auxiliary air heater are listed in Table A-13 in Appendix A.

There are three vertical boreholes, spaced 6.1 m to 6.7 m apart and each reaching a depth of 45.1 m. Davis, et. al. gives additional dimensions and the location of the boreholes [41]. The other parameters required to model the borehole, such as the thermal conductivity and heat capacity of the ground, were determined by Brian Leyde and discussed in [23]. The vertical boreholes were modeled using Type 557. The parameters for this type and their specified values are given in Table A-13 in Appendix A.

The fluid used in the geothermal heat pump is Environol 1000, which is a solution of 75 % water, 20 % ethanol, and 5 % isopropanol (percentages are by weight). The fluid properties required by the borehole and heat pump types were given by the manufacturer's fluid specification catalog [59].

4.3.2 *Results*

4.3.2.1 ASHP vs. GSHP (With Dehumidification)

For the comparison of ground-source vs. air-source heat pumps, the second year thermostat control logic discussed in Section 4.2.1 was used. Figure 43 shows electrical energy consumed by the ASHP using the new thermostat logic versus the GSHP and dehumidifier using the new thermostat logic.

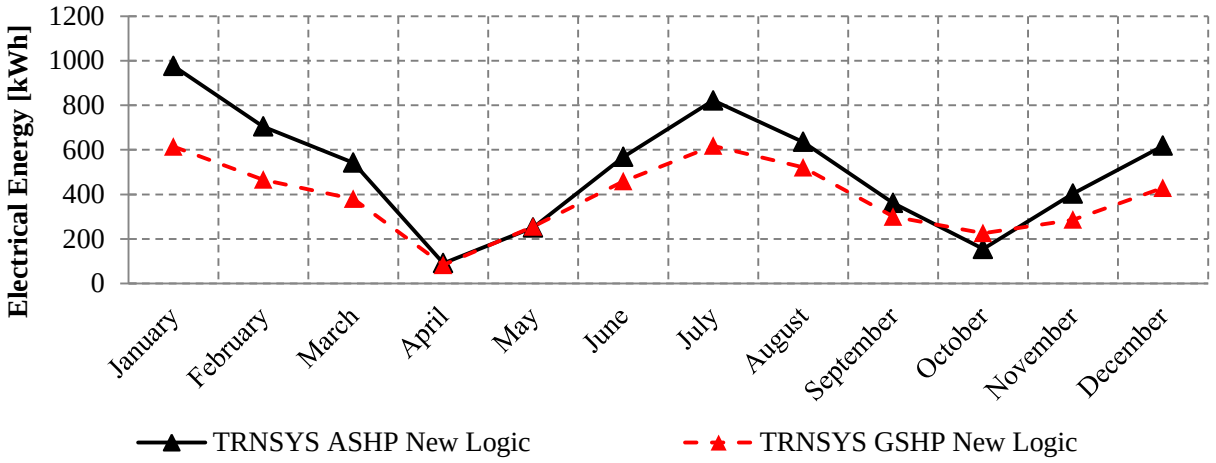

Figure 43. Monthly Average Electrical Energy Consumption of ASHP vs. GSHP with Dehumidifier.

The GSHP system with a dehumidifier reduces the electrical energy required to condition the house. It is a more efficient system than the ASHP largely due to the ground being warmer than the air in the winter and cooler than the air in the summer. Figure 44 shows the monthly average ground and air temperatures over the course of the year.

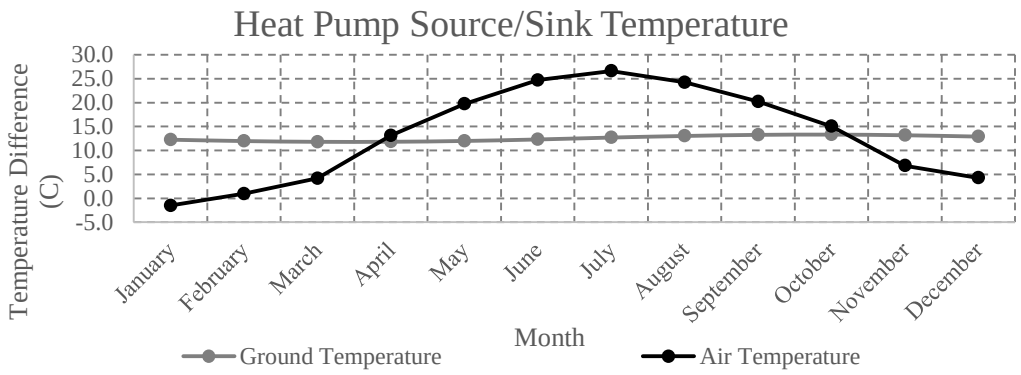

Figure 44. Monthly Average Borehole Ground Temperature and Air Temperature.

Although Figure 43 clearly shows that the GSHP system uses less energy than the ASHP system, useful information can be gained by looking at the energy use by stage and mode. Table 33 lists the energy consumed by each stage of the ASHP and the GSHP, and by the dehumidifier.

Table 33. Annual Thermal Energy and Energy Consumption of ASHP vs. GSHP with Dehumidifier.

	ASHP (kWh)	GSHP with Dehumidifier (kWh)	Percent Difference
Heating Thermal Energy	-8083	-7942	-2%
Cooling Thermal Energy	7370	7490	2%
1st and 2nd Stage Heating	2760	2125	-23%
3rd Stage Heating	0	0	-
Defrost	479	0	-100%
1st and 2nd Stage Cooling	1280	1482	16%
Dehumidification	1408	828	-41%
Standby	228	204	-11%
Total Heating Electrical Energy	3315	2254	-32%
Total Cooling Electrical Energy	2801	2385	-15%
Total Electrical Energy	6116	4639	-24%

Table 33 shows that the heating and cooling thermal energies required by the ASHP system and the GSHP system are almost identical. This is corroborated by the monthly average temperatures and relative humidites of Zones 2 and 3 predicted by the simulations using each type of heat pump. The predicted temperatures are virtually identical. The relative humidity predicted by each simulation is similar, but the relative humidity in the house using the GSHP is somewhat higher than in the house using the ASHP. The dehumidifier has a lower airflow and a lower capacity than the ASHP's dedicated dehumidification mode and it is not able to maintain the relative humidity setpoint in the simulation. Despite a longer runtime during the cooling season, 1513 hr versus the dedicated dehumidification mode's 1207 hr runtime, the condensate from the dehumidifier totaled 906 L over the course of the cooling

season while the dedicated dehumidifier condensed 2145 L during the cooling season. These temperatures and relative humidities can be seen in Figure 45 and Figure 46. Only the cooling season months are shown because it is only during the cooling season that there is control logic applied to the humidity.

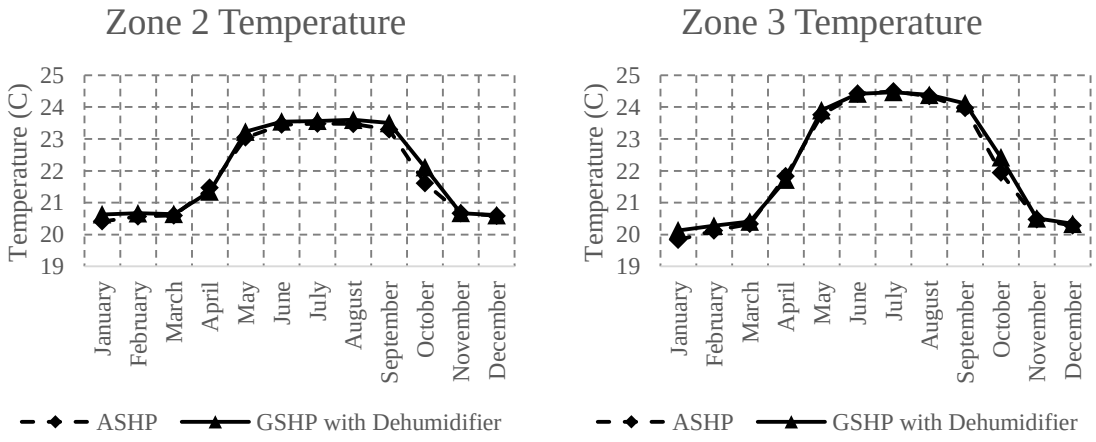

Figure 45. Zone 2 and Zone 3 Air Temperature with ASHP System vs. GSHP with Dehumididifier System.

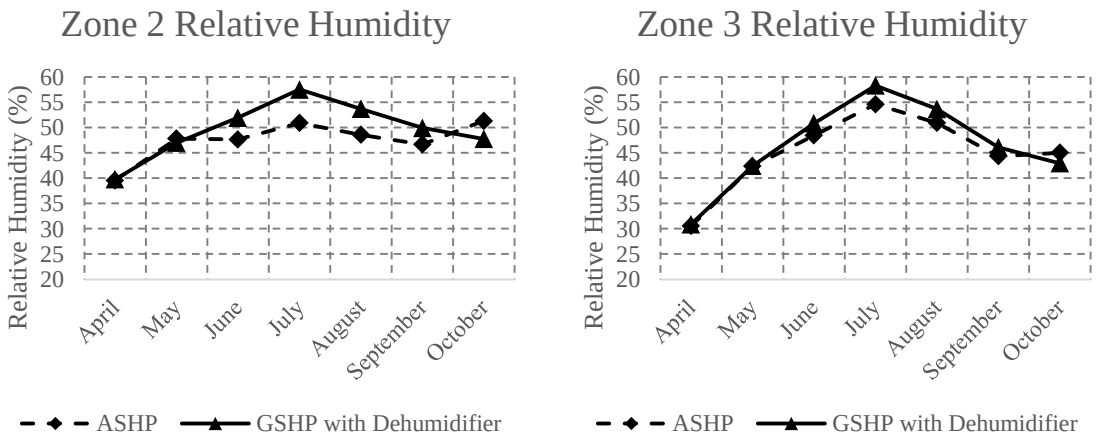

Figure 46. Zone 2 and Zone 3 Air Relative Humidity with ASHP System vs. GSHP with Dehumidifier System.

Overall, the total electrical energy required in heating mode is reduced by 32 % by the GSHP. As with the ASHP system with the new thermostat control logic, the third stage in

heating mode is never activated because the average temperature of Zones 2 and 3 never falls 3.3 ^{0}C below the setpoint. The energy used by the GSHP in both first and second stage cooling is 23 % less than that used by the ASHP in first and second stage. No defrosting is required for the GSHP, which further reduces the energy consumed in heating mode by the GSHP.

The GSHP reduces the total electrical energy required in cooling mode by 15 %. The GSHP requires 16 % more electrical energy for the first and second stage cooling than the ASHP does. This is primarily caused by differences in the dehumidification between the GSHP system and the ASHP system. The dehumidifier in the GSHP system added heat to the supply air because the condenser is located inside the house, while the ASHP dedicated dehumidification mode both dehumidifies and cools the air because the condenser is located in the split-system heat pump's outdoor unit. The TRNSYS simulation predicted the monthly averages of the sensible heat rejected by the dehumidifier to be between 756 W and 778 W. The sensible heat rejected was measured to range between 650 W to 800 W, depending on the relative humidity, which corresponds well to the predicted heat rejected. The energy used by the dehumidifier is lower than the energy used by the ASHP's dedicated dehumidification mode. This is caused by the dehumidifier having a smaller capacity and power consumption than the dedicated dehumidification mode, not because the dehumidifier is more efficient. The average COP (defined here as latent capacity divided by power) of the dehumidifier in July was 0.79, while the COP of the dedicated dehumidification mode was 1.1.

4.3.2.2 ASHP vs. GSHP (With No Dehumidification)

To gain a better sense of the performance of the GSHP system itself compared to the ASHP, simulations were run with the dehumidifier removed and the dedicated dehumidification mode deactivated. Figure 47 shows the electrical consumption of the ASHP with the dedicated dehumidification mode deactivated comparted to the GSHP system without the dehumidifier. Also shown are ASHP and GSHP systems with dehumidification, as was show in Figure 43.

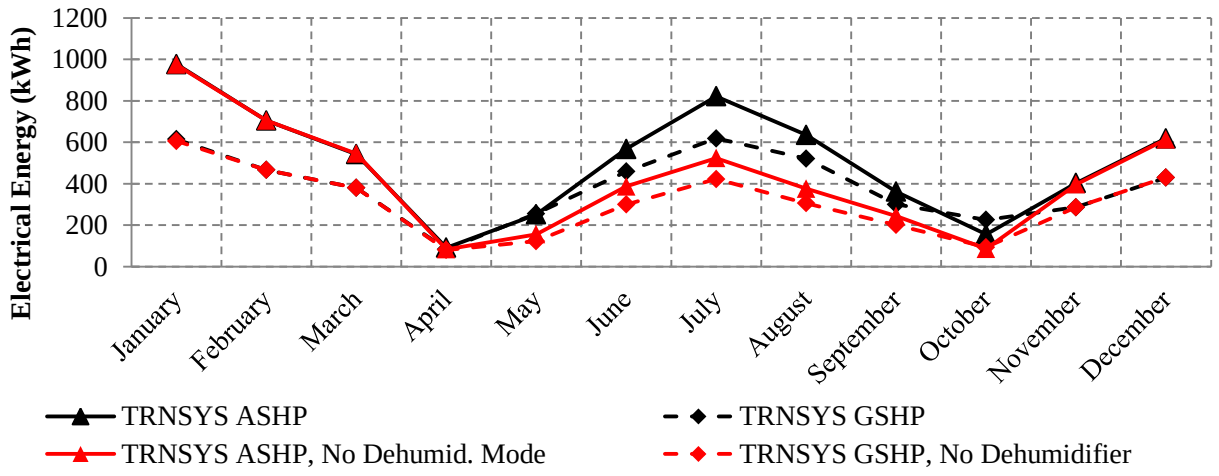

Figure 47. Monthly Average Energy Consumption of ASHP vs. GSHP, With and Without Dehumidfication.

Figure 47 shows that removing the dehumidification function from the ASHP and GSHP systems significantly reduces the electrical energy consumed during the cooling season. Without the dedicated dehumidification mode activated or the dehumidifier in operation, the ASHP and GSHP systems maintain similar indoor comfort conditions. Figure 48 shows the relative humidity in Zones 2 and 3 when the relative humidity is allowed to float. The relative humidity in the house with the GSHP system is only slightly higher when no

dehumidifier is in place. The dehumidifier has low airflow and a relatively small capacity, so it was not able to maintain the relative humidity setpoint when it was operating.

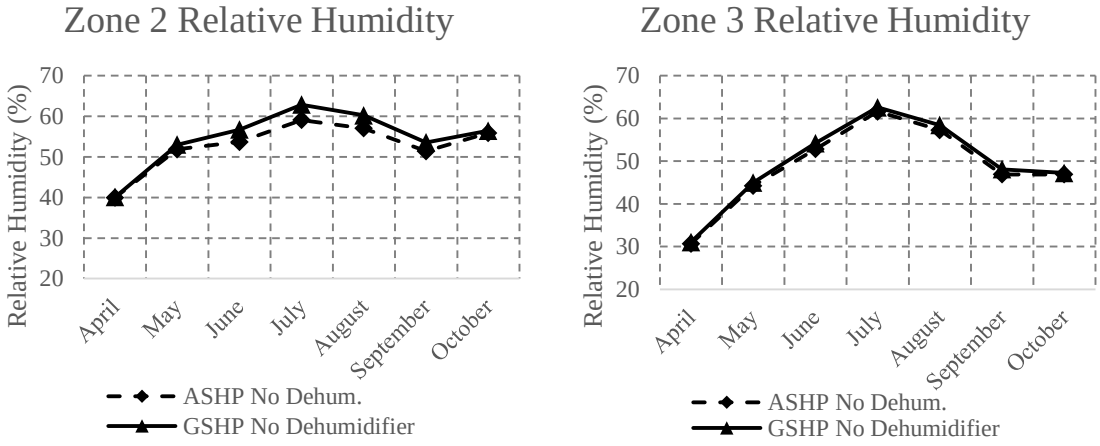

Figure 48. Zone 2 and Zone 3 Air Relative Humidity with ASHP System vs. GSHP with No Dehumidification.

Table 34 shows the energy consumed by each heat pump stage of the ASHP with the dedicated dehumidification mode deactivated and of the GSHP with no dehumidifier. Both systems use the new thermostat control logic, as described in Section 4.2.1.

Table 34. Annual Thermal Energy and Energy Consumption of ASHP vs. GSHP with No Dehumidification.

	ASHP	GSHP	Percent Difference
Heating Thermal Energy	-8030	-8006	0%
Cooling Thermal Energy	6475	5965	-8%
1st Stage Heating	2323	2121	-9%
2nd Stage Heating	423	14	-97%
3rd Stage Heating	0	0	-
Defrost	479	0	-100%
1st Stage Cooling	3038	1268	-58%
2nd Stage Cooling	0	0	-
Dehumidification	0	0	-
Standby	276	289	5%

Total Heating Electrical Energy	3314	2264	-32%
Total Cooling Electrical Energy	1777	1428	-20%
Total Electrical Energy	5092	3692	-27%

Table 34 shows that when only the heat pumps are compared, without the added complication of comparing a system with a dehumidifier to a system with a dedicated dehumidification mode built into the heat pump, the GSHP reduces the energy consumed by 32 % during heating mode and by 19 % during cooling mode. It also shows that with the dehumidification function removed, the GSHP uses less energy in the first and second stages of cooling than the ASHP. As discussed previously, the GSHP is more energy efficient largely because the ground is warmer than the air during the winter and cooler than the air during the summer.

The difference in the heat pump's cooling thermal energy occurs because of differences in the sensible effectiveness of each heat pump. The ASHP removes more latent energy from the air, resulting in a larger thermal load and lower relative humidity. The ASHP ran for 1203 hours and removed 2441 L of condensate, while the GSHP ran for 1210 hours and removed 1901 L of condensate.

4.3.3 *Discussion and Future Work*

The GSHP system is substantially more energy efficient, especially if temperature control is the only concern. To meet a maximum relative humidity setpoint while using the GSHP, a separate dehumidifier may be used. However, the separate dehumidifier modeled here was

predicted to be unable to maintain a maximum relative humidity of 50 % when used with the GSHP. Incorporating a dehumidifier increases the required energy consumption, as was shown in Figure 47. This significant increase in required energy consumption corroborates the importance of correctly sizing the heat pump so that the heat pump may have the opportunity to dehumidify the space.

Future work on comparing a GSHP with an ASHP should include running the simulation for multiple years to predict the effects the ground heat exchanger has on the ground temperature. A dehumidifier with a larger capacity should be modeled and used with the GSHP so the system is able to meet the maximum relative humidity setpoint. It would also be interesting to find and model a GSHP with a dedicated dehumidification mode for a better comparison with the ASHP used in the NZERTF. To make this study more widely applicable, the simulation should be run in locations with different climates.

References

[1] "Green Building Facts | U.S. Green Building Council." *Green Building Facts*. U.S. Green Building Council, 23 Feb. 2015. Web. 9 Dec. 2015. <http://www.usgbc.org/articles/green-building-facts>.

[2] McCook, K. "U.S. Construction Outlook for the 19th Annual CFO Roundtable and Tax Director Workshop." McGraw Hill Construction. Sept. 2013. Web. 9 Dec. 2015. <http://www.ey.com/media/vwCodeLibraries/TDW2013/$File/Construction_Outlook_2013_Joint_McCook_FINAL.pdf>.

[3] Esterly, S., Gelman, R., Haas, K. "2013 Renewable Energy Data Book." U.S. Department of Energy, Energy Efficiency & Renewable Energy. 2013: 25. < http://www.nrel.gov/docs/fy15osti/62580.pdf>.

[4] "Climate Change and President Obama's Action Plan." *The White House.* The White House, President Barack Obama, n.d. Web. 10 Dec. 2015. <https://www.whitehouse.gov/climate-change>.

[5] "Information Hub Overview: Paris COP 21/CMP 11." *Paris COP21: Information Hub*. United Nations: Framework Convention on Climate Change, 26 Nov. 2015. Web. 9 Dec. 2015. <http://newsroom.unfccc.int/cop21parisinformationhub/2015-un-climate-change-conference-information-hub/>.

[6] Beiter, P., Haas, K. "2014 Renewable Energy Data Book." U.S. Department of Energy, Energy Efficiency & Renewable Energy. 2014: 14. < http://www.nrel.gov/docs/fy16osti/64720.pdf>.

[7] "Annual Energy Outlook 2014 Early Release Table Browser." *AEO Table Browser - Energy Information Administration.* U.S. Energy Information Administration, n.d. Web. <http://www.eia.gov/oiaf/aeo/tablebrowser/#release=AEO2014ER&subject=0-AEO2014ER&table=2-AEO2014ER&region=1-0&cases=full2013-d102312a,ref2014er-d102413a>

[8] "What Are the Energy-related Carbon Dioxide Emissions by Source and Sector for the United States?" U.S. Energy Information Administration, 31 Mar. 2015. Web. 9 Dec. 2015. <https://www.eia.gov/tools/faqs/faq.cfm?id=75&t=11>.

[9] Torcellini, P., S. Pless, M. Deru, and D. Crawley. "Zero Energy Buildings: A Critical Look at the Definition." *ACEEE Summer Study* (2006): n. pag. Web. <http://www.nrel.gov/docs/fy06osti/39833.pdf>.

[10] F. Omar, S. T. Bushby, *Simulating Occupancy in the NIST Net-Zero Energy Residential Test Facility*, NIST Technical Note 1817, 2013.

[11] Klein, S., et al. TRNSYS 17: a TRaNsient System Simulation program – Manual. Solar Energy Laboratory, University of Wisconsin. 2012.

[12] Musall E, Weiss T, Lenoir A, Voss K, Garde F, Donn M. Net Zero energy solar buildings: an overview and analysis on worldwide building projects, EuroSun conference, Graz, Austria, 2010.

[13] Norton P, Christensen C. Performance Results from a Cold Climate Case Study for Affordable Zero Energy Homes. National Renewable Energy Laboratory. ASHRAE Winter Conference. Nov. 2007. Web. < http://www.nrel.gov/docs/fy08osti/42339.pdf>.

[14] Athienitis A, Candanedo J, O'Neill B. Solar Buildings Research Network Demonstration Projects: Towards net zero energy consumption. 26th Conference on Passive and Low Energy Architecture, Quebec City, Canada. June 2009. Web. http://www.plea2009.arc.ulaval.ca/Papers/2.STRATEGIES/2.2%20Heating%20and%20Cooling/ORAL/2-2-01-PLEA2009Quebec.pdf.

[15] Noguchi M, Athienitis A, Delisle V, Ayoub J, Berneche B. Net Zero Energy Homes of the Future: A Case Study of the EcoTerra House in Canada. Renewable Energy Congress, Glasgow, Scotland. July 2008. Web. < https://www.nrcan.gc.ca/sites/www.nrcan.gc.ca/files/canmetenergy/files/pubs/2008-112_OP-J_411-PVTZEH_EcoTerra.pdf>.

[16] Doiron M. Whole Building Energy Analysis and Lessons Learned for a Near Net-Zero Energy Solar House. Master's Thesis. Concordia University. Montreal, Canada. Feb. 2011. Web. <http://spectrum.library.concordia.ca/7132/>.

[17] Rober A, Kummert M. Designing net-zero energy buildings for the future climate, not for the past. Journal of Building and Environment. Vol 55. Sept. 2012: 150-158.

[18] Leckner M, Zmeureanu R. Life cycle cost and energy analysis of a Net Zero Energy House with solar combisystem. Journal of Applied Energy. Vol 88 Issue 1. Jan. 2011: 232-241.

[19] Athienitis, Andreas K., and Liam O'Brien. *Modeling, Design, and Optimization of Net-zero Energy Buildings*. Berlin: Ernst & Sohn, 2015.

[20] J. Kneifel, V. Payne, T. Ullah, L. Ng. *Simulated versus Measured Energy Performance of the NIST Net Zero Energy Residential Test Facility Design,* NIST Special Publication 1182, 2015.

[21] J. Kneifel, W. Healy, J. Filliben, M. Boyd. *Energy Performance Sensitivity of a Net-Zero Energy Home to Design and Use Specifications.* Journal of Building Performance Simulation. Feb. 2015.

[22] J. Kneifel. *Annual Whole Building Energy Simulation of the NIST Net Zero Energy Residential Test Facility Design.* NIST Technical Note 1767. Oct. 2012.

[23] B. Leyde, *TRNSYS Modeling of the NIST Net Zero Energy Residential Test Facility*, (Master's Thesis), University of Wisconsin, Madison, 2014.

[24] *Net Zero Energy Residential Test Facility As Built Architectural Plan*, Building Science Corporation. 2009.

[25] *Net-Zero Energy Residential Test Facility (NZERTF) Homepage* NIST: Engineering Laboratory. Web. 9 Dec. 2015. <http://www.nist.gov/el/nzertf/>.

[26] *Chapter 27- Heat, Air, and Moisture Control in Building Assemblies- 2005 ASHRAE Handbook of Fundamentals*, ASHRAE, Inc., Atlanta, GA, 2005.

[27] *ASHRAE Standard 90.2-2007*. ASHRAE, Inc., Atlanta, GA, 2007.

[28] C. M. James, *Heat and Moisture Transfer in a Bed of Gypsum Boards*, (Master's Thesis), University of Saskatchewan, Saskatoon, 2009.

[29] R. Hendron, C Engebrecht, *Building America House Simulation Protocols,* National Renewable Energy Laboratory, Building Technologies Program, U.S. Department of Energy, 2010.

[30] *2013 ASHRAE Handbook - Fundamentals*. ASHRAE, Inc., Atlanta, GA, 2013.

[31] "Soil, Average." MatWeb Material Property Data. Web.

[32] Powder Mill Report Generator, National Water and Climate Center, NRCS, US Dept. of Agriculture. Web.

[33] ASHRAE. 2007. ASHRAE Standard 62.2-2010. Altanta: American Society of Heating, Refrigerating and Air-conditioning Engineers, Inc.

[34] A. H. Fanney, V. Payne, L. Ng, M. Boyd, F. Omar, M. Davis, H. Skye, B. Dougherty, B. Polidoro, W. Healy, B. Pettit, *Net-Zero and Beyond! Design and Performance of NIST's Net-Zero Energy Residential Test Facility*, Energy and Buildings, Vol. 101, 2015.

[35] "Venmar AVS HRV EKO 1.5 Part no. 43901." Product Sheet. Venmar.

[36] "CB/CC Series Engineering Catalog: Condensers & Condensing Units." Aaon, Inc. Rev. B.

[37] "F1 Series Installation, Operation, Maintenance: Indoor Air Handling Units." Aaon, Inc. Rev. B.

[38] "Robertshaw 9801i2 9825ix User's Manual: Deluxe Progammable Thermostat." Invensys Controls America. Jul. 2006.

[39] Certificate of Product Ratings, AHRI, 2014.

[40] 2008 Standard for Performance Rating of Unitary Air-Conditioning & Air-Source Heat Pump Equipment, ANSI/AHRI Standard 210/240, 2008.

[41] M. Davis, W. Healy, M. Boyd, L. Ng, V. Payne, H. Skye, T. Ullah. *Monitoring Techniques for the Net-Zero Energy Residential Test Facility,* NIST Technical Note 1854, 2014.

[42] System Balance, AAON Coil Products, Inc., 2014.

[43] "HPAK Systems Installation Guide." Heliodyne, Inc. V2.1.1.

[44] "Solar Collectors, Technical Specifications." Heliodyne, Inc. 2011.

[45] "Solar Collector Certification and Rating Sheet: Heliodyne, Inc. GOBI 406 001." Solar Rating & Certification Corporation. Mar. 2011.

[46] "Installation, Operation, and Maintenance Manual for Hybrid Electric Heat Pump Water Heater: Base Model 'PBX'." Hubbell Electric Heater Company. 2012.

[47] B. Spam, K. Hudon, D. Christensen, Laboratory Performance Evaluation of Residential Integrated Heat Pump Water Heaters, NREL, 2011.

[48] Uniform Test Method for Measuring the Energy Consumption of Water Heaters. Code of Federal Regulations Title 10, Chapter 11, Subchapter D, Part 430, Subpart B, Appendix E. 2010.

[49] "E19 / 320 Solar Panel." SunPower Corporation. Dec. 2010.

[50] "5000m, 6000m, & 7000m Inverters." Sunpower Corporation. Jun. 2007.

[51] W. De Soto, *Improvement and Validation of a Model for Photovoltaic Array Performance* (Master's Thesis), University of Wisconsin, Madison, 2004.

[52] W. Desoto, S.A. Klein, W.A. Beckman, PV Reference Parameter Determination, 2005. <https://ees-solver.engr.wisc.edu/>.

[53] L. C. Ng, W. V. Payne, *Energy Use Consequences of Ventilating a Net-Zero Energy House*. NIST Technical Note, Forthcoming.

[54] P. Glanville, D. Kosar, J. Stair, Short-Term Performance of Gas-Fired Tankless Water Heater: Laboratory Characterization, ASHRAE Trans. 119 (2013) 1–22.

[55] "Specification Catalog- 3 Series 300A11 Geothermal Heat Pump." Water-Furnace. Sept. 2014.

[56] "Water-source heat pumps – Testing and rating for performance." ANSI/ARI/ASHRAE ISO Standard 13256-2:1998.

[57] "Installer's & Owner's Manual: UltraAire 70H." Therma-Stor LLC. 2012.

[58] “Installer’s & Owner’s Manual: UltraAire DEH 300.” Therma-Stor LLC. 2008.

[59] “Environol Closed Loop Fluid Specification Catalog.” Environol. Mar. 2011.

Appendix A: Parameters

Table A- 1. Infiltration Parameters

	Parameter	Value	Units
Zone 2	Conditioned space volume	447	m^3
	Zone leakage area	135.1	cm^2
	Stack coefficient	0.00029	1/K
	Wind coefficient	0.000325	
Zone 3	Conditioned space volume	360.5	m^3
	Zone leakage area	108.9	cm^2
	Stack coefficient	0.00029	1/K
	Wind coefficient	0.000325	

Table A- 2. Un-tuned HVAC Control Logic

Mode	Setpoint	Turn-on Trigger	First Stage	Second Stage	Third Stage
Heating	21.11 ^{0}C	Deadband (^{0}C)	0.56	1.1	3.3
		Time Delay (min)	N/A	10	40
Cooling	23.89 ^{0}C	Deadband (^{0}C)	1.1	2.8	N/A
		Time Delay (min)	N/A	40	N/A
Dehumidification	50 % RH	Deadband (% RH)	1	N/A	N/A
		Time Delay (min)	N/A	10	N/A

Table A- 3. Un-tuned HRV Parameters

Type	Parameter	Value	Units
HRV Control Type 1269	Return air flow rate Z1	0	m^3/hr
	Return air flow rate Z2	56.4	m^3/hr
	Return air flow rate Z3	114.6	m^3/hr
	Rated air flow rate	246.2	kg/hr
	Sensible effectiveness coefficient a0	1.273	
	Sensible effectiveness coefficient a1	-0.3246	
	Sensible effectiveness coefficient a2	0.0521	
	Rated sensible effectiveness	72	%
	Defrost Temperature Trigger	-5	C
	Time Recirculating	7	min

	Time Operating Defrost Cycle	25	min
Fan Type 111b (two instances)	Rated flow rate	246.2	kg/hr
	Rated power	27	W
	Motor efficiency	0.9	
	Motor heat loss fraction	1	
	Power coefficient 1	0.5256	
	Power coefficient 2	-0.6726	
	Power coefficient 3	1.1477	
HRV Type 667b	Latent effectiveness (input)	0.01	
	On/Off Control Signal (input)	1	

Table A- 4. Un-tuned HVAC Parameters

	Parameter	Value	Units
Heat Pump Type 922	First stage Total air flow rate	536	cfm
	First stage Rated indoor fan power	80	W
	First stage Rated outdoor fan power	240	W
	First stage Rated total cooling capacity	5105	W
	First stage Rated sensible cooling capacity	3931	W
	First stage Rated cooling power	1103	W
	First stage Rated heating capacity	5223	W
	First stage Rated heating power	1971	W
	First stage Rated air flow rate	536	cfm
	Second stage Total air flow rate	800	cfm
	Second stage Rated indoor fan power	85	W
	Second stage Rated outdoor fan power	240	W
	Second stage Rated total cooling capacity	7619	W
	Second stage Rated sensible cooling capacity	5857	W
	Second stage Rated cooling power	1646	W
	Second stage Rated heating capacity	7796	W
	Second stage Rated heating power	2942	W
	Second stage Rated air flow rate	800	cfm

	Third stage Capacity - stage 1 heater	10000	W
Dehumidifying Mode Type 922	First stage Total air flow rate	536	cfm
	First stage Rated indoor fan power	80	W
	First stage Rated outdoor fan power	240	W
	First stage Rated total cooling capacity	5105	W
	First stage Rated sensible cooling capacity	3931	W
	First stage Rated cooling power	1103	W
	First stage Rated heating capacity	1	W
	First stage Rated heating power	1	W
	First stage Rated air flow rate	536	cfm
	Second stage Total air flow rate	360	cfm
	Second stage Rated indoor fan power	80	W
	Second stage Rated outdoor fan power	240	W
	Second stage Rated total cooling capacity	1724	W
	Second stage Rated sensible cooling capacity	24	W
	Second stage Rated cooling power	1103	W
	Second stage Rated heating capacity	1	W
	Second stage Rated heating power	1	W
	Second stage Rated air flow rate	360	cfm
	Third stage Capacity - stage 1 heater	0	W

Table A- 5. Un-tuned SHW Parameters

Type	Parameter	Value	Units
Solar Collectors Type 1b	Number in series	1	
	Collector area	2.1	m^2
	Fluid specific heat	3.5255	kJ/kg-K
	Efficiency mode	1	
	Intercept efficiency (a0)	0.744	
	1st order efficiency coefficient (a1)	3.6707	W/m^2-K

	2nd order efficiency coefficient (a2)	0.00543	W/m^2-K
	Tested flow rate per unit area	79.92	kg/hr-m^2
	Fluid specific heat at test conditions	4.19	kJ/kg-K
	1st-order IAM coefficient	0.0703	
	2nd-order IAM coefficient	0.0902	
Solar Storage Tank Type 534	Number of tank nodes	7	
	Number of ports	2	
	Number of miscellaneous heat flows	0	
	Tank volume	0.3953	m^3
	Tank height	1.5939	m
	Fluid specific heat	4.19	kJ/kg-K
	Fluid density	1000	kg/m^3
	Fluid thermal conductivity	2.14	kJ/hr-m-K
	Fluid viscosity	3.21	kg/m-hr
	Fluid thermal expansion coefficient	0.00026	1/K
	Loss coefficient	0.59	W/m^2-K
	Additional thermal conductivity	0	W/m-K
	Entry node for flow 1	7	
	Exit node for flow 1	1	
	Entry node for flow 2	2	
	Exit node for flow 2	7	
	Flue loss coefficient	0	W/m^2-K
Brine Pump Type 114	Rated flow rate	200	kg/hr
	Fluid specific heat	3.5255	kJ/kg-K
	Rated power	55	W
	Motor heat loss fraction	0	
Water Pump Type 114	Rated flow rate	680	kg/hr
	Fluid specific heat	4.19	kJ/kg-K
	Rated power	55	W
	Motor heat loss fraction	0	
Heat Exchanger Type 91	Heat exchanger effectiveness	0.8	
	Specific heat of source side fluid	3.5255	kJ/kg-K
	Specific heat of load side fluid	4.19	kJ/kg-K
Indoor pipes to/from collectors Type 31	Inside diameter	1.9	cm
	Pipe length	15.24	m
	Loss coefficient	1.42	W/m^2-K
	Fluid density	982	kg/m^3
	Fluid specific heat	3.5255	kJ/kg-K
	Initial fluid temperature	30	C

Outdoor pipes to/from collectors Type 31	Inside diameter	1.27	cm
	Pipe length	6.1	m
	Loss coefficient	1.42	W/m^2-K
	Fluid density	982	kg/m^3
	Fluid specific heat	3.5255	kJ/kg-K
	Initial fluid temperature	30	C
Pipe from Water Mains to SHW Tank Inlet Type 31	Inside diameter	2.54	cm
	Pipe length	7.4	m
	Loss coefficient	13.1	W/m^2-K
	Fluid density	1000	kg/m^3
	Fluid specific heat	4.19	kJ/kg-K
	Initial fluid temperature	30	C

Table A- 6. Un-tuned HPWH Parameters

Type	Parameter	Value	Units
Pipe from SHW Tank to Tempering Valve Type 31	Inside diameter	2.54	cm
	Pipe length	0.945	m
	Loss coefficient	1.96	W/m^2-K
	Fluid density	1000	kg/m^3
	Fluid specific heat	4.19	kJ/kg-K
	Initial fluid temperature	30	C
Pipe from Tempering Valve to HPWH Tank Type 31	Inside diameter	2.54	cm
	Pipe length	2.225	m
	Loss coefficient	1.96	W/m^2-K
	Fluid density	1000	kg/m^3
	Fluid specific heat	4.19	kJ/kg-K
	Initial fluid temperature	30	C
Heat Pump Hot Water Tank Type 534	Number of tank nodes	5	
	Number of ports	2	
	Number of miscellaneous heat flows	1	
	Tank volume	0.189271	m^3
	Tank height	1.143	m
	Fluid specific heat	4.19	kJ/kg-K
	Fluid density	1000	kg/m^3
	Fluid thermal conductivity	2.14	kJ/hr-m-K
	Fluid viscosity	3.21	kg/m-hr
	Fluid thermal expansion coefficient	0.00026	1/K
	Loss coefficient	0.59	W/m^2-K

	Additional thermal conductivity	0	W/m-K
	Entry node for flow 1	5	
	Exit node for flow 1	1	
	Entry node for flow 2	4	
	Exit node for flow 2	4	
	Flue loss coefficient	0	W/m^2-K
	Node for miscellaneous heat gain	2	
Heat Pump Type 938	Density of liquid stream	1000	kg/m^3
	Specific heat of liquid stream	4.19	kJ/kg-K
	Blower power	0	W
	Controller power	0	W
	Total air flow rate	450	cfm
	Rated total cooling capacity	912	W
	Rated sensible cooling capacity	866	W
	Rated compressor power	671	W
	Rated heat rejection	1583	W
Electric Heater Type 1226	Heating capacity (input)	3800	W
	Thermal efficiency	0.99	
Pipe from HPWH Tank to First Floor Type 31	Inside diameter	1	cm
	Pipe length	8.28	m
	Loss coefficient	1.96	W/m^2-K
	Fluid density	1000	kg/m^3
	Fluid specific heat	4.19	kJ/kg-K
	Initial fluid temperature	30	C
Pipe from HPWH Tank to Second Floor Type 31	Inside diameter	1	cm
	Pipe length	12.09	m
	Loss coefficient	1.96	W/m^2-K
	Fluid density	1000	kg/m^3
	Fluid specific heat	4.19	kJ/kg-K
	Initial fluid temperature	30	C

Table A- 7. PV Parameters

Parameter	Value	Units
Module short-circuit current at reference conditions	6.24	amperes
Module open-circuit voltage at reference conditions	64.8	V
Reference temperature	25	C
Reference insolation	1000	W/m^2
Module voltage at max power point and reference conditions	54.7	V

Module current at max power point and reference conditions	5.86	amperes
Temperature coefficient of lsc at ref. cond.	0.0035	A/K
Temperature coefficient of Voc at ref. cond.	-0.1766	V/K
Number of cells wired in series	96	
Number of modules in series	8	
Number of modules in parallel	2	
Module temperature at NOCT	45	C
Ambient temperature at NOCT	20	C
Insolation at NOCT	800	W/m^2
Module area	1.472	m^2
tau-alpha product for normal incidence	0.95	
Semiconductor bandgap	1.12	eV
Value of parameter a at reference conditions	2.527	V
Value of parameter I_L at reference conditions	6.245	amperes
Value of parameter I_0 at reference conditions	4.48E-11	amperes
Module series resistance	0.3897	ohm
Shunt resistance at reference conditions	533.8	ohm
Extinction coefficient-thickness product of cover	0.008	
Maximum inverter power	5300	W/m^2
Maximum inverter voltage	480	V
Minimum inverter voltage	250	V
Night tare	0.25	W

Table A- 8. Tuned HVAC Control Logic

Mode	Setpoint	Turn-on Trigger	First Stage	Second Stage	Third Stage
Heating	20.5	Deadband	0.1	1.1	3.3
		Time Delay	N/A	10	40
Cooling	23.89	Deadband	0.2	2.8	N/A
		Time Delay	N/A	40	N/A
Dehumidification	48	Deadband	2	N/A	N/A
		Time Delay	N/A	6	N/A

Table A- 9. Tuned HRV Parameters

Type	Parameter	Units	Units
HRV Control Type 1269	Return air flow rate Z1	0	m^3/hr
	Return air flow rate Z2	64.35	m^3/hr
	Return air flow rate Z3	130.65	m^3/hr

	Rated air flow rate	246.2	kg/hr
	Sensible effectiveness coefficient a0	1.2616	
	Sensible effectiveness coefficient a1	-0.3246	
	Sensible effectiveness coefficient a2	0.0521	
	Rated sensible effectiveness	72	%
	Defrost Temperature Trigger	-10	C
	Time Recirculating	7	min
	Time Operating Defrost Cycle	22	min
Fan Type 111b (each fan)	Rated flow rate	246.2	kg/hr
	Rated power	31.4	W
	Motor efficiency	0.9	
	Motor heat loss fraction	1	
	Power coefficient 1	0.8677	
	Power coefficient 2	-0.5849	
	Power coefficient 3	0.7172	
HRV Type 667b	Latent effectiveness (input)	0.01	
	On/Off Control Signal (input)	1	

Table A- 10. Tuned HVAC Parameters

	Parameter	Value	Units
First and Second Stage Heat Pump Type 922	First stage Total air flow rate	624	cfm
	First stage Rated indoor fan power	80	W
	First stage Rated outdoor fan power	240	W
	First stage Rated total cooling capacity	5425	W
	First stage Rated sensible cooling capacity	4088	W
	First stage Rated cooling power	1440	W
	First stage Rated heating capacity	5180	W
	First stage Rated heating power	1398	W
	First stage Rated air flow rate	624	cfm
	Second stage Total air flow rate	836	cfm
	Second stage Rated indoor fan power	85	W
	Second stage Rated outdoor fan power	240	W

	Second stage Rated total cooling capacity	7067	W
	Second stage Rated sensible cooling capacity	5360	W
	Second stage Rated cooling power	2420	W
	Second stage Rated heating capacity	8041	W
	Second stage Rated heating power	2126	W
	Second stage Rated air flow rate	836	cfm
	Second stage Capacity - stage 1 heater	0	W
Third Stage Heat Pump Type 922	Third stage Total air flow rate	992	cfm
	Third stage Rated indoor fan power	85	W
	Third stage Rated outdoor fan power	240	W
	Third stage Rated total cooling capacity	1	W
	Third stage Rated sensible cooling capacity	1	W
	Third stage Rated cooling power	1	W
	Third stage Rated heating capacity	5056	W
	Third stage Rated heating power	2056	W
	Third stage Rated air flow rate	992	cfm
	Third stage Capacity - stage 1 heater	10000	W
Dehumidifying Mode Type 922	First stage Total air flow rate	603	cfm
	First stage Rated indoor fan power	80	W
	First stage Rated outdoor fan power	240	W
	First stage Rated total cooling capacity	5997	W
	First stage Rated sensible cooling capacity	4177	W
	First stage Rated cooling power	1820	W
	First stage Rated heating capacity	1	W
	First stage Rated heating power	1	W
	First stage Rated air flow rate	603	cfm
	Second stage Total air flow rate	549	cfm

	Second stage Rated indoor fan power	80	W
	Second stage Rated outdoor fan power	240	W
	Second stage Rated total cooling capacity	1653	W
	Second stage Rated sensible cooling capacity	423	W
	Second stage Rated cooling power	1230	W
	Second stage Rated heating capacity	1	W
	Second stage Rated heating power	1	W
	Second stage Rated air flow rate	549	cfm
	Third stage Capacity - stage 1 heater	0	W

Table A- 11. Tuned SHW Parameters

Type	Parameter	Value	Units
Solar Collectors Type1b	Number in series	1	
	Collector area	2.1	m^2
	Fluid specific heat	3.5255	kJ/kg-K
	Efficiency mode	1	
	Intercept efficiency (a0)	0.744	
	1st order efficiency coefficient (a1)	3.6707	W/m^2-K
	2nd order efficiency coefficient (a2)	0.00543	W/m^2-K
	Tested flow rate per unit area	79.92	kg/hr-m^2
	Fluid specific heat at test conditions	4.19	kJ/kg-K
	1st-order IAM coefficient	0.0703	
	2nd-order IAM coefficient	0.0902	
Solar Storage Tank Type 534	Number of tank nodes	7	
	Number of ports	2	
	Number of miscellaneous heat flows	0	
	Tank volume	0.2953	m^3
	Tank height	1.5939	m
	Fluid specific heat	4.19	kJ/kg-K
	Fluid density	1000	kg/m^3
	Fluid thermal conductivity	2.14	kJ/hr-m-K
	Fluid viscosity	3.21	kg/m-hr

	Fluid thermal expansion coefficient	0.00026	1/K
	Loss coefficient	1	W/m^2-K
	Additional thermal conductivity	0	W/m-K
	Entry node for flow 1	7	
	Exit node for flow 1	1	
	Entry node for flow 2	3	
	Exit node for flow 2	7	
	Flue loss coefficient	0	W/m^2-K
Brine Pump Type 114	Rated flow rate	196	kg/hr
	Fluid specific heat	3.5255	kJ/kg-K
	Rated power	80	W
	Motor heat loss fraction	0	
Water Pump Type 114	Rated flow rate	999	kg/hr
	Fluid specific heat	4.19	kJ/kg-K
	Rated power	80	W
	Motor heat loss fraction	0	
Heat Exchanger Type 91	Heat exchanger effectiveness	0.44	
	Specific heat of source side fluid	3.5255	kJ/kg-K
	Specific heat of load side fluid	4.19	kJ/kg-K
Indoor pipes to/from collectors Type 31	Inside diameter	1.9	cm
	Pipe length	15.24	m
	Loss coefficient	1.42	W/m^2-K
	Fluid density	982	kg/m^3
	Fluid specific heat	3.5255	kJ/kg-K
	Initial fluid temperature	30	C
Outdoor pipes to/from collectors Type 31	Inside diameter	1.27	cm
	Pipe length	6.1	m
	Loss coefficient	1.42	W/m^2-K
	Fluid density	982	kg/m^3
	Fluid specific heat	3.5255	kJ/kg-K
	Initial fluid temperature	30	C
Pipe from Water Mains to SHW Tank Inlet Type 31	Inside diameter	2.54	cm
	Pipe length	7.4	m
	Loss coefficient	13.1	W/m^2-K
	Fluid density	1000	kg/m^3
	Fluid specific heat	4.19	kJ/kg-K
	Initial fluid temperature	20	C

Table A- 12. Tuned HPWH Parameters

Type	Parameter	Value	Units
Pipe from SHW Tank to Tempering Valve Type 31	Inside diameter	2.54	cm
	Pipe length	0.945	m
	Loss coefficient	1.96	W/m^2-K
	Fluid density	1000	kg/m^3
	Fluid specific heat	4.19	kJ/kg-K
	Initial fluid temperature	30	C
Pipe from Tempering Valve to HPWH Tank Type 31	Inside diameter	2.54	cm
	Pipe length	2.225*	m
	Loss coefficient	1.96	W/m^2-K
	Fluid density	1000	kg/m^3
	Fluid specific heat	4.19	kJ/kg-K
	Initial fluid temperature	30	C
Heat Pump Hot Water Tank Type 534	Number of tank nodes	5	
	Number of ports	2	
	Number of miscellaneous heat flows	2	
	Tank volume	0.189	m^3
	Tank height	1.143	m
	Fluid specific heat	4.19	kJ/kg-K
	Fluid density	1000	kg/m^3
	Fluid thermal conductivity	2.14	kJ/hr-m-K
	Fluid viscosity	3.21	kg/m-hr
	Fluid thermal expansion coefficient	0.00026	1/K
	Loss coefficient	0.59	W/m^2-K
	Additional thermal conductivity	0	W/m-K
	Entry node for flow 1	5	
	Exit node for flow 1	1	
	Entry node for flow 2	4	
	Exit node for flow 2	4	
	Flue loss coefficient	0	W/m^2-K
	Node for miscellaneous heat gain	2	
Heat Pump Type 938	Density of liquid stream	1000	kg/m^3
	Specific heat of liquid stream	4.19	kJ/kg-K
	Blower power	5	W
	Controller power	0	W
	Total air flow rate	450	cfm
	Rated total cooling capacity	1231	W
	Rated sensible cooling capacity	1169	W

	Rated compressor power	794	W
	Rated heat rejection	2025	W
Electric Heater Type 1226	Heating capacity (input)	3600	W
	Thermal efficiency	1	
Pipe from HPWH Tank to First Floor Type 31	Inside diameter	1	cm
	Pipe length	8.28	m
	Loss coefficient	1.96	W/m^2-K
	Fluid density	1000	kg/m^3
	Fluid specific heat	4.19	kJ/kg-K
	Initial fluid temperature	30	C
Pipe from HPWH Tank to Second Floor Type 31	Inside diameter	1	cm
	Pipe length	12.09	m
	Loss coefficient	1.96	W/m^2-K
	Fluid density	1000	kg/m^3
	Fluid specific heat	4.19	kJ/kg-K
	Initial fluid temperature	30	C

* this value is 7.165 m for July 1 – Sept 26

Table A- 13. GSHP System Parameters

Type	Parameter	Value	Units
Borehole Type 557a	Storage volume	22873.12	m^3
	Borehole depth	45.72	m
	Header depth	1.22	m
	Number of boreholes	3	
	Borehole radius	0.0488	m
	No. of boreholes in series	1	
	Number of radial regions	1	
	Number of vertical regions	10	
	Storage thermal conductivity	8.748	kJ/hr-m-K
	Storage heat capacity	2549	kJ/m^3-K
	Negative of u-tubes/bore	-1	
	Outer radius of u-tube pipe	0.016093	m
	Inner radius of u-tube pipe	0.0127	m
	Center-to-center half distance	0.03429	m
	Fill thermal conductivity	2.617	kJ/hr-m-K
	Pipe thermal conductivity	1.62	kJ/hr-m-K
	Gap thermal conductivity	5.04	kJ/hr-m-K

	Gap thickness	0	m
	Reference borehole flow rate	1700	kg/hr
	Reference temperature	23.89	C
	Pipe to pipe heat transfer	-1	
	Fluid specific heat	4.396	kJ/kg-K
	Fluid density	980.7	kg/m^3
	Insulation indicator	0	
	Insulation height fraction	0	
	Insulation thickness	0	m
	Insulation thermal conductivity	0	kJ/hr-m-K
	Number of simulation years	2	
	Maximum storage temperature	76.67	C
	Initial surface temperature of storage volume	12.67	C
	Initial thermal gradient of storage volume	0	
	Number of preheating years	1	
	Maximum preheat temperature	13.68	C
	Minimum preheat temperature	12.34	C
	Preheat phase delay	242	day
	Average air temperature- preheat years	11.67	C
	Amplitude of air temperature - preheat years	14	deltaC
	Air temperature phase delay - preheat years	263	day
	Number of ground layers	4	
	Thermal conductivity of layer	8.748	kJ/hr-m-K
	Heat capacity of layer	2549	kJ/m^3-K
	Thickness of layer	91.44	m
First Stage Heat Pump Type 919	Humidity mode	2	
	Number of water flow steps	3	
	Number of water temps. - cooling	10	
	Number of water temps. - heating	8	
	Number of wet bulb steps	8	
	Number of dry bulb steps - cooling	10	
	Number of dry bulb steps - heating	9	
	Number of airflow steps - cooling	2	
	Number of airflow steps - heating	2	
	Density of liquid stream	980.7	kg/m^3
	Specific heat of liquid stream	4.396	kJ/kg-K
	Specific heat of DHW fluid	4.19	kJ/kg-K

	Blower power	372	W
	Controller power	10	W
	Capacity of stage -1 auxiliary	0	W
	Capacity of stage -2 auxiliary	0	W
	Total air flow rate	710	cfm
	Rated total cooling capacity	5273	W
	Rated sensible cooling capacity	4273.5	W
	Rated cooling power	922	W
	Rated heating capacity	3943	W
	Rated heating power	1048	W
	Rated air flow rate	600	cfm
	Rated liquid flow rate	0.4	L/s
Second Stage Heat Pump Type 919	Humidity mode	2	
	Number of water flow steps	3	
	Number of water temps. - cooling	10	
	Number of water temps. - heating	8	
	Number of wet bulb steps	8	
	Number of dry bulb steps - cooling	10	
	Number of dry bulb steps - heating	9	
	Number of airflow steps - cooling	2	
	Number of airflow steps - heating	2	
	Density of liquid stream	980.7	kg/m^3
	Specific heat of liquid stream	4.396	kJ/kg-K
	Specific heat of DHW fluid	4.19	kJ/kg-K
	Blower power	372	W
	Controller power	10	W
	Capacity of stage -1 auxiliary	0	W
	Capacity of stage -2 auxiliary	0	W
	Total air flow rate	882	cfm
	Rated total cooling capacity	6686	W
	Rated sensible cooling capacity	5192	W
	Rated cooling power	1520	W
	Rated heating capacity	4962	W
	Rated heating power	1437	W
	Rated air flow rate	800	cfm
	Rated liquid flow rate	0.5	L/s
Third Stage Heat Pump Type 919	Humidity mode	2	
	Number of water flow steps	3	
	Number of water temps. - cooling	10	

	Number of water temps. - heating	8	
	Number of wet bulb steps	8	
	Number of dry bulb steps - cooling	10	
	Number of dry bulb steps - heating	9	
	Number of airflow steps - cooling	2	
	Number of airflow steps - heating	2	
	Density of liquid stream	980.7	kg/m^3
	Specific heat of liquid stream	4.396	kJ/kg-K
	Specific heat of DHW fluid	4.19	kJ/kg-K
	Blower power	372	W
	Controller power	10	W
	Capacity of stage -1 auxiliary	4800	W
	Capacity of stage -2 auxiliary	0	W
	Total air flow rate	974	cfm
	Rated total cooling capacity	1	W
	Rated sensible cooling capacity	1	W
	Rated cooling power	1	W
	Rated heating capacity	5016	W
	Rated heating power	1427	W
	Rated air flow rate	800	cfm
	Rated liquid flow rate	0.5	L/s
Dehumidifier Type 921	Humidity Mode	2	
	Number of Condenser Temperatures	3	
	Number of Evaporator Flows	3	
	Number of Indoor Wet Bulbs	2	
	Number of Indoor Dry Bulb Temperatures	2	
	Blower Power Draw	200	W
	Rated Evaporator Flowrate	115	cfm
	Rated Total Cooling Capacity	293	W
	Rated Sensible Cooling Capacity	1	W
	Rated Power	520	W

Appendix B: Monthly Data

Table B- 1. Un-Tuned Thermal Load

	Heating Mode			Cooling Mode			Total Thermal Energy		
Month	Measured Energy [kW-hr]	TRNSYS Energy [kW-hr]	Percent Error [%]	Measured Energy [kW-hr]	TRNSYS Energy [kW-hr]	Percent Error [%]	Measured Energy [kW-hr]	TRNSYS Energy [kW-hr]	Percent Error [%]
Jan-14	-2156.9	-2299.4	7%	0.0	0.0	0%	-2156.9	-2299	7%
Feb-14	-1634.7	-1708.8	5%	0.0	0.0	0%	-1634.7	-1709	5%
Mar-14	-1423.5	-1371.2	-4%	0.0	0.0	0%	-1423.5	-1371	-4%
Apr-14	-252.7	-257.3	2%	66.8	46.0	-31%	-185.9	-211	14%
May-14	0.0	-5.4	0%	603.0	497.8	-17%	603	492	-18%
Jun-14	0.0	0.0	0%	1559.7	1284.9	-18%	1559.7	1285	-18%
Jul-13	0.0	0.0	0%	2122.9	1911.7	-10%	2122.9	1912	-10%
Aug-13	0.0	0.0	0%	1392.1	1348.1	-17%	1392.1	1348	-17%
Sep-13	0.0	-3.9	0%	937.2	808.7	-14%	937.2	805	-14%
Oct-13	-56.4	-215.7	282%	306.4	222.8	-27%	250	7	-97%
Nov-13	-832.1	-1086.1	31%	1.7	0.0	-100%	-830.4	-1086	31%
Dec-13	-1351.0	-1607.9	19%	0.0	0.0	0%	-1351	-1608	19%
Total	-7707.3	-8555.6	11%	6989.8	6120.1	-15%	-717.5	-2435	398%

Table B- 2. Un-Tuned Heat Pump Electrical Energy

	Total Heating Season Energy			Total Cooling Season Energy			Total Energy		
Month	Measured Energy [kW-hr]	TRNSYS Energy [kW-hr]	Percent Error [%]	Measured Energy [kW-hr]	TRNSYS Energy [kW-hr]	Percent Error [%]	Measured Energy [kW-hr]	TRNSYS Energy [kW-hr]	Percent Error [%]
Jan-14	1254.8	1220.9	-3%	0.0	0.0	0%	1254.8	1220.9	-3%
Feb-14	753.1	744.9	-1%	0.0	0.0	0%	753.1	744.9	-1%
Mar-14	650.4	555.4	-15%	0.0	0.0	0%	650.4	555.4	-15%
Apr-14	113.2	63.2	-44%	13.6	11.9	-12%	126.8	75.2	-41%
May-14	0	2.9	0%	177.7	128.1	-28%	177.7	130.9	-26%
Jun-14	0	0.0	0%	511.3	324.1	-37%	511.3	324.1	-37%
Jul-13	0	0.0	0%	700.8	527.5	-25%	700.8	527.5	-25%
Aug-13	0	0.0	0%	551.0	371.2	-33%	551.0	371.2	-33%
Sep-13	0	2.8	0%	345.5	206.9	-40%	345.5	209.6	-39%
Oct-13	33.6	52.0	55%	142.3	61.6	-57%	175.9	113.6	-35%
Nov-13	396.4	377.0	-5%	15.7	0.0	-100%	412.1	377.0	-9%
Dec-13	581.5	608.1	5%	0.0	0.0	0%	581.5	608.1	5%
Total	**3783.0**	**3627.2**	**-4%**	**2457.9**	**1631.2**	**-34%**	**6240.9**	**5258.4**	**-16%**

Table B-2 Continued. Un-Tuned Heat Pump Electrical Energy

	First and Second Stage Heating			Third Stage Resistive Heat			Defrost		
Month	Measured Energy [kW-hr]	TRNSYS Energy [kW-hr]	Percent Error [%]	Measured Energy [kW-hr]	TRNSYS Energy [kW-hr]	Percent Error [%]	Measured Energy [kW-hr]	TRNSYS Energy [kW-hr]	Percent Error [%]
Jan-14	692.9	798.1	15%	411.2	422.8	3%	136.4	0.0	-100%
Feb-14	541.8	608.4	12%	97.9	136.5	39%	98.5	0.0	-100%
Mar-14	459.5	462.6	1%	104.0	92.8	-11%	65.4	0.0	-100%
Apr-14	70.6	60.6	-14%	9.3	2.7	-71%	0.9	0.0	-100%
May-14	0.0	0.9	0%	0.0	2.0	0%	0.0	0.0	-100%
Jun-14	0.0	0.0	0%	0.0	0.0	0%	0.0	0.0	-100%
Jul-13	0.0	0.0	0%	0.0	0.0	0%	0.0	0.0	-100%
Aug-13	0.0	0.0	0%	0.0	0.0	0%	0.0	0.0	-100%
Sep-13	0.0	0.6	0%	0.0	2.2	0%	0.0	0.0	-100%
Oct-13	20.0	50.0	150%	11.9	2.0	-83%	1.7	0.0	-100%
Nov-13	267.5	348.7	30%	64.7	28.3	-56%	38.3	0.0	-100%
Dec-13	443.2	551.0	24%	35.5	57.2	61%	81.5	0.0	-100%
Total	**2495.6**	2880.7	15%	**734.5**	746.5	2%	**422.7**	**0.0**	-100%

Table B-2 Continued. Un-Tuned Heat Pump Electrical Energy

	First & Second Stage Cooling			Dehumidification Mode			Standby		
Month	Measured Energy [kW-hr]	TRNSYS Energy [kW-hr]	Percent Error [%]	Measured Energy [kW-hr]	TRNSYS Energy [kW-hr]	Percent Error [%]	Measured Energy [kW-hr]	TRNSYS Energy [kW-hr]	Percent Error [%]
Jan-14	0.0	0.0	0%	0.0	0.0	0%	14.3	0.0	-100%
Feb-14	0.0	0.0	0%	0.0	0.0	0%	14.9	0.0	-100%
Mar-14	0.0	0.0	0%	0.0	0.0	0%	21.5	0.0	-100%
Apr-14	13.6	3.6	-74%	0.0	8.4	0%	32.4	0.0	-100%
May-14	125.7	52.3	-58%	21.5	75.8	252%	30.5	0.0	-100%
Jun-14	290.7	162.0	-44%	204.4	162.1	-21%	16.2	0.0	-100%
Jul-13	442.6	208.6	-53%	245.6	318.9	30%	12.6	0.0	-100%
Aug-13	287.4	121.9	-58%	246.4	249.3	1%	17.2	0.0	-100%
Sep-13	208.3	89.7	-57%	113.8	117.2	3%	23.4	0.0	-100%
Oct-13	50.0	15.1	-70%	59.9	46.5	-22%	32.4	0.0	-100%
Nov-13	-14.3	0.0	-100%	30.0	0.0	-100%	25.9	0.0	-100%
Dec-13	-0.2	0.0	-100%	0.2	0.0	-100%	21.3	0.0	-100%
Total	**1403.9**	**653.0**	**-53%**	**921.8**	**978.2**	**6%**	**262.5**	**0.0**	**-100%**

Table B- 3. Tuned Thermal Load

	Heating Mode			Cooling Mode			Total Thermal Energy		
Month	Measured Energy [kW-hr]	TRNSYS Energy [kW-hr]	Percent Error [%]	Measured Energy [kW-hr]	TRNSYS Energy [kW-hr]	Percent Error [%]	Measured Energy [kW-hr]	TRNSYS Energy [kW-hr]	Percent Error [%]
Jan-14	-2156.9	-2225.9	3%	0.0	0.0	0%	-2156.9	-2226	3%
Feb-14	-1634.7	-1637.9	0%	0.0	0.0	0%	-1634.7	-1638	0%
Mar-14	-1423.5	-1303.7	-8%	0.0	0.0	0%	-1423.5	-1304	-8%
Apr-14	-252.7	-164.5	-35%	66.8	33.9	-49%	-185.9	-131	-30%
May-14	0.0	-4.8	0%	603.0	554.2	-8%	603.0	549	-9%
Jun-14	0.0	0.0	0%	1559.7	1484.8	-5%	1559.7	1485	-5%
Jul-13	0.0	0.0	0%	2122.9	2156.6	2%	2122.9	2157	2%
Aug-13	0.0	0.0	0%	1620.6	1488.9	-8%	1620.6	1489	-8%
Sep-13	0.0	0.0	0%	937.2	890.0	-5%	937.2	890	-5%
Oct-13	-56.4	-142.6	153%	306.4	270.7	-12%	250.0	128	-49%
Nov-13	-832.1	-1005.0	21%	1.7	0.0	-100%	-830.4	-1005	21%
Dec-13	-1351.0	-1541.8	14%	0.0	0.0	0%	-1351.0	-1542	14%
Total	-7707.3	-8026.2	4%	7218.3	6879.0	-5%	-489.0	-1147	135%

Table B- 4. Tuned Heat Pump Electrical Energy

	Total Heating Season Energy			Total Cooling Season Energy			Total Energy		
Month	Measured Energy [kW-hr]	TRNSYS Energy [kW-hr]	Percent Error [%]	Measured Energy [kW-hr]	TRNSYS Energy [kW-hr]	Percent Error [%]	Measured Energy [kW-hr]	TRNSYS Energy [kW-hr]	Percent Error [%]
Jan-14	1254.8	1129.9	-10%	0.0	0.0	0%	1254.8	1129.9	-10%
Feb-14	753.1	669.1	-11%	0.0	0.0	0%	753.1	669.1	-11%
Mar-14	650.4	528.5	-19%	0.0	0.0	0%	650.4	528.5	-19%
Apr-14	113.2	85.4	-25%	13.6	13.6	0%	126.8	99.0	-22%
May-14	0	1.1	0%	177.7	236.9	33%	177.7	238.0	34%
Jun-14	0	0.0	0%	511.3	551.2	8%	511.3	551.2	8%
Jul-13	0	0.0	0%	700.8	859.8	23%	700.8	859.8	23%
Aug-13	0	0.0	0%	551.0	615.9	12%	551.0	615.9	12%
Sep-13	0	0.0	0%	345.5	353.6	2%	345.5	353.6	2%
Oct-13	33.6	47.2	40%	142.3	149.5	5%	175.9	196.7	12%
Nov-13	396.4	371.7	-6%	15.7	0.0	-100%	412.1	371.7	-10%
Dec-13	581.5	569.4	-2%	0.0	0.0	0%	581.5	569.4	-2%
Total	**3783.0**	**3402.2**	**-10%**	**2457.9**	**2780.4**	**13%**	**6240.9**	**6182.6**	**-1%**

Table B-4 Continued. Tuned Heat Pump Electrical Energy

	First and Second Stage Heating			Third Stage Resistive Heat			Defrost		
Month	Measured Energy [kW-hr]	TRNSYS Energy [kW-hr]	Percent Error [%]	Measured Energy [kW-hr]	TRNSYS Energy [kW-hr]	Percent Error [%]	Measured Energy [kW-hr]	TRNSYS Energy [kW-hr]	Percent Error [%]
Jan-14	692.9	645.0	-7%	411.2	346.9	-16%	136.4	122.7	-10%
Feb-14	541.8	522.8	-4%	97.9	45.2	-54%	98.5	84.2	-14%
Mar-14	459.5	405.0	-12%	104.0	45.1	-57%	65.4	54.4	-17%
Apr-14	70.6	41.4	-41%	9.3	9.2	-1%	0.9	0.8	-17%
May-14	0.0	1.1	100%	0.0	0.0	0%	0.0	0.0	0%
Jun-14	0.0	0.0	0%	0.0	0.0	0%	0.0	0.0	0%
Jul-13	0.0	0.0	0%	0.0	0.0	0%	0.0	0.0	0%
Aug-13	0.0	0.0	0%	0.0	0.0	0%	0.0	0.0	0%
Sep-13	0.0	0.0	0%	0.0	0.0	0%	0.0	0.0	0%
Oct-13	20.0	37.1	86%	11.9	8.1	-32%	1.7	1.9	15%
Nov-13	267.5	308.6	15%	64.7	3.1	-95%	38.3	34.1	-11%
Dec-13	443.2	480.8	8%	35.5	4.9	-86%	81.5	62.0	-24%
Total	**2495.6**	2441.8	-2%	**734.5**	462.5	-37%	**422.7**	360.2	-15%

Table B-4 Continued. Tuned Heat Pump Electrical Energy

	First & Second Stage Cooling			Dehumidification Mode			Standby		
Month	Measured Energy [kW-hr]	TRNSYS Energy [kW-hr]	Percent Error [%]	Measured Energy [kW-hr]	TRNSYS Energy [kW-hr]	Percent Error [%]	Measured Energy [kW-hr]	TRNSYS Energy [kW-hr]	Percent Error [%]
Jan-14	0.0	0.0	0%	0.0	0.0	0%	14.3	15.3	7%
Feb-14	0.0	0.0	0%	0.0	0.0	0%	14.9	16.9	14%
Mar-14	0.0	0.0	0%	0.0	0.0	0%	21.5	23.9	11%
Apr-14	13.6	5.9	-56%	0.0	7.7	0%	32.4	34.0	5%
May-14	125.7	94.5	-25%	21.5	113.1	426%	30.5	29.2	-4%
Jun-14	290.7	281.0	-3%	204.4	254.4	24%	16.2	15.8	-2%
Jul-13	442.6	383.6	-13%	245.6	470.9	92%	12.6	5.3	-58%
Aug-13	287.4	221.9	-23%	246.4	380.5	54%	17.2	13.5	-22%
Sep-13	208.3	161.2	-23%	113.8	168.8	48%	23.4	23.6	1%
Oct-13	50.0	28.6	-43%	59.9	89.7	50%	32.4	31.2	-4%
Nov-13	-14.3	0.0	-100%	30.0	0.0	-100%	25.9	25.8	0%
Dec-13	-0.2	0.0	0%	0.2	0.0	-100%	21.3	21.8	2%
Total	**1403.9**	1176.7	-16%	**921.8**	1485.2	61%	**262.5**	256.1	-2%

Table B- 5. Un-Tuned DHW Temperatures

Month	Measured T_{SHWin} [^{0}C]	TRNSYS T_{SHWin} [^{0}C]	Measured T_{SHWout} [^{0}C]	TRNSYS T_{SHWout} [^{0}C]	Measured T_{HPWHin} [^{0}C]	TRNSYS T_{HPWHin} [^{0}C]	Measured $T_{HPWHout}$t [^{0}C]	TRNSYS $T_{HPWHout}$ [^{0}C]
Jan-14	12.7	12.5	23.6	25.6	23.7	25.3	51.3	51.2
Feb-14	11.6	12.0	25.9	30.1	25.6	29.6	51.3	51.2
Mar-14	12.3	13.2	29.6	34.2	28.8	33.4	51.3	51.4
Apr-14	14.7	15.0	40.8	45.7	38.9	42.0	49.9	49.5
May-14	17.9	17.6	46.4	52.6	44.2	45.8	50.9	48.3
Jun-14	20.9	19.9	52.1	61.6	46.1	47.4	50.7	47.0
Jul-13	23.2	21.7	52.7	61.4	43.2	47.4	51.6	47.0
Aug-13	23.1	22.1	40.6	55.7	35.7	46.5	51.8	47.7
Sep-13	23.3	22.0	47.6	58.2	41.8	46.9	51.5	47.2
Oct-13	21.2	20.0	40.6	42.2	37.6	40.3	51.6	50.2
Nov-13	17.9	17.3	31.3	32.3	30.5	31.7	52.0	51.6
Dec-13	14.9	14.6	22.8	23.6	23.3	23.4	51.8	51.2

Table B- 6. Tuned DHW Temperatures

Month	Measured T_{SHWin} [^{0}C]	TRNSYS T_{SHWin} [^{0}C]	Measured T_{SHWout} [^{0}C]	TRNSYS T_{SHWout} [^{0}C]	Measured T_{HPWHin} [^{0}C]	TRNSYS T_{HPWHin} [^{0}C]	Measured $T_{HPWHout}$t [^{0}C]	TRNSYS $T_{HPWHout}$ [^{0}C]
Jan-14	12.7	12.6	23.6	23.6	23.7	23.4	51.3	51.3
Feb-14	11.6	12.2	25.9	27.0	25.6	26.6	51.3	51.6
Mar-14	12.3	13.3	29.6	30.2	28.8	29.7	51.3	51.8
Apr-14	14.7	15.1	40.8	39.6	38.9	37.8	49.9	51.2
May-14	17.9	17.7	46.4	45.2	44.2	42.2	50.9	50.6
Jun-14	20.9	20.0	52.1	51.0	46.1	45.7	50.7	49.1
Jul-13	23.2	21.8	52.7	49.1	43.2	46.4	51.6	50.9
Aug-13	23.1	22.1	40.6	39.6	35.7	37.8	51.8	51.2
Sep-13	23.3	22.0	47.6	44.8	41.8	42.5	51.5	50.8
Oct-13	21.2	20.0	40.6	37.6	37.6	36.6	51.6	51.5
Nov-13	17.9	17.3	31.3	29.1	30.5	28.6	52.0	50.8
Dec-13	14.9	14.7	22.8	22.0	23.3	21.8	51.8	50.5

Appendix C: Alternate DHW Configurations

System 1: Standard Electric Resistance Water Heater (Baseline)

Tank Schematic

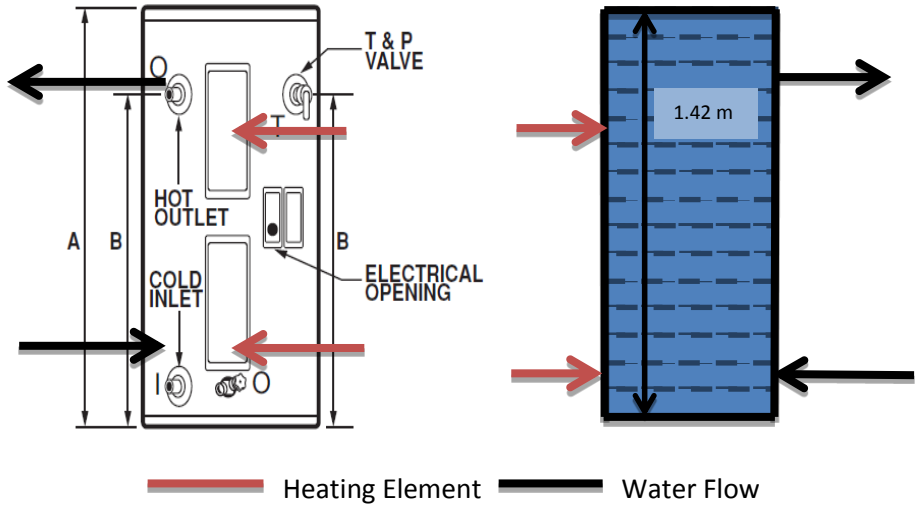

Figure 49. Standard Electric Water Heater Schematic.

Controls

Table 35. Standard Electric Water Heater Controls.

	Setpoint	Node
Top Element	49 ^{0}C ± 2.8 ^{0}C	5
Bottom Element	49 ^{0}C ± 8.3 ^{0}C	14

The bottom element will not turn on if top element is on. The temperature sensor for each element is located in the same node in which the element is located.

Type Parameters

Table 36. Standard Electric Water Heater Parameters

Type	Parameter	Value	Units
Storage Tank Type 534	Number of tank nodes	15	
	Number of ports	1	
	Number of miscellaneous heat flows	2	
	Tank volume	0.1893	m^3
	Tank height	1.422	m
	Fluid specific heat	4.19	kJ/kg-K

	Fluid density	1000	kg/m^3
	Fluid thermal conductivity	0.6	W/m-K
	Fluid viscosity	3.21	kg/m-hr
	Fluid thermal expansion coefficient	0.00026	1/K
	Top loss coefficient	0.355	W/m^2-K
	Edge loss coefficient	0.355	W/m^2-K
	Bottom loss coefficient	0.355	W/m^2-K
	Additional thermal conductivity	0	W/m^2-K
	Entry node	14	
	Exit node	3	
	Flue overall loss coefficient	0	kJ/hr-K
	Node for miscellaneous heat gain-1	3	
	Node for miscellaneous heat gain-2	13	
Pipe to Tank Type 31	Inside diameter	2.54	cm
	Pipe length	7.4	m
	Loss coefficient	13.1	W/m^2-K
	Fluid density	1000	kg/m^3
	Fluid specific heat	4.19	kJ/kg-K
	Initial fluid temperature	20	C
Electric Heaters (1 & 2) Type 1226	Heating capacity*	3800	W
	Thermal efficiency*	1	

*Type input, not a parameter

System 2: 80 Gallon SHW with Heating Element Enabled

Tank Schematic

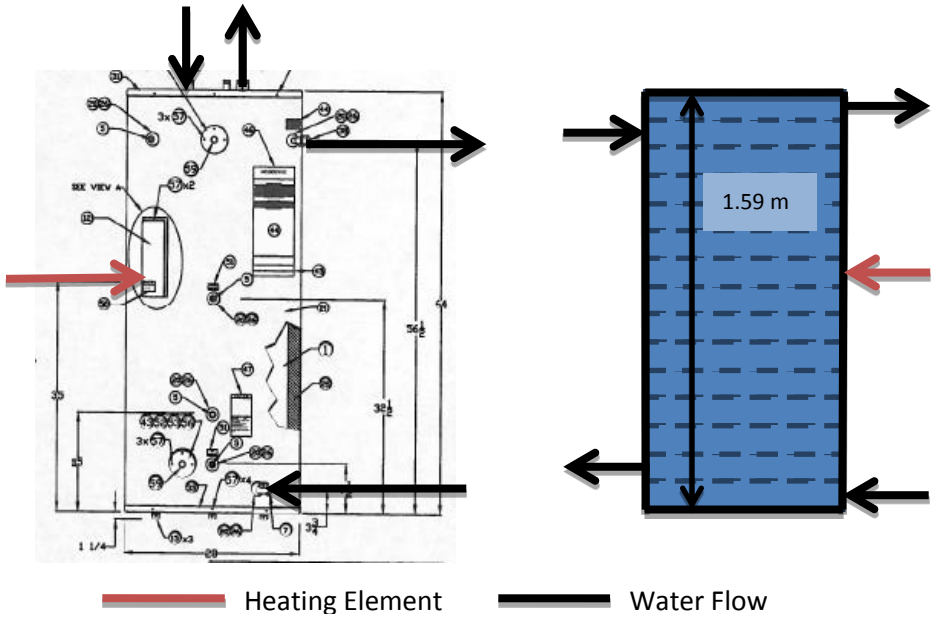

Figure 50. 80 Gallon SHW Tank Schematic

System Schematic

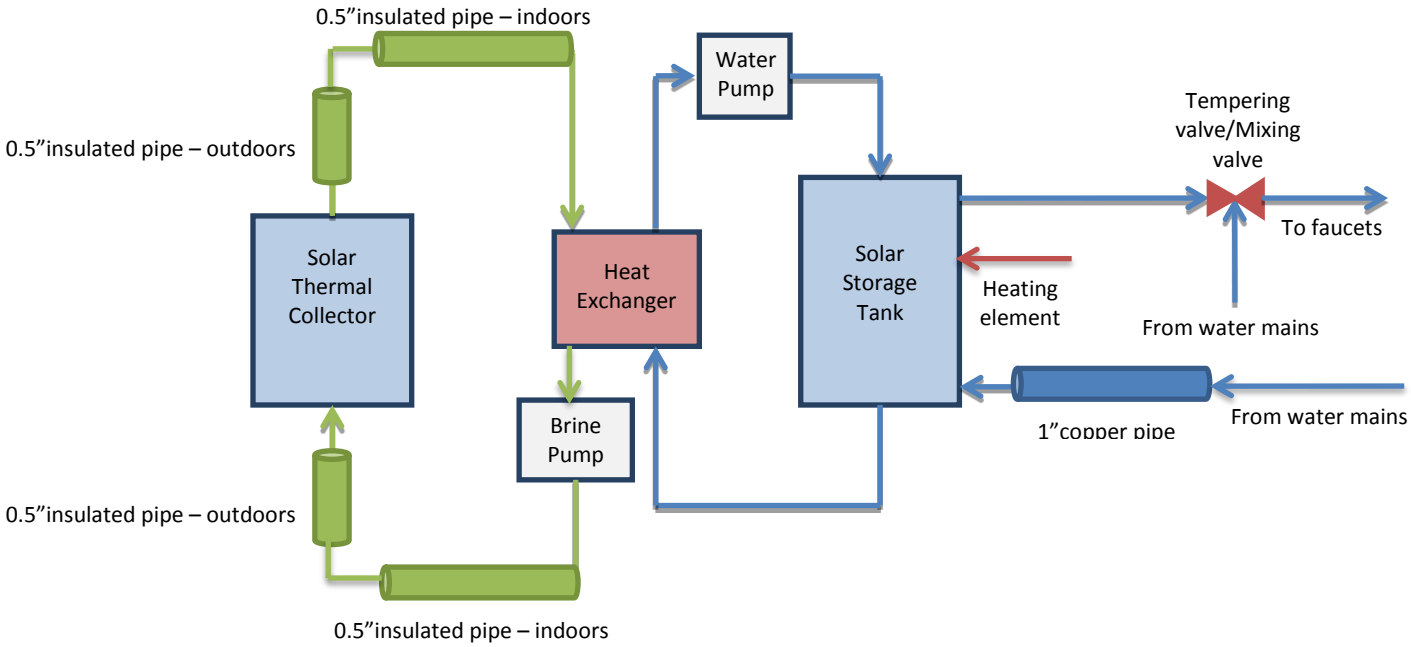

Figure 51. 80 Gallon SHW System Schematic

Controls

Heating element is located at node 7 and is set to 49 ^{0}C ± 2.8 ^{0}C.

The circulating pumps will turn on when the temperature differential between node 14 (near the bottom) and the solar panel outlet temperature is 10 ^{0}C or greater and will turn off when the differential is 3 ^{0}C or less. The pumps will not run if the temperature at node 14 reaches 71 ^{0}C, the shutoff temperature. When a water draw occurs, the water exiting the solar storage tank is tempered to 49 ^{0}C, if needed, using water from the water mains.

Type Parameters

Table 37. 80 Gallon SHW Parameters

Storage Tank Type 534	Number of tank nodes	15	
	Number of ports	2	
	Number of miscellaneous heat flows	1	
	Tank volume	0.2953	m^3
	Tank height	1.594	m
	Fluid specific heat	4.19	kJ/kg-K
	Fluid density	1000	kg/m^3
	Fluid thermal conductivity	0.6	W/m-K
	Fluid viscosity	3.21	kg/m-hr
	Fluid thermal expansion coefficient	0.00026	1/K
	Top loss coefficient	1.0	W/m^2-K
	Edge loss coefficient	1.0	W/m^2-K
	Bottom loss coefficient	1.0	W/m^2-K
	Additional thermal conductivity	0	W/m^2-K
	Entry node-1	15	
	Exit node-1	1	
	Entry node-2	2	
	Exit node-2	14	
	Flue overall loss coefficient	0	kJ/hr-K
	Node for miscellaneous heat gain	7	

Pipe to Tank Type 31	Inside diameter	2.54	cm
	Pipe length	7.4	m
	Loss coefficient	13.1	W/m^2-K
	Fluid density	1000	kg/m^3
	Fluid specific heat	4.19	kJ/kg-K
	Initial fluid temperature	20	C
Electric Heaters (1 & 2) Type 1226	Heating capacity*	4500	W
	Thermal efficiency*	1	
Solar Panels Type 539 (two instances)	Number in series	1	
	Collector area	2.1	m^2
	Fluid specific heat	3.5255	kJ/kg-K
	Collector test mode	1	
	Intercept efficiency (a0)	0.744	
	1st order efficiency coefficient (a1)	3.6707	W/m^2-K
	2nd order efficiency coefficient (a2)	0.00543	W/m^2-K
	Tested flow rate per unit area	79.92	
	Fluid specific heat at test conditions	4.19	kJ/kg-K
	1st-order IAM coefficient	0.0703	
	2nd-order IAM coefficient	0.0902	
	Minimum flowrate	0	kg/hr
	Maximum flowrate	101.15	kg/hr
	Capacitance of collectors	8.437	kJ/K
	Number of nodes	10	
	Initial Temperatures	20	C
Brine Pump Type 114	Rated flow rate	196	kg/hr
	Fluid specific heat	3.5255	kJ/kg-K
	Rated power	80	W
	Motor heat loss fraction	0	
Water Pump Type 114	Rated flow rate	999	kg/hr
	Fluid specific heat	4.19	kJ/kg-K
	Rated power	80	W

	Motor heat loss fraction	0	
Heat Exchanger Type 91	Heat exchanger effectiveness	0.44	
	Specific heat of source side fluid	3.5255	kJ/kg-K
	Specific heat of load side fluid	4.19	kJ/kg-K
Indoor pipes to/from collectors Type 31	Inside diameter	1.9	cm
	Pipe length	15.24	m
	Loss coefficient	1.42	W/m^2-K
	Fluid density	982	kg/m^3
	Fluid specific heat	3.5255	kJ/kg-K
	Initial fluid temperature	30	C
Outdoor pipes to/from collectors Type 31	Inside diameter	1.27	cm
	Pipe length	6.1	m
	Loss coefficient	1.42	W/m^2-K
	Fluid density	982	kg/m^3
	Fluid specific heat	3.5255	kJ/kg-K
	Initial fluid temperature	30	C

*Type input, not a parameter

System 3: 120 Gallon SHW with Heating Element Enabled

Tank Schematic

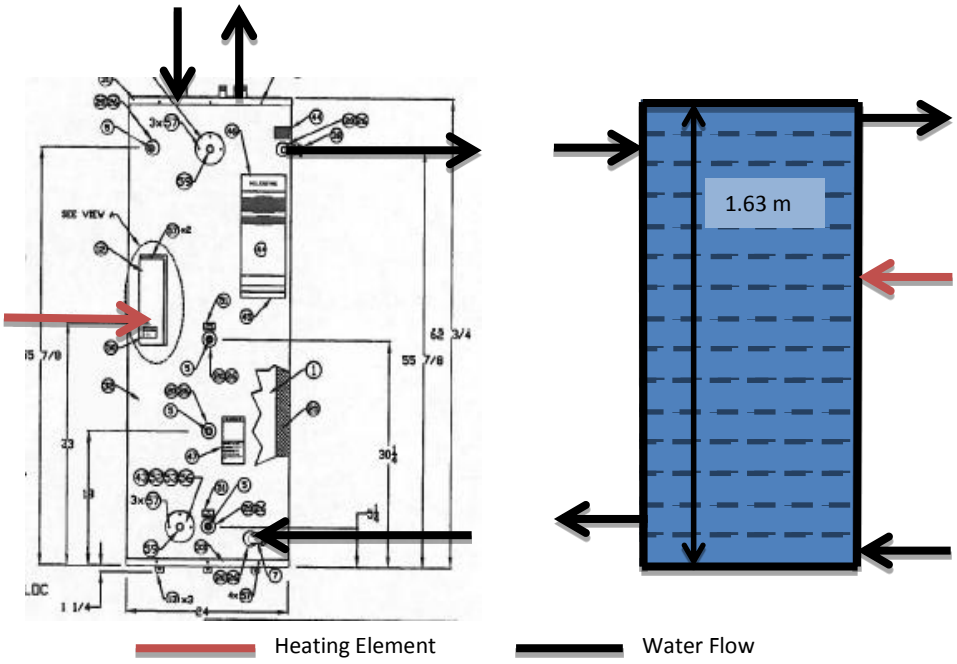

Figure 52. 120 Gallon SHW Tank Schematic

Controls

The control logic used in the 120 gallon SHW system is identical to that which is used in the 80 gallon SHW system, except that the heating element is located at node 6.

Type Parameters

The types and parameters used in the 120 gallon SHW system are identical to that which is used in the 80 gallon SHW system, except for the storage tank, Type 534.

Table 38. 120 Gallon SHW Parameters

Storage Tank Type 534	Number of tank nodes	15	
	Number of ports	2	
	Number of miscellaneous heat flows	1	
	Tank volume	0.424	m^3
	Tank height	1.626	m
	Fluid specific heat	4.19	kJ/kg-K
	Fluid density	1000	kg/m^3
	Fluid thermal conductivity	0.6	W/m-K

	Fluid viscosity	3.21	kg/m-hr
	Fluid thermal expansion coefficient	0.00026	1/K
	Top loss coefficient	1.0	W/m^2-K
	Edge loss coefficient	1.0	W/m^2-K
	Bottom loss coefficient	1.0	W/m^2-K
	Additional thermal conductivity	0	W/m^2-K
	Entry node-1	15	
	Exit node-1	1	
	Entry node-2	2	
	Exit node-2	14	
	Flue overall loss coefficient	0	kJ/hr-K
	Node for miscellaneous heat gain	6	

System 4: 50 Gal HPWH

Tank Schematic

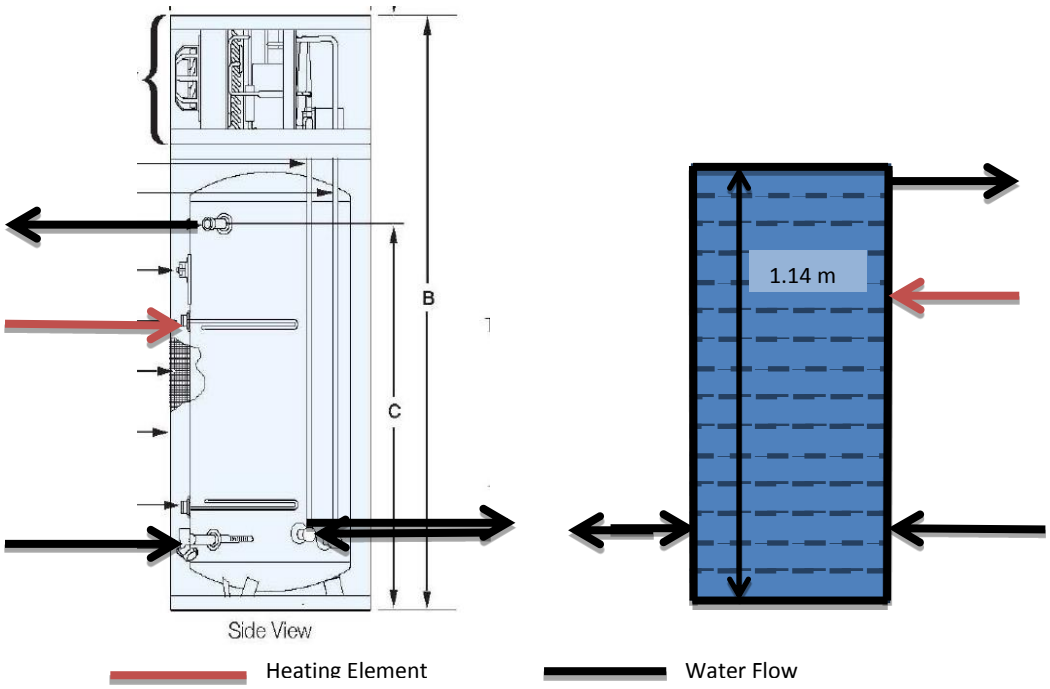

Figure 53. 50 Gallon HPWH Tank Schematic.

System Schematic

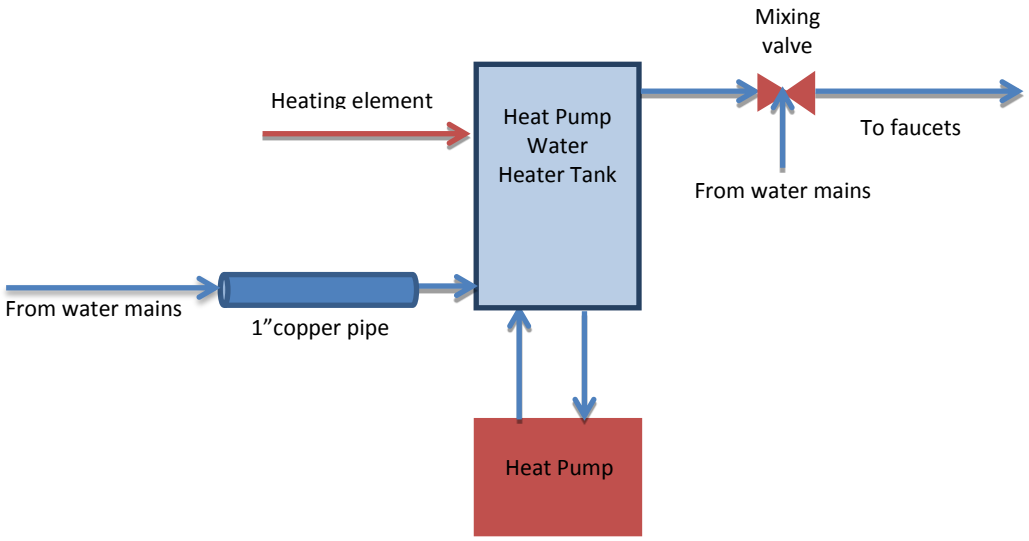

Figure 54. 50 Gallon HPWH System Schematic.

Controls

Table 39. 50 Gallon HPWH Controls.

	Setpoint	Node
Top Element	49 ^{0}C ± 1.1 ^{0} C	13
Bottom Element	49 ^{0}C +4.4/-16.8 ^{0}C	5

The heat pump will not turn on if the heating element is on.

Type Parameters

Table 40. 50 Gallon HPWH Parameters.

Heat Pump Water Heater Tank Type 534	Number of tank nodes	15	
	Number of ports	2	
	Number of miscellaneous heat flows	1	
	Tank volume	0.189271	m^3
	Tank height	1.143	m
	Fluid specific heat	4.19	kJ/kg-K
	Fluid density	1000	kg/m^3
	Fluid thermal conductivity	0.59	W/m-K
	Fluid viscosity	3.21	kg/m-hr
	Fluid thermal expansion coefficient	0.00026	1/K
	Loss coefficient	0.59	W/m^2-K
	Additional thermal conductivity	0	W/m-K
	Entry node for flow 1	13	
	Exit node for flow 1	1	

	Entry node for flow 2	13	
	Exit node for flow 2	13	
	Flue loss coefficient	0	W/m^2-K
	Node for miscellaneous heat gain	5	
Heat Pump Type 938	Density of liquid stream	1000	kg/m^3
	Specific heat of liquid stream	4.19	kJ/kg-K
	Blower power	5	W
	Controller power	0	W
	Total air flow rate	450	cfm
	Rated total cooling capacity	1231	W
	Rated sensible cooling capacity	1169	W
	Rated compressor power	794	W
	Rated heat rejection	2025	W
Electric Heater Type 1226	Heating capacity (input)*	3600	W
	Thermal efficiency*	1	

*Type input, not a parameter

The heat pump's measured standby power of 6.92 W was also included in the model.

System 5: 80 Gal HPWH

Controls

The controls used in the 80 gal HPWH are identical to those used in the 50 gal HPWH

Type Parameters

The types and parameters used in the 80 gal HPWH are identical to those used in the 50 gal HPWH, except for the tank dimensions.

Table 41. 80 Gallon HPWH Tank Dimensions.

	Value	Units
Tank volume	0.30283	m^3
Tank height	1.321	m

System 6: 80 gal SHW + 50 gal HPWH

System Schematic

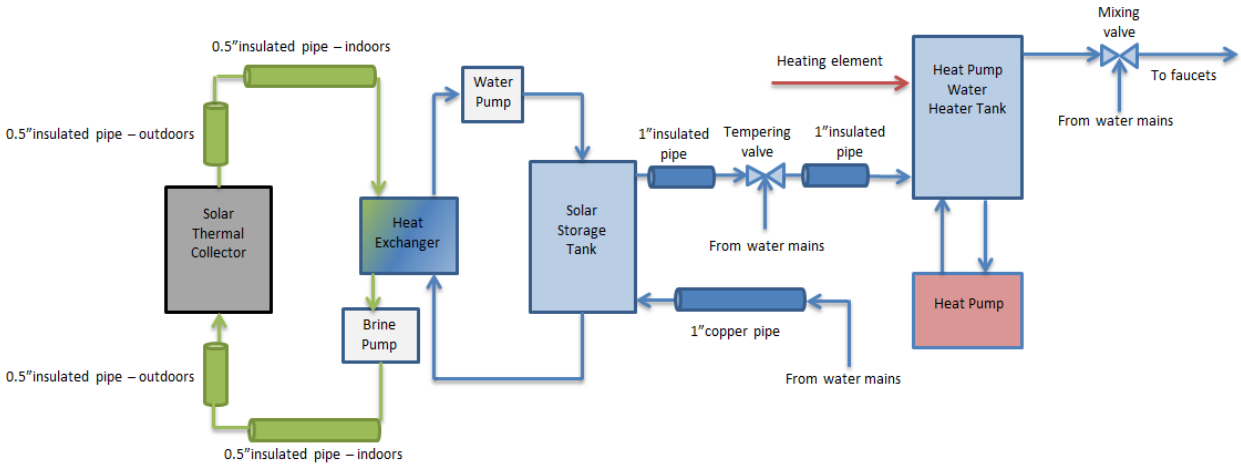

Figure 55. 80 Gallon SHW + 50 Gallon HPWH System Schematic.

Controls

The controls used in the combined 80 gallon SHW and HPWH system are the same as those used in the 80 gallon SHW system and HPWH systems individually, except that there is no heating element activated within the solar storage tank.

Type Parameters

The types and parameters used in the combined 80 gallon SHW and HPWH system are the same as those used in the 80 gallon SHW system and HPWH systems individually, except that there is added piping between the solar storage tank and the HPWH tank.

Table 42. 80 Gallon SHW + 50 Gallon HPWH Parameters.

Pipe from SHW Tank to Tempering Valve Type 31	Inside diameter	2.54	cm
	Pipe length	0.945	m
	Loss coefficient	1.96	W/m^2-K
	Fluid density	1000	kg/m^3
	Fluid specific heat	4.19	kJ/kg-K
	Initial fluid temperature	20	C
Pipe from Tempering Valve to HPWH Tank Type 31	Inside diameter	2.54	cm
	Pipe length	2.225	m
	Loss coefficient	1.96	W/m^2-K
	Fluid density	1000	kg/m^3
	Fluid specific heat	4.19	kJ/kg-K

	Initial fluid temperature	20	C

System 7: 120 gal SHW + 50 gal HPWH

Controls

The controls used in the combined 120 gallon SHW and HPWH system are the same as those used in the 120 gallon SHW system and HPWH systems individually, except that there is no heating element activated within the solar storage tank.

Type Parameters

The types and parameters used in the combined 120 gallon SHW and HPWH system are the same as those used in the 120 gallon SHW system and HPWH systems individually, except that there is added piping between the solar storage tank and the HPWH tank. The added piping is identical to the piping added between the tanks in the 80 gallon SHW and HPWH system.

System 8: 80 gal SHW + Tankless Water Heater (TWH)

System Schematic

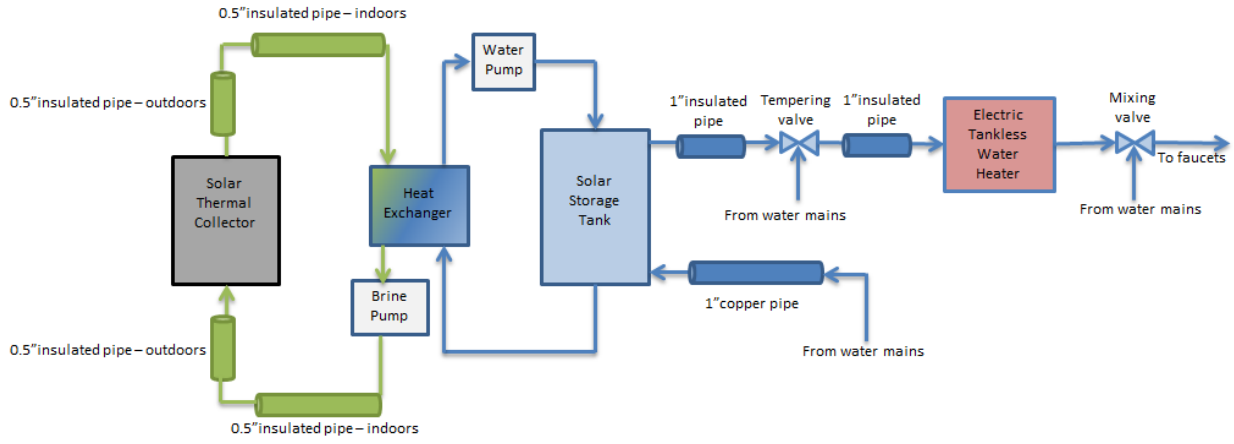

Figure 56. 80 Gallon SHW + TWH System Schematic.

Controls

The controls for the 80 gallon SHW system are identical to those used in for the 80 gallon SHW system in other DHW configurations. The tankless water heater setpoint is 48.9 ^{0}C ± 2.8 ^{0}C. This water heater has two stages of capacity: 12.5 kW and 25 kW.

Parameters

The types and parameters for the 80 gallon SHW system are identical to those used in the 80 gallon SHW plus 50 gallon HPWH configuration. Listed below are the parameters for the electric tankless water heater.

Table 43. 80 Gallon SHW + TWH System Parameters.

Tankless Water Heater Type 940	Thermal capacitance	12.6	kJ/K
	Initial temperature	40	C
	Minimum flowrate	56.8	kg/hr
	Efficiency of device	1	
	Heating capacity	25000	W
	Surface area	0.4645	m^2
	Modulation steps	2	
	Temperature deadband	5.6	deltaC
	Minimum input fration: modulating control	N/A	
	Efficiency of pilot light	N/A	
	Pilot light energy	0	W
	Fluid specific heat	4.19	kJ/kg-K
	On-time delay	0	hr
	Electrical energy - standby mode	2	W
	Electrical energy - heating mode	25000	W
	Setpoint Temperature*	51.7	C
	Heat loss coefficient*	9.1	W/m^2-K
	Auxiliary heat input*	0	W

*Type input, not a parameter